

———— Study for the Scientific Students' Association ————

András György Szanthoffer

**The Combustion Chemistry of
Syngas/NO_x Gas Mixtures**

Supervisors:

**Tamás Turányi, Professor of Chemistry
István Gyula Zsély, Assistant Professor**

Department of Physical Chemistry



———— Eötvös Loránd University ————
—— Faculty of Science ——
— Budapest, 2021. —

Acknowledgments

First of all, I would like to thank my supervisors, Tamás Turányi and István Gyula Zsély for their support during my three years at the Chemical Kinetics Laboratory of ELTE. Tamás Turányi gave me this interesting project three years ago and always carefully reviewed my reports including this treatise. István Gyula Zsély provided me with valuable technical advice throughout the project that ensured the flow of the work.

This thesis could have never been completed without the software development work of Máté Papp who always implemented my requests into the *Optima++* framework readily.

I am also grateful to Márton Kovács whose work guided me in the sensitivity analysis of the thermodynamic parameters in kinetic models.

I also have to express my gratitude to Tibor Nagy for developing the *Minimal Spline Fit* computer program that I used in the estimation of the standard deviation of experimental datasets.

The work was supported by NKFIH grant OTKA K132109 of the Hungarian National Research, Development and Innovation Office.

Contents

1. Introduction	4
2. The objectives of the present study	6
3. Literature review and data collection.....	7
3.1. Indirect experimental techniques in combustion chemistry	7
3.1.1. Spatially homogeneous reactor models	8
3.1.2. Burner stabilized flames (BSF)	12
3.2. Collection of indirect experimental data on syngas/NO _x systems.....	14
3.2.1. The reburning process for non-hydrocarbon fuels	17
3.2.2. The sensitizing effects of NO and NO ₂ on H ₂ /CO combustion	18
3.3. Detailed kinetic reaction mechanisms	20
3.3.1. The CHEMKIN mechanism format	20
3.3.2. The investigated reaction mechanisms.....	23
4. Applied methods.....	26
4.1. The preparation of RKD format experimental data files	26
4.2. The simulation of gas-phase combustion systems.....	27
4.3. Modifications of the investigated mechanisms	28
4.4. The quantitative comparison of reaction mechanisms	30
4.4.1. The error function.....	31
4.4.2. Estimating the standard deviation of the experimental data	32
4.4.3. The standard deviation of different experimental data types	36
4.5. Local sensitivity analysis.....	40
4.5.1. Sensitivity analysis of thermodynamic properties	42
5. Results and discussion.....	45
5.1. The comparison of syngas/NO _x combustion mechanisms	45
5.1.1. Jet stirred reactor simulations.....	47
5.1.2. Shock tube simulations.....	48
5.1.3. Flow reactor simulations	49
5.1.4. Burner stabilized flame simulations	50
5.2. The comparison of the results with <i>FlameMaster</i> and <i>OpenSMOKE++</i>	51

5.3. Overview of mechanism performance comparisons	55
5.4. Results of the sensitivity analysis	62
5.4.1. Kinetic parameters.....	62
5.4.2. Thermodynamic parameters	67
6. Conclusions and outlook.....	69
Appendix	70
References	97

1. Introduction

The term “syngas” (a shortened form of *synthesis gas*) is a synonym for “wet CO” in the field of combustion chemistry. Syngas is the mixture of hydrogen (H_2) and carbon monoxide (CO), and possible additional diluted species such as carbon dioxide (CO_2) and/or water vapor (H_2O), etc. “Wet CO” is distinct from “dry CO”, where the latter is pure CO gas in the absence of any hydrogen compound. The distinction is important because the combustion characteristics of the two gas mixtures are very different. From a practical point of view, only the combustion of wet CO is relevant [1].

Syngas can be produced by the gasification of coal or biomass [2-4]. The resulting gas mixture can then be used for electricity production in gas turbines (GT), internal combustion engines, and boilers [5]. The use of syngas as a fuel may provide a clean (low emission), well-controllable and efficient way of energy production; therefore, it is relevant in environmental protection [5]. To design new syngas-based engines or power plants, accurate chemical kinetic models are needed that can describe the combustion of syngas mixtures under conditions relevant to the industrial application. In recent years, several kinetic mechanisms have been published that aimed to describe the combustion of syngas mixtures [6-11]. In the work of Varga et al. [11], a collection of syngas combustion mechanisms (published before 2016) can be found.

The accurate modeling of syngas combustion is important from another aspect as well. Today, in most internal combustion engines, the main fuel is a hydrocarbon or a hydrocarbon mixture. However, it is well-known that the oxidation kinetics of hydrocarbons has a hierarchical nature [1]. It means that, at high temperatures, small molecules and radicals control the oxidation kinetics of fuels with a larger carbon number. In this mechanism, CO is a very important intermediate species [9]. The combustion mechanism of syngas (H_2/CO) is the basis of all high-temperature hydrocarbon oxidation [11].

Nowadays, a great interest can be seen toward the exploration of the combustion mechanisms of gas mixtures that contain also nitrogen compounds. The reason for this is that one of the most important issues of recent times is the reduction of the emission of air pollutants. Air pollutants are predominantly formed in the combustion of fossil fuels during energy production. These processes take place in, for example, the industry, the heating of households, and transportation. One of the most important groups of air pollutants is nitrogen oxides. Based on quantity and stability, the most significant nitrogen oxides are nitric oxide

(NO), nitrogen dioxide (NO₂), and nitrous oxide (N₂O), and these compounds will be referred to as NO_x here. This study investigates the combustion of syngas (H₂/CO) mixtures that also contain at least one of the NO_x species.

The NO_x compounds have several harmful effects on the environment and the human health. NO and NO₂ significantly contribute to the formation of *acid rain* in the troposphere and are major constituents of *photochemical smog*. N₂O is inert, not soluble in water, so it has a large residence time in the troposphere, and therefore it can reach also the stratosphere. The molar absorption coefficient of N₂O is large in the IR range but it is small in the UV/VIS range, hence N₂O is a *greenhouse gas*. Moreover, it can be converted to NO, and NO catalyzes the decomposition of ozone in the stratosphere; therefore, N₂O indirectly contributes to the *destruction of the ozone layer*. More details on the role of the NO_x compounds in the atmosphere can be found in the book of Seinfeld and Pandis [12]. Due to these harmful effects of the NO_x compounds, the minimization of NO_x emission is crucial during the energy-producing processes, and in the meanwhile, the efficiency of the energy production should not deteriorate significantly. To find an optimum of these two purposes, it is necessary to know the chemistry of the reactions that occur in the combustion chambers of engines and gas turbines.

Though in gas turbines and reciprocating engines, the nitrogen is initially predominantly present in the form of N₂ that comes from the air (oxidizer), the investigation of fuel/oxidizer gas mixtures doped with NO_x compounds is itself very important. First, NO_x compounds, even in very small amounts, have a significant effect on most combustion systems such as syngas/oxidizer mixtures: by opening new reaction paths, and most importantly by altering the H/O radical pool during combustion, they can change the reaction rate substantially. This property is called the *sensitizing effect*. This effect was demonstrated in several combustion systems, from low to high temperatures for various fuels [13-19]. The investigation of syngas/NO_x systems is of particular importance as Ahmed et al. [20] showed that the NO_x formation and the kinetic fuel–NO_x interactions are still not explored appropriately in hydrogen and syngas combustion systems.

Second, if too much NO_x is formed during the operation of a power plant or a means of transport, then the NO_x emission must be reduced. Several methods have been developed for this purpose. To improve the techniques of controlling the NO_x-emission of combustion systems, better knowledge of NO_x chemistry is inevitable.

2. The objectives of the present study

The Chemical Kinetics Laboratory at ELTE Eötvös Loránd University [21] deals with the computer modeling of gas-phase combustion processes. The group aims to evaluate the performance of combustion models based on experimental data from the literature and to develop new combustion mechanisms for various combustion systems. The work presented in this study was carried out within the frame of this research group. My research investigated the combustion of gas mixtures in which the fuel was syngas (H_2/CO), and NO_x species were also added to the mixture.

The aims of this study can be summarized as follows:

- (i) Collection of experimental data on the combustion of syngas/ NO_x gas mixtures from the literature and preparing data files that are suitable for simulation programs to model these experiments.
- (ii) Collection of recent, detailed reaction mechanisms from the literature that can describe the combustion of syngas/ NO_x combustion systems.
- (iii) Simulation of the collected experiments with the mechanisms using two different numerical solver packages.
- (iv) Quantitative evaluation of the performance of the mechanisms under various conditions, based on the simulation and experimental results.
- (v) Comparison of the performance of the mechanisms in a quantitative way.
- (vi) Comparison of the simulation results obtained by the two solver packages.
- (vii) Investigation of the best-performing model by sensitivity analysis to identify the parameters that are most influential on the model outputs.
- (viii) Discussion of further research opportunities.

3. Literature review and data collection

In this section, the experimental techniques often applied for the investigation of the combustion chemistry of syngas/NO_x gas mixtures are introduced first (Section 3.1). After that, I present the data that were collected from the literature and that will be used in this study for the comparison of the performance of the mechanisms (Section 3.2). Finally, I show the recent reaction mechanisms that can describe the combustion of syngas/NO_x systems and that were investigated in this work (Section 3.3.2). The structure of gas-phase combustion mechanisms is also discussed briefly based on the CHEMKIN reaction mechanism format (Section 3.3.1).

3.1. Indirect experimental techniques in combustion chemistry

In Section 1, it was discussed why the computer modeling of syngas/NO_x combustion systems is important in practice. When a reaction mechanism is being developed, researchers rely on various types of data: results of theoretical chemistry calculations, direct experimental data, and indirect experimental data. The results of *theoretical chemistry calculations* [22-25] are primarily used to determine the thermochemical data of a species or to estimate the rate coefficient of a selected reaction at different pressures and temperatures. The latter purpose can also be achieved by performing *direct experiments* [26-29].

In the case of *indirect experiments*, a quantity that is characteristic of the whole reaction, i. e., the whole set of reaction steps, not only one reaction step, is measured. When a reaction mechanism has been constructed, it must be validated against experimental data, which means that indirect experiments are simulated with the mechanism, and the simulation results are compared to the results of the indirect experiments. The more accurate the predictions of the mechanism compared to the indirect experimental results, the better the performance of the model.

Since the main aim of this treatise is to compare the performance of several combustion mechanisms of syngas/NO_x systems, some indirect experimental techniques that are relevant for this research are introduced in this section. These methods can be divided into two groups. One group contains methods in which the experiment can be simulated by a homogeneous gas mixture model (see [30] and p. 339. in [31]). These techniques are discussed in Section 3.1.1. The homogeneity of the gas mixture can be approximated experimentally by premixing the

reactants to aim the “perfect” mixing of the reactor zone. The computer simulation of these systems is called *zero-dimensional* (0D) because the physical–chemical properties do not depend on any spatial coordinate in the simulation. The experimental studies of flames belong to the other group. The computer simulation of flames is more complicated than that of homogeneous systems because flames can only be simulated by spatially one- or more-dimensional models. In this study, *one-dimensional* (1D) flames are treated (Section 3.1.2) whose physical-chemical properties are a function of the distance from the flat burner plate (burner stabilized flames).

3.1.1. Spatially homogeneous reactor models

3.1.1.1. Jet stirred reactor (JSR)

The main part of a *jet stirred reactor* (JSR), which is often called the *perfectly stirred reactor* (PSR), is a spherical reactor with a wall made of glass or quartz placed in a thermostat to keep the reactor at constant temperature (Figure 1, Figure 2). After the preheating section, the reactant gases that are usually highly diluted with the bath gas are continuously introduced into the reactor at a given mass flow rate through nozzles that point in different directions causing a turbulent flow in the reactor. In this construction, it can be assumed that the gases are perfectly mixed in the sphere, and therefore the reaction mixture can be considered homogeneous. The temperature in the reactor is measured by thermocouples (Figure 2) and the pressure is kept constant. At the opposite side of the sphere relative to the inlet, an outlet valve can be found. This valve is opened at a given pressure such that a steady state is maintained in the reactor. When the steady state has evolved, the outlet gas mixture is sampled and analyzed by the appropriate analytical techniques. The important experimental parameters in JSR measurements are the residence time in the reactor and the volume of the reactor [32–34]. The residence time is usually denoted by τ , and it is the time that the inlet gases spend in the reactor, on average, between the inlet and the outlet. If the mass flow rate of the reactants is set to constant in the experiments, the residence time decreases with increasing temperature.

Note that preheating and high dilution of the reactants are needed to minimize the temperature fluctuations in the reactor caused by the heat effects of the chemical reaction. This way, the temperature of the reactor may be kept at a constant value within a few kelvins. Note, however, that if the gas mixture is not highly diluted or if the reaction has very large

heat effects, the temperature of the reactor may vary significantly, and, in this case, the isothermal steady state modeling approach may not be valid for this experiment type. A more detailed theoretical and practical overview of the jet stirred reactors used in combustion studies can be found in Chapter 8 of the book of Battin-Leclerc et al. [35].



Figure 1. The jet stirred reactor used at the Laboratoire Réactions et Génie des Procédés (Nancy, France). Source of the figure: p. 186. of the book of Battin-Leclerc et al. [35].

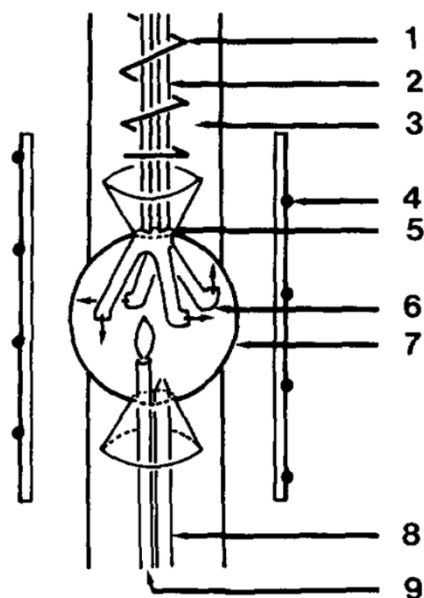


Figure 2. The schematic of a jet stirred reactor. 1: preheating resistor, 2: capillary for the inlet of the fuel-bath gas mixture, 3: inlet of the oxidizer-bath gas mixture (main flow), 4: heating resistor, 5: point of mixing, 6: injectors, 7: the spherical reactor, 8: gas outlet valve and sampling, 9: thermocouple. Source of the figure: Dagaut et al. [32].

3.1.1.2. Shock tube (ST): measuring the ignition delay time

The *shock tube* (ST) is a 5–10-meter-long steel tube with a diameter of 60 mm, typically. The tube is divided into two compartments by a membrane which is also called a diaphragm (Figure 3). In one of the compartments (the *driver section*), there is the high-pressure (ca. 50 atm) driver gas which is an inert gas (usually Ar or N₂). In the other compartment (the *driven section*), the investigated low-pressure fuel–oxidizer–diluent gas mixture is located.

At the start of the measurement, the diaphragm is ruptured mechanically (e. g., by a sudden increase of the pressure), and a shock wave starts propagating in the tube towards its low-pressure end, this is the so-called *incident shock wave*. This propagating shock wave compresses the gas mixture in the tube; consequently, the temperature and the pressure of the gas located in front of the shock wave increase suddenly. As the shock wave reaches the low-

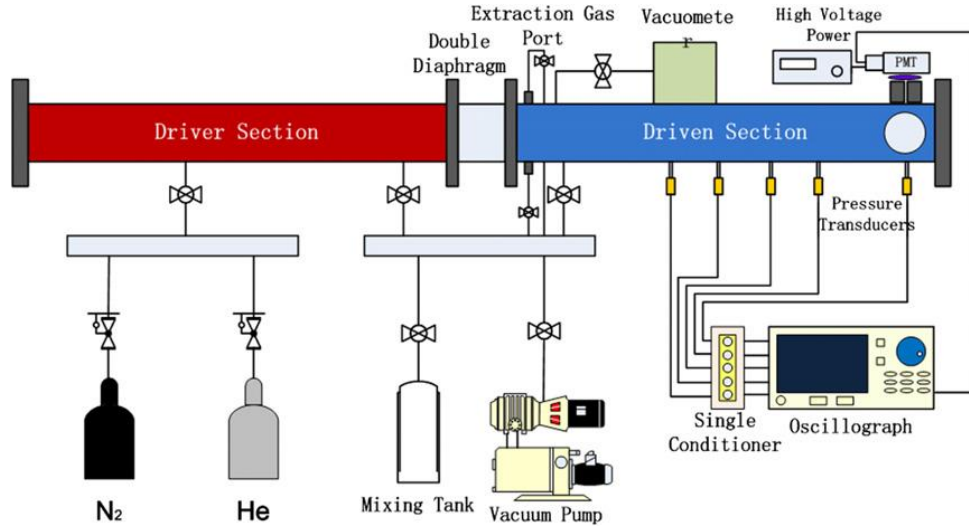


Figure 3. The schematic representation of a shock tube used in the work of Zhang et al. [36].

pressure end of the tube, it is reflected back from the wall, and the so-called *reflected shock wave* starts propagating in the opposite direction (towards the originally high-pressure end of the tube). The reflected shock wave has the same effect on the gas mixture as the incident shock wave; therefore, another sudden increase in the temperature and the pressure of the gas mixture can be observed. Nowadays, in almost all measurements, the experimental conditions are designed such that the ignition takes place due to the reflected shock wave, and the incident shock wave has only the role of pre-heating the mixture. The reason for this is that the computer simulation of the ignition behind the reflected shock wave is simpler and more reliable.

Due to the ignition, the pressure and the temperature of the gas mixture often increase suddenly, once more. However, since the gas mixtures are usually highly diluted, the pressure and temperature increase are often not very significant. In these cases, the start of the ignition is usually indicated by the sudden increase of the concentration of intermediate species that are typically highly reactive radicals. The concentrations of these radicals are measured by an optical spectroscopy technique. The ignition of a high-pressure and -temperature gas mixture does not take place immediately upon the arrival of the reflected shock wave, but only after a certain amount of time when the radical concentrations are so large that they can induce the ignition. The elapsed time between the compression (i. e., the arrival of the reflected shock wave) and the ignition is called the *ignition delay time* (usually denoted by τ , τ_{ign} , or IDT), and the shock tube is most often used for measuring this quantity.

The ignition delay time can be detected in many ways, depending on the actual experimental device. Recently, Zhang et al. [37] collected 37 different ignition delay time

detection methods in methane combustion experiments. In the work of Burke et al. [38], several modern experimental constructions of shock tubes are shown, which are applicable for the determination of ignition delay times.

3.1.1.3. Tubular flow reactor (FR)

The *tubular flow reactor* (FR), which is often referred to as *plug flow reactor*, is a quartz or glass tube which is heated (thermostated) by electric cartridges from the outside. At one end of the tube, the reactant gases and the inert bath gas(es) enter the tube in separate inlets, and they flow through the tube with a constant flow speed. The chemical reaction takes place in the tube (at the preselected temperature), and then, at the other end of the tube, the outlet gas mixture is cooled down, and the concentrations of some chemical species are measured by the appropriate analytical technique(s). To approximate the conditions of homogeneous combustion, a mixing zone is placed before the reaction zone where the reactant gases can mix. A schematic of a tubular flow reactor is given in Figure 4. The temperature is measured by thermocouples in the reactor along the tube, and the pressure is also recorded.

Note, that to ensure a uniform temperature profile in the reaction zone, the inlet gases are preheated by separate thermostats. However, a really uniform temperature profile still cannot be created along the whole tube despite this effort; the ends of the tube are always cooler than the reaction zone (the middle part). Sometimes, the authors publish the experimentally measured temperature profiles along the reactor axis (Figure 5). In these cases, the simulations of flow reactor experiments can be performed using these temperature profiles, the length and the diameter of the reactor, and the flow velocity of the inlet gas mixture as inputs. As can be seen in Figure 5, it usually can be achieved that the reaction zone has a constant temperature within a few kelvins. Therefore, in the lack of experimental

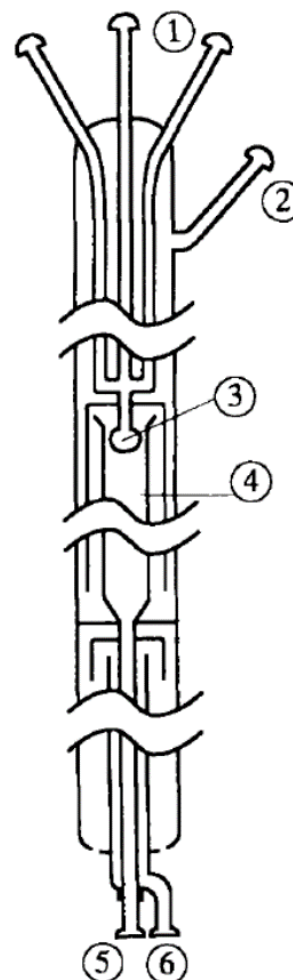


Figure 4. Schematic of a tubular flow reactor. 1: inlets for reactants, 2: inlet for inert bath gases (main flow), 3: reactant mixing zone and injection into the main flow, 4: reaction zone, 5: outlet, 6: cooling air. Source of the figure: Glarborg et al. [39].

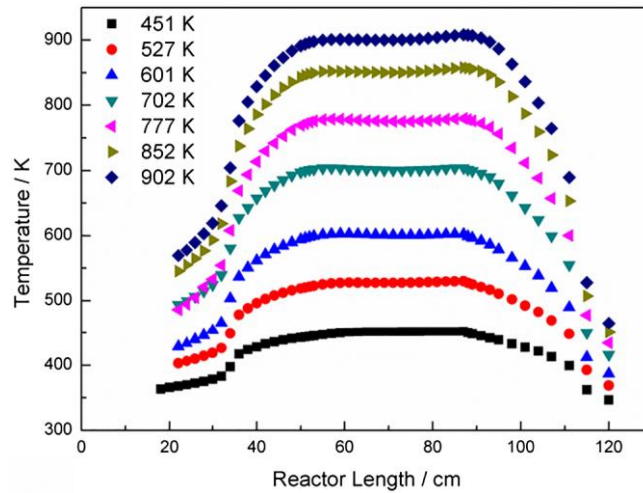


Figure 5. Experimentally measured temperature profiles along the axis of a tubular flow reactor at different isothermal zone temperatures at 30 bar during ammonia oxidation [41]. Source of the figure: Song et al. [41].

temperature profiles, it is a good approximation that the reaction takes place at a constant temperature. In these cases, the residence time of the gas mixture in the reaction zone and the isothermal temperature are used as input parameters for the simulations. Of course, the latter approximation is less accurate.

There are two types of flow reactor experiments widely used in combustion chemistry: measuring outlet concentrations or measuring concentration–time profiles. In the first case, the outlet concentration of some species is measured as described above. Usually, these measurements are carried out at different reaction temperatures and the outlet concentrations are plotted as a function of temperature [14, 39, 40], but other properties can also be chosen as the independent variable such as the initial concentration of a species [39, 40] or the residence time [40]. In the case of concentration–time profile measurements, the concentrations of some species are measured as a function of reaction time at constant temperature and pressure. The different reaction times are ensured by sampling the flowing gas mixture at different axial positions compared to the point of mixing. The distances are then converted to reaction times by taking into account the mass flow rates of the gases.

A detailed theoretical and practical description of flow reactor experiments in combustion chemistry can be found in Chapter 9 of the book of Battin-Leclerc et al. [35].

3.1.2. Burner stabilized flames (BSF)

The investigation of flames reveals additional important physical properties of the investigated system. For the validation of combustion mechanisms, 1D experiments are

frequently applied, because there are widely used computer codes that can relatively easily simulate such experiments. The modeling of two- or three-dimensional experiments is computationally more challenging and expensive. In this section, one type of one-dimensional experiments with flames is introduced, namely, the investigation of the structure of burner stabilized premixed flat flames.

In a typical burner stabilized flame experiment, the concentration profiles of some species are measured in the flame. The most frequently used experimental device is the so-called *flat flame burner* (Figure 6). In this case, the flame is stabilized on the burner head, and the flame is assumed to be stationary. In these experiments, the concentrations of some species are measured as a function of the distance from the burner plate by a quartz sampling nozzle or an appropriate spectroscopy method [42-44]. In Figure 7, the schematic of an experimental setup is shown from the work of Seery et al. [42] in which molecular beam sampling with mass spectroscopy was applied to analyze the structure (composition) of the flame.

In these measurements, there is heat loss from the flame towards the burner plate, so the flame front is not adiabatic. The computer simulation of these flames is rather challenging without knowing the experimental temperature profile above the burner; therefore, the temperature of the flame is also usually measured as a function of the distance from the burner plate. This temperature distribution is used as an input parameter for the computer simulations.

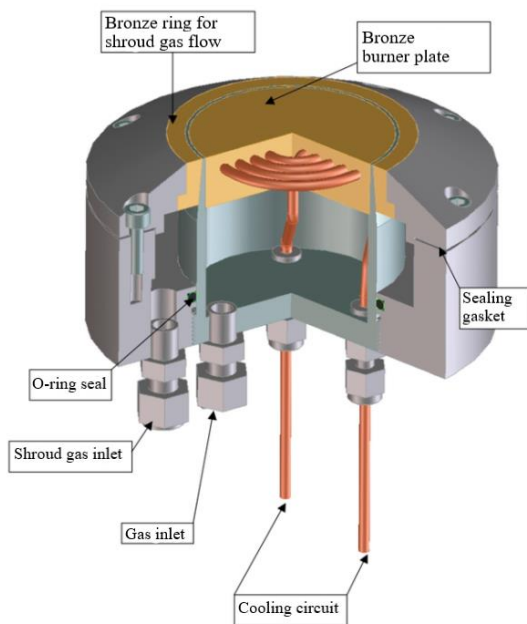


Figure 6. The cross-section of a flat flame burner. The figure was modified from [45].

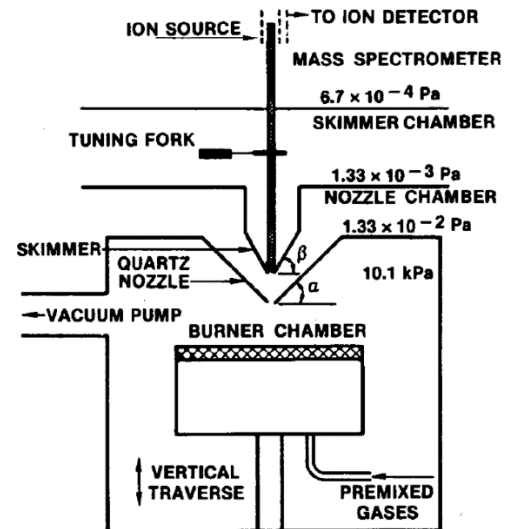


Figure 7. The experimental setup of a flat flame burner measurement using molecular beam sampling and mass spectroscopy for analyzing the flame structure. The figure was modified from the work of Seery et al. [42].

3.2. Collection of indirect experimental data on syngas/NO_x systems

In this section, the collected indirect experimental data from the literature are presented and the main features of the data collection are discussed. Table 1 and Table 2 contain the collected indirect experimental data that are used in this study for mechanism comparison. Table 1 summarizes the main targets of the experiments, and Table 2 contains the experimental conditions in more detail.

In Table 2, the composition of the gas mixture is characterized by the so-called *equivalence ratio*, Φ , which is often denoted by φ . This quantity is defined as follows:

$$\Phi = \frac{\frac{n_{\text{fuel}}}{n_{\text{oxidizer}}}}{\left(\frac{n_{\text{fuel}}}{n_{\text{oxidizer}}} \right)_{\text{stoichiometric}}}, \quad (1)$$

where n is the molar amount of the component. Hence, Φ describes whether the gas mixture is fuel-rich or fuel-lean, compared to the stoichiometry of the main combustion reaction. If $\Phi < 1$, the mixture is fuel-lean, if $\Phi > 1$, it is fuel-rich, and if $\Phi = 1$, it is referred to as stoichiometric. Table 2 also shows that the oxidizer was O₂ in most experiments, and the inert bath gas (diluent) was N₂. In a few cases, O₂ was replaced by N₂O as the oxidizer, and in these experiments, N₂ was replaced by Ar.

Table 1. The main targets of the indirect experiments on H₂/CO/NO_x systems.

Reference	Apparatus	Main target
Dagaut (2003) [33]	JSR	reburning with H ₂ /CO
Dagaut (2003) [34]		sensitizing effects of NO on H ₂ /CO oxidation, reburning with H ₂ /CO
Dean (1978) [46]	ST	ignition of H ₂ /CO with N ₂ O as oxidizer
Kopp (2012) [47]		ignition of H ₂ /CO with N ₂ O as oxidizer
Hulgaard (1993) [48]	FR	decomposition of N ₂ O in the presence of CO
Roesler et al (1995) [49]		sensitizing effects of NO on moist CO oxidation
Glarborg (1995) [50]		sensitizing effects of NO/NO ₂ on moist CO oxidation
Glarborg (1996) [39]		sensitizing effects of NO on moist CO oxidation
Alzueta (1997) [51]		reburning with CO
Mueller (1999) [15]		sensitizing effects of NO/NO ₂ on moist CO oxidation (up to 10 atm)
Glarborg (2000) [52]		reburning with H ₂ /CO
Rasmussen (2008) [14]		sensitizing effects of NO/NO ₂ on H ₂ /CO oxidation (up to 100 atm)
Dindi (1991) [53]	BSF	structure of CO/N ₂ O flames at low p
Vandooren (1997) [43]		structure of H ₂ /CO/N ₂ O/Ar flames at low p

As seen in Table 1, the indirect experiments may be grouped into three categories based on the targets of the investigations. The main groups are the reburning process of non-hydrocarbon fuels, the sensitizing effects of NO/NO₂ on syngas combustion, and the combustion of syngas/N₂O systems. The first two processes are discussed in Sections 3.2.1 and 3.2.2 in more detail.

Table 2. Indirect experiments on H₂/CO/NO_x systems and the experimental conditions.

Reference	App. ^a	Profile	XML/Ds./Dp. ^b	Fuel	Ox. ^c	Dopant	Dil. ^d	p / atm	T / K	Φ
Dagaut (2003) [33]	JSR	$c_{\text{out}}\text{--}\Phi$	2/9/96	H ₂ /CO	O ₂	NO	N ₂	1.0	1100, 1400	0.5–2.5
Dagaut (2003) [34]		$c_{\text{out}}\text{--}T$	3/8/87	H ₂ /CO	O ₂	NO	N ₂	1.0	800–1400	0.1, 1.0, 2.0
Subtotal:			5/17/183							
Dean (1978) [46]	ST	IDT– T	4/4/47	H ₂ /CO	N ₂ O	–	Ar	1.2–2.2	2000–3000	3.0, 11.6
Kopp (2012) [47]			2/2/33	H ₂ /CO	N ₂ O	–	Ar	1.4, 10.4	1650–2250	3.1
Subtotal:			6/6/80							
Hulgaard (1993) [48]	FR	c_{out}	2/4/24	CO	N ₂ O/(O ₂)	–	N ₂	1.0	950–1400	–
Roesler (1995) [49]		$c\text{--}t$	2/2/38	CO	O ₂	NO/H ₂ O	N ₂	1.0	1000	0.1, 1.0
Glarborg (1995) [50]		c_{out}	10/19/280	CO	O ₂	NO/(NO ₂)/H ₂ O	N ₂	1.05	800–1400	0.01–0.02
Glarborg (1996) [39]		c_{out}	4/4/60	CO	O ₂	NO/H ₂ O	N ₂	1.05	800–1300	0.01
Alzueta (1997) [51]		c_{out}	1/3/66	CO	O ₂	NO	N ₂	1.0	900–1400	1.3
Mueller (1999) [15]		$c\text{--}t$	11/22/394	CO	O ₂	NO/H ₂ O	N ₂	0.5–10.0	950–1010	0.3
Glarborg (2000) [52]		c_{out}	13/24/153	CO	O ₂	NO/H ₂ O	N ₂	1.0	1200–1800	0.1–10
Rasmussen (2008) [14]		c_{out}	3/15/195	H ₂ /CO	O ₂	NO/NO ₂	N ₂	20, 50, 100	600–900	0.06
Subtotal:			46/93/1210							
Dindi (1991) [53]	BSF	$c\text{--}$	1/18/175	CO	N ₂ O	–	–	0.07	298 ^f	1.0, 1.32, 1.5
Vandooren (1997) [43]		HAB ^e	3/11/186	H ₂ /CO	N ₂ O	–	Ar	0.04	300 ^f	1.19
Subtotal:			4/29/361							
Total:			61/145/1834							

^a: Apparatus, ^b: Number of XML files/datasets/data points, ^c: Oxidizer, ^d: Diluent, ^e: Height above the burner, ^f: Unburnt gas temperature.

3.2.1. The reburning process for non-hydrocarbon fuels

The **reburning process** is a method to reduce the NO_x emission of practical combustors. It reduces the NO formed during the combustion back to N₂ by the clever modification of the combustion process [54]. It is based on the observation of Myerson et al. [55] that the reaction of hydrocarbon radicals with NO is fast. The practically applied method based on this reaction was developed by Wendt et al. [56], in which the fuel is used to reduce the NO in the exhaust gas mixture.

In reburning, the combustion of the gas mixture is carried out as a three-stage combustion process. In the first stage, the gas mixture is usually moderately fuel-lean and the temperature may be high to ensure efficient combustion, and therefore a significant amount of NO_x is usually formed from the combustion air and/or from fuel-bound nitrogen. The second stage is the so-called *reburning zone* where the secondary, so-called *reburning fuel* is added to the gas mixture to reduce the NO_x formed in the first stage as efficiently as possible. The last stage is the so-called *burnout zone*, where excess air is introduced to the system (fuel-lean conditions) to complete the combustion. In this stage, the temperature should be relatively low to avoid the high-temperature Zeldovich NO formation [57]. The prompt NO formation which is relevant in fuel-rich mixtures [58-61] is suppressed by the application of excess air. From now on, the term “reburning” will be used to refer to the second stage of the process where the NO_x is reduced by the reburning fuel.

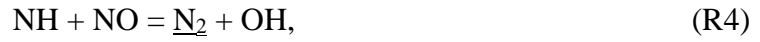
When the reburning fuel is a hydrocarbon, which is the most common scenario, the attack of CH_n radicals on NO is the initiation reaction of the reburning process:



However, it is also possible to use H₂, CO, or syngas as the reburning fuel, and in this case, the CH_n radicals are not present in significant amounts [52] under reburning conditions. Therefore, other reactions than (R1) initiate the process. The reburning process for syngas (a non-hydrocarbon fuel) is discussed here based mainly on the work of Glarborg et al. [52]. The experimental and theoretical investigation of this process is important because most gas mixtures obtained by the gasification of coal, biomass, etc., and used as fuel (such as syngas) have a very low or negligible hydrocarbon content. Therefore, these studies may have implications on the potential application of these gas mixtures as reburning fuels.

At medium temperatures (900–1800 K), which is relevant for the reburning process, the primary scheme for the removal of NO starts with the H radical (stemming from the O/H radical pool) attacking the NO (R2). This reaction requires a third-body colliding partner and

produces the HNO intermediate. Then, the HNO reacts with another H radical, and the key product of the reaction is the NH intermediate (R3). This NH radical reacts with another NO molecule and converts it to N₂ either directly (R4) or in a two-step process through N₂O (R5)–(R6).



The key step in the (R2)–(R6) scheme is the reaction of the HNO intermediate with H in (R3), because two important reactions compete with it, which convert the HNO species back to NO, and thus, they impede the NO reduction:



If the conditions are reducing ($\Phi > 1$), the H₂ and CO concentrations may be large enough to make the following reactions important:



The resulting NH would then react via the (R4)–(R6) scheme, and thus would reduce the NO back to N₂. (R9) and (R10) are not important below 1400 K according to Dagaut et al. [34]. Above 1400 K, the role of these reactions is not completely clear [52].

Note, that there is another route that can lead to NH from HNO, which involves the formation of H₂NO and HNOH intermediates, but this pathway is not important under conditions relevant for reburning.

3.2.2. The sensitizing effects of NO and NO₂ on H₂/CO combustion

Several experiments in Table 1 studied the sensitizing effects of NO and NO₂ on the combustion of syngas mixtures; therefore, this topic is summarized here shortly, based mainly on the work of Glarborg et al. [50] and Mueller et al. [15].

In small concentrations, NO promotes the oxidation of CO and H₂ at medium temperatures (ca. 850–1250 K) due to the reaction



which produces reactive OH radicals from unreactive HO₂ radicals from the H/O radical pool. The resulting OH radicals may then react with H₂ and CO as



to form catalytic cycles which oxidize H₂ and CO. Thus, the oxidation of CO and H₂ may begin at a noticeably lower temperature in the presence of a small amount of NO than in the absence of this dopant.

In higher concentrations, NO may act as an inhibitor for H₂ and CO oxidation through the following sequence of chain termination (radical recombination) reactions, if they are



more important than (R11):

where X and Y are reactive radicals from the H/O radical pool, H, O, or OH. Dagaut et al. [34] showed that reaction (R14) competes with (R11), and the importance of the (R14)–(R15) scheme increases with increasing equivalence ratio. Note also that carbonaceous species are not present in (R11)–(R15), so NO influences the oxidation of syngas mainly via the H/O radical pool.

The sensitizing effects of NO₂ may be similar to that of NO but the situation may also be a bit more complicated. It is discussed more thoroughly in the works of Glarborg et al. (1995) [50] and Mueller et al. (1999) [15] which include also NO₂ in the gas mixtures.

3.3. Detailed kinetic reaction mechanisms

The computer modeling of combustion systems is carried out by constructing detailed reaction mechanisms that can describe the investigated system(s) and can be interpreted by an appropriate combustion simulation code. Nowadays, the aim of developing detailed reaction mechanisms is the accurate theoretical description of combustion systems, rather than the parameterization of the rate of a single overall reaction. To facilitate the development of combustion mechanisms, it was necessary to introduce a common format in which the reaction mechanisms are published, and which can be interpreted by the widely used simulation programs, so that published reaction mechanisms can be utilized by any user having an appropriate simulation package.

Approximately 35 years ago, the so-called CHEMKIN reaction mechanism format was introduced, which soon became widespread, and almost all combustion simulation programs can interpret mechanisms in this format today. In Section 3.3.1, the basics of the GAS-PHASE KINETICS part of the CHEMKIN simulation code are discussed briefly, based on version 17.0 of the Chemkin Theory Manual of the ANSYS software developer company [62], and the Theory Manual [63] and Input Manual [64] of the CHEMKIN version 4.0.2. In Section 3.3.2, the reaction mechanisms investigated in this work are introduced. These models are capable of simulating syngas/NO_x/O₂ combustion systems.

3.3.1. The CHEMKIN mechanism format

CHEMKIN format mechanism text files are divided into blocks:

- **ELEMENTS** block: a list of the symbols of the chemical elements that constitute the species in the mechanism.
- **SPECIES** block: a list of the chemical species in the mechanism.
- **THERMO** block: the thermodynamic data of the species listed in the SPECIES block. These data can also be given in a separate text file.
- **REACTIONS** block: contains the equations of the reaction steps and the corresponding rate parameters. The rate coefficient (k) of a reaction step depends on the temperature and may also depend on the pressure and the composition of the gas mixture. Most reactions take place in both directions, but usually, only the rate coefficient in one of the

directions is given. The rate coefficient in the opposite direction (k_{-1}) can be calculated from the equilibrium constant (K) as follows:

$$k_{-1} = \frac{k}{K}. \quad (2)$$

The equilibrium constant can be calculated from the thermodynamic data of the reactants according to basic thermodynamic relations.

- **TRANS** file: contains properties from which the viscosity, the coefficient of thermal conductivity, and the diffusion coefficient of the species defined in the SPECIES block can be calculated. The required properties for each species are the geometry index (0 for atoms, 1 for linear molecules, and 2 for nonlinear molecules), the Lennard-Jones parameters, the dipole moment, the polarizability, and the rotational relaxation collision number. These data are necessary for one- or more dimensional simulations (e. g., laminar premixed flames) but not needed for zero-dimensional computations such as ignition delay time simulations. They are given in a separate file.

3.3.1.1. The thermodynamic parameters of the species

Most gas kinetics programs like the CHEMKIN simulation package assume that the gas mixture is ideal and is in thermal equilibrium. This has two implications. First, the temperature of the gas mixture and the temperature of each species are the same, and second, the standard thermodynamic properties of the species depend only on the temperature, but not on the pressure.

The CHEMKIN simulation package first defines the standard isobar molar heat capacity of the species ($c_{p,i}^\ominus$ for species i), because, from this, any other standard thermodynamic property can be calculated by integration. In principle, the temperature dependence of the heat capacity can be given by a polynomial of arbitrary degree. The CHEMKIN package uses the convention of the NASA polynomials [65, 66] which gives the heat capacity as a polynomial of degree four in temperature (T):

$$\frac{c_{p,i}^\ominus}{R}(T) = a_{1,i} + a_{2,i}T + a_{3,i}T^2 + a_{4,i}T^3 + a_{5,i}T^4, \quad (3)$$

where R is the gas constant ($8.314 \text{ J mol}^{-1} \text{ K}^{-1}$), and a_1 – a_5 are the coefficients (parameters). Consequently, the standard molar enthalpy of formation (H_i^\ominus) and the standard molar entropy (S_i^\ominus) of species i can be given as follows:

$$\frac{H_i^\ominus}{RT}(T) = a_{1,i} + \frac{a_{2,i}}{2}T + \frac{a_{3,i}}{3}T^2 + \frac{a_{4,i}}{4}T^3 + \frac{a_{5,i}}{5}T^4 + \frac{a_{6,i}}{T}, \quad (4)$$

$$\frac{S_i^\ominus}{R}(T) = a_{1,i} \ln T + a_{2,i}T + \frac{a_{3,i}}{2}T^2 + \frac{a_{4,i}}{3}T^3 + \frac{a_{5,i}}{4}T^4 + a_{7,i}, \quad (5)$$

where a_6 and a_7 are the new coefficients coming from the integrations in equations (6)–(7). Equations (3)–(5) accord with the well-known thermodynamic relations between these quantities:

$$H_i^\ominus(T) = \int c_{p,i}^\ominus(T) dT, \quad (6)$$

$$S_i^\ominus(T) = \int \frac{c_{p,i}^\ominus(T)}{T} dT. \quad (7)$$

Hence, if we know coefficients a_1 – a_7 , we know the temperature dependence of the standard thermodynamic quantities using equations (3)–(5). If these three state functions are known, then using the basic thermodynamic relations [62, 67] any other thermodynamic quantity needed for the simulations can be calculated at any temperature and pressure.

It is important to note that in the whole relevant temperature interval, we usually cannot describe the temperature dependence of these standard quantities with one polynomial accurately; therefore, the coefficients of the polynomials must be given separately in several temperature ranges. By default, the CHEMKIN format allows the definition of the thermodynamic functions in two temperature intervals, so in this case, 14 NASA coefficients need to be provided.

3.3.1.2. The temperature and pressure dependence of the rate coefficient

In the case of a high-temperature, gas-phase system, the temperature dependence of the rate coefficient is usually described by the so-called *extended Arrhenius equation*:

$$k = A \cdot T^n \cdot \exp\left(-\frac{E}{RT}\right), \quad (8)$$

where A , n , and E are the three Arrhenius parameters that characterize temperature dependence the rate coefficient. In CHEMKIN format mechanism files, these three parameters are applied.

Note, that it is possible that the same set of reactants give the same products via different reaction routes, and different Arrhenius parameters belong to these different reaction pathways. This may be the case for multi-channel reactions. In this case, to indicate that there is more than one pathway for a given reaction, it is required to give the same reaction more

than once in the CHEMKIN input file. This is not allowed in CHEMKIN by default; therefore, if one wishes to include reactions of this type, the “DUP” or “DUPLICATE” keyword must be provided after each reaction equation corresponding to a duplicate reaction. Mathematically, the rate coefficient of a duplicate reaction is calculated as the sum of the rate coefficients of all reaction channels at the actual temperature (and pressure). Note, that duplicate reactions can frequently be replaced by one single reaction via the mathematical refitting of the rate parameters.

The rate coefficient may also depend on the pressure. In reaction mechanisms, many conventions may be used to describe the pressure dependence of the rate coefficient. These are the Lindemann model [68], the Troe parameterization [69, 70], the SRI parameterization [71], the PLOG formalism [72], and the Chebyshev polynomials [73, 74]. They can be used for different kinds of elementary reactions. A more detailed description of these formulations can be found in Chapter 2 of the book of Turányi and Tomlin [31].

3.3.2. The investigated reaction mechanisms

In this section, I present the reaction mechanisms investigated in this study. These mechanisms were published in the literature not earlier than 1999, and their main features are summarized here. They are capable of modeling syngas/NO_x combustion systems, though originally they were designed to describe more complicated systems such as those that contain methane and larger hydrocarbons as well. Therefore, when one performs simulations on the syngas/NO_x systems, it is enough to use only the part of the mechanism that is relevant in the combustion of the target system, in our case, syngas/NO_x systems. This decreases the computational time of the simulations substantially, especially in the case of one-dimensional simulations. However, the question arises: which parts of the mechanisms could be omitted?

According to Glarborg et al. [75], a mechanism that aims to describe the nitrogen chemistry in hydrocarbon combustion should include the following sub-mechanisms:

- i) hydrocarbon oxidation sub-mechanism (core: CO/H₂ oxidation),
- ii) oxidation of reactive nitrogenous species such as NH₃, HCN, HNCO,
- iii) interactions (coupling) between hydrocarbon and nitrogen chemistry such as prompt NO formation [58-61] and reburning.

Recently, Olm et al. [30, 76] tested the performance of several detailed reaction mechanisms published not earlier than 1999 on a very large collection of hydrogen and syngas indirect experimental data. Based on these works, Varga et al. [11] performed a

mechanism optimization jointly for hydrogen and syngas combustion systems in 2016, and their optimized mechanism had a better overall performance on the same set of experimental data than any mechanism published earlier. In their optimized mechanism, only three carbonaceous species were included, CO, CO₂, and HCO. It is not recommended to exclude all carbon species except for CO, CO₂, and HCO from the “reduced” mechanism initially without further analysis such as sensitivity analysis or reaction pathway analysis [31]. For instance, Zhang et al. [77] showed that the HOCO chemistry in a syngas/NO_x combustion mechanism has a non-negligible impact on the CO and CO₂ concentrations at high pressure in the case of H₂/CO/O₂/N₂/NO_x mixtures. Furthermore, according to Glarborg et al. [75], almost any fuel-derived radical can be involved in the fuel oxidation–nitrogen chemistry interactions; therefore, it is worth including the C₁ species in the “reduced” mechanisms for the syngas/NO_x mixtures, at least initially.

Therefore, when one investigates syngas/NO_x systems, it is a good practice to include only those species (and the corresponding reactions) that do not contain more than one carbon atom in the mechanism. For instance, the Wang-2020 model that was designed for the combustion of syngas/NO_x systems contains only species complying with this criterion. Besides that, the nitrogen chemistry sub-mechanism should also be included. If species that contain both nitrogen and one carbon atom such as HCN, HNCO, etc. are included in the mechanism, it is worth including them in the “reduced” mechanism as well, in order not to lose these reaction pathways without further analysis.

In Table 3, some features of the selected mechanisms are summarized. The number of species and the number of reactions were calculated after that the species (and the corresponding reactions) with more than one carbon atom had been removed from the original mechanisms, and these numbers are listed in the second and the third column of the table. From now on, these “reduced” mechanisms are meant by the identifiers in the first column. After these numbers, the number of species and that of reactions in the full mechanisms are shown in parentheses. Significant differences can be observed between the number of species and reactions in the various mechanisms. This can be traced back to the fact that the mechanisms were developed to describe different combustion systems. Moreover, the mechanisms are usually validated most extensively against experiments performed on their main target systems. Depending on whether the mechanism aims to describe one or more target systems or is a comprehensive reaction mechanism for C/H/N/O systems, its complexity may vary significantly.

Table 3. Reaction mechanisms that can simulate the combustion of syngas/NO_x/NH₃ gas mixtures. The mechanisms are listed in chronological order (the year in the mechanism identifiers refers to the publication year of the corresponding mechanism).

Mechanism	Species ^a	Reactions ^a	Main target	Ref.
GRI3.0-1999	40 (53)	231 (325)	natural gas ignition & flame propagation (including NO formation, and removal by reburning)	[78]
SanDiego-2004 ^b	36 (71)	140 (323)	NO _x emission in hydrocarbon flames	[79]
Tian-2009	60 (84)	506 (703)	species profiles in premixed NH ₃ /CH ₄ /O ₂ /Ar flames at low pressure	[80]
Konnov-2009	60 (129)	598 (1231)	small hydrocarbon combustion, NO _x formation and reburning, prompt NO formation (via NCN)	[61]
POLIMI-2014 ^d	32 (32)	173 (173)	combustion of H ₂ /CO/O ₂ /NO _x systems	[81, 82]
GDFKin-2016	45 (123)	350 (934)	modeling of NO formation in premixed natural gas/O ₂ /N ₂ flames at low pressure	[83]
Zhang-2017	43 (43)	251 (251)	pyrolysis and oxidation of hydrogen/NO _x and syngas/NO _x systems	[77]
SanDiego-2018 ^c	33 (68)	129 (311)	NO _x emission in hydrocarbon flames	[79]
Okafor-2018	49 (59)	281 (356)	NO concentration profile and LBV of premixed CH ₄ /NH ₃ /air flames	[84]
Glarborg-2018	80 (149)	674 (1374)	formation of N-containing air pollutants in the combustion of light hydrocarbons (CH ₄), $p \leq 1$ atm	[75]
Shrestha-2019	64 (125)	609 (1090)	NO _x chemistry during methanol and ethanol oxidation	[19]
POLIMI-2019 ^e	64 (159)	519 (2459)	the sensitizing effects of NO and NO ₂ on CH ₄ oxidation in JSRs at low T	[18, 85]
Han-2020	35 (35)	177 (177)	LBV of premixed syngas/NH ₃ /air flames	[86]
Wang-2020 ^f	43 (43)	253 (253)	syngas combustion with NO _x chemistry (update of Zhang-2017)	[87]
Konnov-2021	77 (255)	742 (3038)	LBV of premixed CH ₄ /HCOOH/air flames	[88]

^a: See text.

^{b, c}: The mechanisms are composed of the 2016/12/14 version of hydrocarbon oxidation, and the 2004/12/09 (b) and the 2018/07/23 (c) version of the nitrogen chemistry sub-mechanism by the Combustion Research Group at the University of California, respectively.

^{d, e}: “Previous kinetic mechanism (Version 1412) December 2014” (d) and “C₁–C₃ + NO_x mechanism (Version 2003, March 2020)” (e) models of the CRECK Modeling Group at Politecnico di Milano, respectively.

^f: The detailed kinetic mechanism of Wang et al. [87] was used because the indirect experiments investigated in this study were not used for the construction of the skeletal mechanism of the authors.

4. Applied methods

4.1. The preparation of RKD format experimental data files

A large part of my work was to extract the relevant information from the publications discussed in Section 3.2, and then, prepare data files in a specified file format, which contain all the necessary information about the experiments needed to perform the simulation of them. This file format is also briefly introduced here.

Due to the accumulation of experimental data in the combustion chemistry literature, there has been a demand for a database that facilitates and standardizes data storing, handling, and manipulation. An example of this is the PrIME database of Michael Frenklach [89] which contains models, model parameters, and experimental data from the field of combustion chemistry.

ReSpecTh [90] is an online database, which is a result of the collaboration of the ELKH-ELTE Complex Chemical Systems Research Group [91], the Laboratory of Molecular Structure and Dynamics [92], and the Chemical Kinetics Laboratory [21] of ELTE Eötvös Loránd University. It contains a large amount of literature data in the field of reaction kinetics (“Re”), spectroscopy (“Sp”), and thermochemistry (“Th”). The reaction kinetics section includes direct and indirect experimental data, reaction mechanisms, and computer programs that can be utilized for mechanism development.

Indirect experimental data are available in the so-called RKD (ReSpecTh Kinetics Data) format whose latest version is v2.3 [93]. It is essentially an extension of the file format used in the PrIME database [89]. Each measurement is stored in a separate XML (Extensible Markup Language) data file and each file has a unique identifier. The advantage of the use of XML files for data storage is that these files can easily be handled by computer programs and are also well readable by humans.

An RKD format XML measurement file contains all information about the experiment such as the experimental conditions and the measurement results, which is necessary to reproduce the experiment by computer simulations and to compare the theoretical and experimental results. In addition, it includes bibliographic information about the experiment so that the original data source can easily be found in the literature. The files have a straightforward structure: each structural unit starts with an opening `<...>` and ends with a closing `</...>` label and these units can be embedded into each other.

I prepared RKD format XML files from indirect experimental data listed in Section 3.2. My files were originally prepared in an earlier version, v2.2, of the RKD format because, at the time of this process, it was the latest version. Later, however, I updated them to v2.3. Altogether, 61 data files were constructed (see Table 2).

4.2. The simulation of gas-phase combustion systems

To be able to compare the performance of different combustion mechanisms, first, we must perform simulations with the mechanisms on the target experimental systems. The simulations were carried out with the help of the *Optima++* program package [94] developed by the Chemical Kinetics Laboratory at ELTE Eötvös Loránd University. The version of *Optima++* available on [94] can be executed from the command line. The current version (v2.3.0) of *Optima++* is compatible with the *CHEMKIN-II* [95], *FlameMaster* (FM) [96], and *OpenSMOKE++* (OS) [97-100] simulation packages. In this study, *FlameMaster* (version 4.2.1) and *OpenSMOKE++* (version 0.12.0) were used for the simulations. These packages can simulate all experiment types investigated in this study.

The necessary input files (CHEMKIN format mechanism file and RKD format XML file) have been discussed in Section 3. In the first step, *Optima++* creates an appropriate binary file from the plain text mechanism file that can be interpreted by the solver (FM or OS). After that, *Optima++* interprets the XML file(s) provided by the user and prepares the necessary input files for the solver. Then, the solver performs the requested simulation(s), and the results of the simulation(s) are printed in a plain text output file by *Optima++*.

The numerical solution of spatially 0D experiments is relatively easy, but 1D (premixed flame) simulations require much more computational effort. This is because in this case, the stationary solution of a partial differential equation needs to be found, as the physical–chemical properties are not only a function of time but that of one spatial coordinate as well. To find this stationary solution, a reasonable initial estimation of the solution has to be provided in the case of FM. In contrast to FM, OS can perform the 1D simulations without the initial estimations (“empty database”), though in this case, the simulation time increases significantly. The key to performing successful 1D simulations with FM is to find a good initial estimation of the solution for our target system, that is, an existing solution file for a system as similar to the system in question as possible. It is also advantageous if the original simulation was carried out with the same mechanism. Therefore, for the flame simulation with

FM, I first performed the simulations with OS and used the obtained solution files for FM simulations.

Instead of looking for a continuous solution as a function of the distance from the burner plate, the solvers perform the computations on grid points and look for a stationary solution for each grid point. A solution file contains the stationary values of the physical–chemical quantities (temperature, concentrations, etc.) at each grid point. I carried out my flame simulations applying approximately 600 grid points, which ensured the required accuracy, and at the same time, the simulations did not take too long.

4.3. Modifications of the investigated mechanisms

In Section 3.3.2, the investigated reaction mechanisms have already been introduced. However, some of them had been modified before they were used for simulations. In this section, these modifications are discussed.

As it has been mentioned in Section 3.1.1.2, ignition delay times are usually determined using the concentration profile of a species in the gas mixture. This species was CO_2 in the measurements of Dean et al. [46], and in the Kopp et al. [47] measurements, it was the excited OH radical (OH^*). In Table 4, however, we can see that only a few of the mechanisms contain the OH^* species and its reactions (OH^* submechanism). With the other mechanisms, the reproduction of the IDT measurements of Kopp et al. [47] is not impossible. To overcome this issue, the OH^* submechanism of the syngas combustion mechanism of Kéromnès et al. [7] was added to the mechanisms that lack this part, and the ST-IDT simulations were carried out using these modified mechanisms. This OH^* submechanism is also included in the optimized syngas combustion model of Varga et al. [11]. I chose this submechanism for this purpose because the model is the best syngas combustion mechanism published not later than 2016 and it was constructed using an optimization method on a large set of experimental data. Also, this mechanism was developed in the Chemical Kinetics Laboratory at ELTE Eötvös Loránd University, and to follow the hierarchical mechanism development strategy of the group, it was a logical choice.

Table 4. Some features of the investigated mechanisms that are related to the modification of some mechanisms.

Mechanism	OH* submechanism	Rate coefficient of (R16)
GRI3.0-1999	—	—
SanDiego-2004	—	—
Tian-2009	—	—
Konnov-2009	—	—
POLIMI-2014	—	—
GDFKin-2016	—	—
Zhang-2017	original	Kosarev et al. [101]
SanDiego-2018	—	—
Okafor-2018	—	—
Glarborg-2018	original	—
Shrestha-2019	original	—
POLIMI-2019	—	—
Han-2020	original	—
Wang-2020	original	Mulvihill et al. [27]
Konnov-2021	original	Mulvihill et al. [27]

Though the Tian-2009 model included the carbon atom species (C) and its reactions, the thermochemical data of it were not included in the THERMO file of the mechanism. Therefore, I took the thermochemical data of C from version 1.122 (created in 2016) of the thermochemical database of ATcT (Active Thermochemical Tables) [102-105] and used them in Tian-2009 to allow the simulations. These data are also included in the Glarborg-2018 model.

Among the mechanisms in Table 4, only Zhang-2017, Wang-2020, and Konnov-2021 contain the direct reaction of N₂O and H₂:



This reaction may be important in the combustion of gas mixtures that contain both N₂O and H₂ (Vandooren et al. [43], Dean et al. [46], Kopp et al. [47]). According to Mulvihill et al. [27], (R16) is important only if the H₂/N₂O mixture is not too dilute. Until 2018, only one direct measurement was carried out to determine the rate coefficient of this reaction. It was performed by Kosarev et al. [101] in a shock tube in 2007. Zhang et al. [77] used the rate coefficient determined by Kosarev et al. [101] in the Zhang-2017 model,

$$k_{16} = 2.1 \cdot 10^{14} \cdot \exp(-16356 \text{ K} / T) \text{ cm}^3 / \text{mol s}.$$

In 2018, however, Mulvihill et al. [27] performed new measurements, and they proposed a new rate coefficient for (R16) based on H₂O concentration–time measurements performed in a shock tube using a dilute H₂/N₂O/Ar gas mixture. Their rate coefficient was 30 times smaller,

$$k_{16}^{\text{mod}} = 7.0 \cdot 10^{12} \cdot \exp(-16356 \text{ K} / T) \text{ cm}^3 / \text{mol s}$$

than that of Kosarev et al [101].

Mulvihill et al. [27] suggested that their rate coefficient (k_{16}^{mod}) should be used in future mechanisms if (R16) is included in the model, instead of that by Kosarev et al. [101]. Kovács et al. [106] and Szanthoffer et al. [107] also showed that the rate coefficient measurements of Mulvihill et al. [27] are probably more accurate. Therefore, in Zhang-2017, the original rate parameters of (R16) were replaced by the parameters of Mulvihill et al [27]. The model obtained this way is called “Zhang-2017_mod” from now on. In the Wang-2020 and Konnov-2021 models, k_{16}^{mod} was used as the rate coefficient of (R16), so in that case, no modification was needed.

Finally, it is worth noting that although the investigated mechanisms were published in CHEMKIN format, some of them contained some syntactical errors (e. g., whitespace in wrong place, etc.). In these cases, I had to modify the text files so that *Optima++* could interpret them. In this work, I made good use of the text editor *Notepad++*.

4.4. The quantitative comparison of reaction mechanisms

In Section 3.1, it was mentioned that the goodness of a mechanism can be characterized by how accurately it can reproduce the results of indirect experimental measurements. In the case of a large number of indirect experimental data and the comparison of many reaction mechanisms, it can be beneficial to use a quantitative method for the comparison. In this section, a method for this purpose is introduced, which has been applied several times successfully in the Chemical Kinetics Laboratory of ELTE Eötvös Loránd University for different chemical systems [11, 30, 76, 106, 108-111]. At the moment, a new version of *Optima++* is being developed in the aforementioned research group which has a graphical user interface and is capable of performing the quantitative comparison of reaction mechanisms. I actively participated in the development of the mechanism comparison part of the program by testing it and suggesting improvements to make it more flexible and

user-friendly. All performance comparisons were carried out by this development version of *Optima++*.

4.4.1. The error function

Let us assume that we have collected N indirect experimental datasets from the literature based on which we would like to evaluate the agreement between the mechanism and the experimental data. These datasets are stored in N_{XML} experimental data files. $N \geq N_{\text{XML}}$ always, because one XML file may contain more than one dataset; for example, the concentrations of several species can be measured during a flow reactor experiment. Let the i -th dataset consist of N_i data points and let P_i denote the number of datasets in the XML to which the i -th dataset belongs. The agreement between the simulation results and the experimental data is described by the following average *error function*:

$$E = \frac{1}{N_{\text{XML}}} \sum_{i=1}^N \frac{1}{N_i} \cdot \frac{1}{P_i} \sum_{j=1}^{N_i} \left(\frac{Y_{ij}^{\text{sim}} - Y_{ij}^{\text{exp}}}{\sigma(Y_{ij}^{\text{exp}})} \right)^2 \quad (9)$$

where

$$Y_{ij} = \begin{cases} y_{ij}, & \text{if } \sigma(y_{ij}^{\text{exp}}) \approx \text{constant} \\ \ln y_{ij}, & \text{if } \sigma(\ln(y_{ij}^{\text{exp}})) \approx \text{constant} \end{cases} \quad (10)$$

where y_{ij}^{exp} and $\sigma(y_{ij}^{\text{exp}})$ are the j -th data point in the i -th dataset and its standard deviation, respectively. The corresponding y_{ij}^{sim} value is obtained by performing a simulation of the indirect experiment with the reaction mechanism. If a measured (experimental) data point can be characterized by an absolute error (the magnitude of the error is independent of the magnitude of the y_{ij}^{exp} value), $Y_{ij} = y_{ij}$ is taken in equation (9). This is true for some species concentration measurements. If, on the other hand, y_{ij}^{exp} is characterized by a relative error (the absolute error is linearly proportional to y_{ij}^{exp}), $Y_{ij} = \ln y_{ij}$. This approach is applicable for ignition delay time and some species concentration measurements. Note, that the error function can be defined for each XML (E_{XML}), dataset (E_i), and data point (E_{ij}) as follows:

$$E_{\text{XML}} = \sum_{i \in \text{XML}} \frac{1}{N_i} \frac{1}{P_i} \sum_{j=1}^{N_i} \left(\frac{Y_{ij}^{\text{sim}} - Y_{ij}^{\text{exp}}}{\sigma(Y_{ij}^{\text{exp}})} \right)^2, \quad (11)$$

$$E_i = \frac{1}{N_i} \sum_{j=1}^{N_i} \left(\frac{Y_{ij}^{\text{sim}} - Y_{ij}^{\text{exp}}}{\sigma(Y_{ij}^{\text{exp}})} \right)^2, \quad (12)$$

$$E_{ij} = \left(\frac{Y_{ij}^{\text{sim}} - Y_{ij}^{\text{exp}}}{\sigma(Y_{ij}^{\text{exp}})} \right)^2. \quad (13)$$

Since the experimental data points are assumed to have a normal distribution, the E function follows a chi-square distribution, and because it is normalized by N_{XML} and $N_i \cdot P_i$, the expected value of E is one. If the value of E is unity ($E = 1$), it means that the mechanism can reproduce the experimental data as accurately as precisely the data can be measured experimentally (the precision is characterized by the standard deviation), on average. Since there is a square after the second summation in equation (9), a mechanism that describes the experimental data less accurately than that has $E > 1$. In principle, the value of E can be smaller than one, but in practice, it is never the case. The smaller the value of E , the better the performance of the mechanism. Note, that if the E value is not greater than 4 and 9, it means that the model can reproduce the experimental data on average within their $\pm 2\sigma$ and $\pm 3\sigma$ uncertainty limits, respectively.

The normalization by the standard deviation in equation (9) is necessary in order not to overweight the experimental data measured with large uncertainty. However, its inclusion in the formula raises some problems as well because the experimental uncertainty is very often not published appropriately in the literature. In these cases, the standard deviation must be estimated as discussed in the next section.

4.4.2. Estimating the standard deviation of the experimental data

Because we use equation (9) to compare the performance of the mechanisms, we need to know the standard deviation of the experimental data. These data are sometimes published together with the experimental results, but, unfortunately, this information is in many cases not complete or missing. Therefore, to be able to apply equation (9), we need to estimate the standard deviation of the experimental data.

For this purpose, I used the *Minimal Spline Fit* program of Tibor Nagy [112, 113]. On the webpage of the ReSpecTh database, Version January 5 (2020) of the program can be found. I have used an earlier version of the program that lacked some of the functionalities of the latest version. In this section, I describe the procedure of the estimation of the standard deviation (“noise”) of the experimental data using this program.

Let us assume that we have a dataset composed of (x_i, y_i) data points ($i = 1, \dots, N$). The program performs the least-squares fitting of polynomials with increasing order ($n = 0, 1, 2, \dots$) and that of Akima splines [114] with increasing number of control points ($n = 3, 4, 5, \dots$), also called *knots*. Akima splines are functions composed of cubic polynomials between the control points, and they are continuously differentiable at the control points. Though the fitting of polynomials is simple and fast, the application of splines has some advantages compared to it. In the case of higher-order polynomials, the fitted curve often shows unnatural oscillation, which can be eliminated by using splines. Besides that, more precise fits can be achieved by splines than polynomials.

The program also computes the standard deviation (noise) of the dataset based on the fitted curves. Using goodness-of-fit measures provided by the program and visual inspection of the fitted curves, we can identify the curve that describes the trend of the experimental dataset (the “noise-free” data) the best. We can estimate the statistical standard deviation of the data points in the dataset by the standard deviation corresponding to this optimal fit.

The fitting is performed by minimizing the root-mean-square deviation ($RMSD_{\text{fit}}$) of the fitting function ($y_{\text{fit}}(x)$) from the input data (y_i):

$$RMSD_{\text{fit}} = \sqrt{\frac{1}{N} \sum_{i=1}^N [y_{\text{fit}}(x_i; \mathbf{p}) - y_i(x_i)]^2}, \quad (14)$$

where \mathbf{p} is the parameter set to be optimized. In the case of a polynomial of degree n , the parameter set is the $n + 1$ coefficients, $\mathbf{p} = \{a_0, \dots, a_n\}$, while in the case of a spline with n control points, the positions of the control points ($X_1, \dots, X_n, Y_1, \dots, Y_n$) are optimized, $\mathbf{p} = \{\mathbf{X}, \mathbf{Y}\} = \{X_1 \equiv x_1, \dots, X_n \equiv x_N, Y_1, \dots, Y_n\}$. As can be seen, in the latter case, the first and the last control points are fixed at x_1 and x_N , respectively. Therefore, the number of parameters of the fitting function, p , is $p = n + 1$ in the case of polynomials, while it is $p = 2n - 2$ in the case of splines. The number of degrees of freedom, ν , is

$$\nu = N - p. \quad (15)$$

The $RMSD_{\text{fit}}$ quantity is not the appropriate metric for estimating the standard deviation of the dataset because it does not take into account the number of degrees of freedom of the fit. For this purpose, the standard deviation of the fit (σ_{fit}) can be used:

$$\sigma_{\text{fit}} = \sqrt{\frac{N}{\nu}} RMSD_{\text{fit}}. \quad (16)$$

The program also helps to decide which model describes the experimental data the best by providing the so-called *Akaike information criterion* values (AIC) [115]:

$$AIC = 2p + N + N \cdot \ln \left(\frac{2\pi \cdot RMSD_{\text{fit}}^2}{N} \right), \quad (17)$$

which penalizes underfitting as well as overfitting. The lower the AIC value, the better the model. However, when the number of data points is small ($N \lesssim 2p^2$), the corrected AIC value ($AICc$) gives a better metric for the goodness-of-fit [116-118]:

$$AICc = AIC + \frac{2p(p+1)}{N-p-1}. \quad (18)$$

When $N \gg 2p^2$, the $AICc$ value converges to AIC .

Equation (14) can be used to estimate the $RMSD_{\text{fit}}$ if we assume that the experimental data follow Gaussian (normal) distribution. In this case, the measured data can be characterized by an absolute error and σ_{fit} gives this absolute estimated standard deviation according to equation (16). However, as it was mentioned in Section 4.4.1, in some cases, the data can be characterized by a relative error. If the relative error is small, $y_{\text{fit}}(x_i; \mathbf{p}) / y_i(x_i) \approx 1$, this is approximately equivalent to saying that the original data follow lognormal distribution. In this case, the $\{y_i\}$ data are transformed to $\ln\{y_i\}$, and the $RMSD_{\text{fit}}$ is calculated on the transformed data as follows (cf. equation (14)):

$$RMSD_{\text{fit}} = \sqrt{\frac{1}{N} \sum_{i=1}^N [\ln(y_{\text{fit}}(x_i; \mathbf{p})) - \ln(y_i(x_i))]^2}. \quad (19)$$

The σ_{fit} value calculated according to equation (16) corresponds to the estimated standard deviation of the transformed data which we assume to follow Gaussian (normal) distribution, and it estimates the relative error of the dataset, as long as the relative error is not too large, which we assume in all cases. Note, that if equation (19) is applied for the estimation of $RMSD_{\text{fit}}$, then the zero concentration values must be excluded from the dataset for the fitting.

Note, that the program also allows us to transform the $\{x_i\}$ values to estimate the standard deviation of the dataset. This was applied in the case of ignition delay time measurements, where the $\log \tau$ data are usually plotted against the inverse temperature (T^{-1}) [13, 27, 47, 77, 119-121].

It is important to note, that even though the $AICc$ values and the calculated relative probabilities facilitate choosing the optimal model, in some cases, the predicted optimal model seems incorrect based on the visual inspection of the dataset and the fitted curve. Therefore, the *Minimal Spline Fit* program also prepares plots of the experimental data and the fitted curves with the help of *Gnuplot*. For this reason, the visual inspection of the data and the fitted curves is always recommended.

An example for the estimation of the standard deviation of a dataset can be seen in Figure 8 and the corresponding statistics are summarized in Table 5. It is a species concentration measurement in a burner stabilized flame performed by Vandooren et al. [43]. The example shows the CO mole fraction in the flame as a function of the distance from the burner measured by molecular beam mass spectrometry. In this case, we assume that the experimental data have a constant relative error (see in Section 4.4.3.2); therefore, the fitting is carried out on the transformed data (Figure 8, right). Three curves are shown in this figure, two Akima splines, and one polynomial. It can be seen from Table 5 that the Akima spline with 5 control points (red curve) predicts the smallest standard deviation (σ_{fit}), and its $AICc$ value is much lower than that of the Akima spline with 4 control points (blue curve). Still, the $n = 4$ Akima spline was chosen as the optimal model. Though the $n = 5$ spline describes the data rather accurately, it shows an unnatural behavior at around 0.5 cm distance from the burner: it changes convexity with a relatively sharp breaking point, which is not expected physically. The polynomial with 5 parameters is also shown in the figure (green curve). At small distances, it describes the data smoothly, but at larger distances when the CO concentration starts to stagnate, it shows unnatural wiggles, which is also not expected

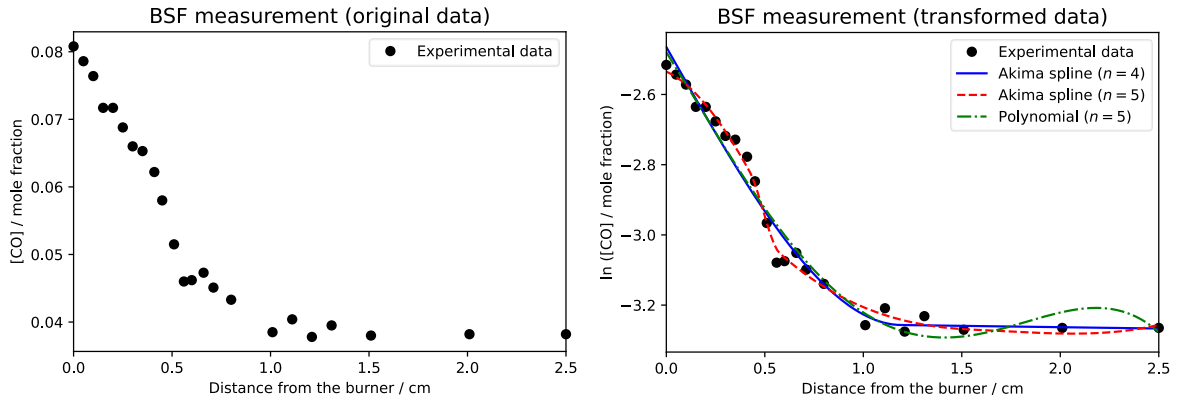


Figure 8. The estimation of the standard deviation of a concentration profile in a burner stabilized flame. Experimental data is from the work of Vandooren et al. [43]. In the figure to the left, the original data are seen, and in the figure to the right, the transformed data can be seen and some of the fitted functions. The Akima spline with $n = 4$ control points was chosen as the optimal model.

Table 5. Statistics of the fitted curves in Figure 8. The relative probability is only calculated for splines, and the spline with the lowest $AICc$ value is the reference whose relative probability is one.

Model	n	ν	$RMSD_{\text{fit}}$	σ_{fit}	AIC	$AICc$
Akima spline	4	17	0.0412	0.0479	-141.535	-136.285
Akima spline	5	15	0.0226	0.0280	-165.195	-154.909
Polynomial	5	18	0.0440	0.0500	-140.479	-136.950

physically, and which is typical behavior of polynomial functions. The physically most realistic model seems to be the Akima spline with $n = 4$. Even though it is less accurate than the spline with more control points, it can describe the experimental data smoothly both at small distances where the CO concentration decreases steeply and at larger distances where the CO concentration seems to reach a constant value, and the transition between the two behaviors is also smooth. Using this model function, the relative error of the dataset is 4.79%, as can be seen from Table 5, which is a realistic experimental error. I estimated the standard deviations of the other datasets following similar arguments as described above.

4.4.3. The standard deviation of different experimental data types

In the preceding section, the basic principles of the estimation of the standard deviation of the experimental data were discussed; however, the estimated standard deviation is sometimes unrealistically small. Therefore, for each measurement type, I applied a minimum standard deviation (σ_{\min}) based on previous experience. A standard deviation smaller than this threshold value cannot belong to any dataset of that measurement type.

In many cases, the experimental uncertainty (σ_{\exp}) of the measured data was also reported, and in this case, we should take into account both kinds of standard deviation when calculating the overall standard deviation (σ) used in equation (9). The general principle was as follows. The sum of squares of the experimental and the random standard deviations was taken, and the square root of this value was considered the standard deviation of the data:

$$\sigma = \sqrt{\sigma_{\text{fit}}^2 + \sigma_{\text{exp}}^2}. \quad (20)$$

If this σ was not smaller than σ_{\min} , then this value was accepted. If it was smaller than σ_{\min} , σ_{\min} was taken as σ . In the cases when no experimental error was provided, σ_{\min} replaced σ_{\exp} in equation (20):

$$\sigma = \sqrt{\sigma_{\text{fit}}^2 + \sigma_{\min}^2}, \quad (21)$$

which is inherently not smaller than σ_{\min} , so this value was always accepted.

In the next sections, I summarize the procedures that I applied in this study to calculate the standard deviation of different types of experimental data.

4.4.3.1. Ignition delay time measurements

In the investigated ST-IDT experiments, the experimental uncertainties were not provided. Based on previous experience [11, 13, 27, 30, 76, 108, 119-121], the data in an ignition delay time measurement dataset have a constant relative error; therefore, equation (19) was used to estimate the $RMSD_{fit}$. The standard deviation was estimated for each dataset. All the IDT measurements investigated here were performed at low pressure (< 20 atm), and in this case, the typical experimental uncertainty ($\pm 2\sigma$) is $\pm 10\%$. Therefore, the minimum standard deviation was $\sigma_{min} = 0.05$ (5%) in IDT measurement datasets. The overall standard deviations (σ) of the (transformed) ST-IDT measurement datasets are summarized in Table A2, together with the experimental details.

4.4.3.2. Species concentration measurements

As can be seen in Table 2, the concentrations of some species are measured in JSR, FR, and BSF experiments as functions of other quantities such as temperature, time, initial composition, residence time, or distance from the burner. In the case of JSR, FR experiments, and the BSF measurements of Dindi et al. [53], the measured species are H_2 , CO , CO_2 , O_2 , N_2 , NO , NO_2 , and N_2O . The concentrations of these species may be measured by various means, of which optical spectroscopy and gas chromatography (GC) were applied.

In these measurements, if the experimental uncertainty is published, it is very often given as: “The experimental uncertainty of species X is $\pm x\%$ but not less than y ppm” (see “relative error with absolute minimum limits” in Table 6. Therefore, I assumed constant relative error for the measured data points (I fitted polynomials and splines to the logarithm of the data), but for each data point, it was checked whether the absolute value of the standard deviation was smaller than a minimum absolute standard deviation. If it was smaller, then the minimum absolute standard deviation was assigned to that data point, and absolute error was chosen as the error type. To avoid using unrealistically small standard deviations, a minimum relative (σ_{min}^{rel}) and absolute (σ_{min}^{abs}) error were defined for each species (Table 7) based on previous experience from the literature.

Table 6. Reported experimental error types of the species concentration measurements in the case of the investigated experiments.

Ref.	Measured species	Measurement technique ^a	Error type
JSR			
Dagaut (2003) [34]	H ₂ , CO, CO ₂	GC (H ₂ , CO, CO ₂), FT-IR (CO, CO ₂)	no error is reported
Dagaut (2003) [33]	H ₂ , CO, CO ₂ , NO	GC (H ₂ , CO, CO ₂), FT-IR (CO, CO ₂ , NO)	no error is reported
FR			
Hulgaard (1993) [48]	NO, N ₂ O	UV spectroscopy (NO), IR spectroscopy (N ₂ O)	relative error with absolute minimum limits
Roesler (1995) [49]	CO	IR spectroscopy	no error is reported
Glarborg (1995) [50]	CO, CO ₂ , NO, NO ₂	UV and IR spectroscopy	relative error with absolute minimum limits
Glarborg (1996) [39]	CO	UV and IR spectroscopy	relative error with absolute minimum limits
Alzueta (1997) [51]	CO, CO ₂ , NO	UV and IR spectroscopy	relative error with absolute minimum limits
Mueller (1999) [15]	CO, NO, NO ₂	IR spectroscopy (CO), FT-IR (NO, NO ₂)	relative error (with absolute minimum limits in the case of NO)
Glarborg (2000) [52]	CO, CO ₂ , NO	GC (CO, CO ₂), Spectroscopic methods (CO, CO ₂ , NO)	relative error with absolute minimum limits
Rasmussen (2008) [14]	CO, CO ₂ , NO, NO ₂ , O ₂	GC (CO, CO ₂ , O ₂), Chemiluminescence analyzer (NO, NO ₂)	relative error
BSF			
Dindi (1991) [53]	CO, N ₂ O, CO ₂ , NO, N ₂ , O ₂	GC	relative error
Vandooren (1997) [43]	N ₂ O, H, NO, CO, CO ₂ , O ₂ , N ₂ , H ₂ , H ₂ O, O, OH	MBMS	no error is reported

^a: GC = gas chromatography, FT-IR = Fourier Transform Infrared spectroscopy, UV = ultraviolet, IR = infrared, MBMS = molecular beam mass spectrometry

Table 7. The minimum overall relative and absolute errors defined for each species for concentration measurements.

Species	$\sigma_{\min}^{\text{rel}}$	$\sigma_{\min}^{\text{abs}} / \text{ppm}$
H ₂	0.025 (2.5%)	5
CO	0.025 (2.5%)	5
CO ₂	0.025 (2.5%)	5
O ₂	0.025 (2.5%)	5
N ₂	0.025 (2.5%)	5
NO	0.025 (2.5%)	5
NO ₂	0.025 (2.5%)	5
N ₂ O	0.05 (5%)	10

In the BSF measurements of Vandooren et al. [43], the species concentrations were measured by molecular beam mass spectrometry (MBMS) in the flame, and no experimental uncertainties were provided. A similar measurement series was carried out by Miller et al. [122] on a slightly different system, and the relative and absolute errors provided there were used as minimum values for the Vandooren et al. [43] measurements.

For each dataset, the relative error was estimated using *Minimal Spline Fit*, and the procedure described in Section 4.4.3 was performed using $\sigma_{\min}^{\text{rel}}$ the minimum value. Let us denote the resulting σ value by σ^{rel} . Then, for each data point, the absolute standard deviation was calculated as (concentration value $\cdot \sigma^{\text{rel}}$). If this value was not smaller than $\sigma_{\min}^{\text{abs}}$ of the respective species, then σ^{rel} was accepted and relative error was considered for that data point. If it was smaller than $\sigma_{\min}^{\text{abs}}$, then $\sigma_{\min}^{\text{abs}}$ was assigned to that data point and absolute error was considered. Consequently, in this type of measurement, data points within one dataset could have different error types (absolute or relative).

Note, that when the measured concentration of a species was zero, it was omitted from the relative error estimation, and $\sigma_{\min}^{\text{abs}}$ of the respective species was assigned to that data point as an absolute error. Note also, that in a few cases, it was not possible to fit an appropriate model function to the dataset, for instance, because the number of data points in the dataset was too small. In these cases, if the experimental error was provided, $\sigma_{\min}^{\text{rel}}$ was assigned to σ_{fit} , but if it was not provided, $\sigma_{\min}^{\text{rel}}$ was assigned to both as σ_{fit} and σ_{exp} , so σ was $\sqrt{2}\sigma_{\min}^{\text{rel}}$ in the latter cases.

Finally, another issue may occur when estimating the standard deviation of the logarithmically transformed concentration data, which was also discussed in the work of Kawka et al. [108]. It is not a good strategy to assign a relative error to concentration values that are relatively small within a dataset, because on the logarithmic scale, these data points would artificially be overweighted in the fitting process and bias the error function. Sometimes, if these points were included in the dataset in the model fitting process, no appropriate model function could be found, but when these points were excluded, the other points could be described well by a model function. Therefore, concentration values that were at least ten times smaller than the largest value were sometimes excluded from the fitting process. The σ_{rel} value – that was calculated based on the relative standard deviation estimated for all the other data points in the dataset – was assigned as a relative error to these points.

The overall standard deviations (σ) of the species concentration measurement datasets are summarized in Table A1 for the JSR measurements, Table A3 for the FR measurements, and Table A4 for the BSF measurements, together with the experimental details.

4.5. Local sensitivity analysis

As can be seen in Table 3, detailed chemical kinetic mechanisms are usually composed of several hundred or thousand reaction steps and thermodynamic and transport properties, which means that they contain a huge set of parameters. To develop an existing model further and to construct reduced reaction mechanisms that can be used for, for instance, computational fluid dynamics (CFD) calculations, we need to know which parameters of the model are important under various conditions. An input model parameter (for example, the preexponential factor of a rate coefficient) is considered important under a given circumstance if its change strongly influences the output of the mathematical model (for example, a computed laminar burning velocity, ignition delay time, or concentration). In other words, a parameter is *important* or *influential*, if a small alteration of its value results in a large change of the result computed with the model. To explore the importance of the model parameters under given conditions, one can apply the methods of *sensitivity analysis* [31], which can be divided into two groups: local and global sensitivity analysis methods. In my work, I only applied the local sensitivity analysis, therefore only that is discussed here.

In the case of local sensitivity analysis, we investigate how much the model prediction changes due to a small change of the value of a parameter close to its nominal value. Let us denote the i -th model result by Y_i and the j -th input model parameter by p_j . The partial derivative

$$s_{ij} \equiv \frac{\partial Y_i}{\partial p_j} \quad (22)$$

is called the first-order *local sensitivity coefficient*. The greater the absolute value of s_{ij} , the more influential the j -th model parameter on the i -th model result.

The local sensitivity coefficient calculated according to equation (22) has a dimension which is the dimension of the model result divided by that of the parameter. Therefore, it shows how much the model output changes in its own unit due to a unit change in the value of the parameter (in its own unit). Since both the model parameters and the model results may have various units, the $\{s_{ij}\}$ coefficients also have different units, which means that the s_{ij} values cannot be compared to each other. Therefore, to make the different sensitivity coefficients comparable to each other, we introduce the unitless *normalized local sensitivity coefficient*, defined as follows:

$$sn_{ij} \equiv \frac{p_j}{Y_i} \frac{\partial Y_i}{\partial p_j} = \frac{\partial \ln \tilde{Y}_i}{\partial \ln \tilde{p}_j}, \quad (23)$$

where \tilde{Y}_i and \tilde{p}_j are the dimensionless i -th model result and j -th parameter, respectively. Now, the values of the $\{sn_{ij}\}$ coefficients are independent of the units of the model results and parameters, and according to this definition, sn_{ij} gives the percentage that the i -th model output changes due to a 1% change in the value of the j -th parameter. Consequently, the normalized sensitivity coefficients are comparable to each other.

The local sensitivity coefficients can usually be determined numerically only, and many numerical methods exist to determine the sensitivity coefficients. The simplest method to obtain local sensitivity coefficients is the *brute force method* that applies the *finite difference approximation* as follows:

$$s_{ij} \approx \frac{Y'_i - Y_i}{p'_j - p_j} = \frac{\Delta Y_i}{\Delta p_j}, \quad (24)$$

where p'_j is the j -th parameter after its original value (p_j) was changed (perturbed) by Δp_j , and Y'_i is the i -th model result obtained with the perturbed value of p_j in the model. If we insert equation (24) in the definition of the normalized sensitivity coefficient (equation (23)), we get

$$sn_{ij} \approx \frac{p_j}{Y_i} \frac{\Delta Y_i}{\Delta p_j} = \frac{p_j}{Y_i} \cdot \frac{Y'_i - Y_i}{p'_j - p_j} = \frac{p_j}{p'_j - p_j} \cdot \frac{Y'_i - Y_i}{Y_i} = \frac{1}{\underbrace{\frac{p'_j - p_j}{p_j}}_{f_{\text{pert}}}} \cdot \frac{Y'_i - Y_i}{Y_i}, \quad (25)$$

where f_{pert} is called the *perturbation factor* which gives how much the j -th parameter was changed in percentage compared to its original value. I applied a constant perturbation factor to compute the local sensitivity coefficients of the kinetic parameters of the model.

Although the calculation of the sensitivity coefficients using the brute force method is simple, it may provide inaccurate coefficients. One reason for this is that equation (24) is only accurate if there is a linear relationship between the model result and the parameter, but in the case of reaction kinetic models, it is rarely the case. The linear approximation is approximately valid only if the perturbation of the parameter is small. However, if the perturbation is too small, Y'_i and Y_i may be very close to each other, and so the obtained sensitivity coefficient will have a large relative error because computers can only store numbers up to a limited number of decimal digits. Consequently, to obtain reliable and accurate sensitivity coefficients, the parameter perturbation should be neither too large nor too

small. In the case of kinetic parameters, I applied $f_{\text{pert}} = 0.05$ which corresponds to a 5% increase of the rate parameters, which is usually sufficient.

Even though the normalized sensitivity coefficients are dimensionless, their direct comparison is difficult in the case of a large number of data points because their scaling is different. Therefore, to facilitate the evaluation of the results of the sensitivity analysis, let us rescale the normalized sensitivity coefficients and define the *scaled normalized local sensitivity coefficient* (\tilde{sn}_{ij}) as follows:

$$\tilde{sn}_{ij} = \frac{sn_{ij}}{\max_j \{|sn_{ij}|\}} \quad (26)$$

which means that we compute the sn_{ij} coefficients for a given data point (Y_i) for all parameters ($\{p_j\}$), and we divide each sn_{ij} by the one whose absolute value is maximal for that data point. Therefore, the resulting \tilde{sn}_{ij} values will be scaled into the $[-1,1]$ interval. This way, we can say, for example, that parameter j is important for data point i if

$$|\tilde{sn}_{ij}| \geq 0.1 \quad (27)$$

for that data point, and this criterion can be applied for each simulation result.

4.5.1. Sensitivity analysis of thermodynamic properties

Kovács et al. [123] performed local sensitivity analysis on the thermodynamic parameters (see Section 3.3.1.1) of reaction mechanisms. Similar studies have been done by Turányi et al. [124], Zádor et al. [125], and Langer et al. [126] previously. The method of Kovács et al. [123] was used in this study for the sensitivity analysis of the thermodynamic parameters. As discussed in Section 3.3.1.1, the temperature dependence of the thermodynamic properties of the species is described by NASA polynomials (equations (3)–(5)). For the better readability of the text, these equations are repeated here for species k :

$$\frac{c_{p,k}^{\ominus}}{R}(T) = a_{1,k} + a_{2,k} T + a_{3,k} T^2 + a_{4,k} T^3 + a_{5,k} T^4, \quad (28)$$

$$\frac{H_k^{\ominus}}{RT}(T) = a_{1,k} + \frac{a_{2,k}}{2} T + \frac{a_{3,k}}{3} T^2 + \frac{a_{4,k}}{4} T^3 + \frac{a_{5,k}}{5} T^4 + \frac{a_{6,k}}{T}, \quad (29)$$

$$\frac{S_k^{\ominus}}{R}(T) = a_{1,k} \ln T + a_{2,k} T + \frac{a_{3,k}}{2} T^2 + \frac{a_{4,k}}{3} T^3 + \frac{a_{5,k}}{4} T^4 + a_{7,k}. \quad (30)$$

We are interested in how much the three thermodynamic parameters, $c_{p,k}^{\ominus}$, H_k^{\ominus} , and S_k^{\ominus} , influence the model outputs; therefore, the following perturbations were applied separately:

- To investigate the effect of $c_{p,k}^{\ominus}$: only $a_{1,k}$ was perturbed by an absolute value of +0.01, which is equivalent to a constant +0.08314 J / (mol K) shift of the $c_{p,k}^{\ominus}$, independent of temperature. Note, that the perturbation of $a_{1,k}$ influences the values of H_k^{\ominus} and S_k^{\ominus} as well, and this perturbation depends on temperature.
- To investigate the effect of H_k^{\ominus} : only $a_{6,k}$ was perturbed by an absolute value of +3 K, which resulted in a constant +0.01 change in $a_{6,k} / T$ at 300 K. This caused a +24.79 J / mol shift of H_k^{\ominus} , independent of temperature.
- To investigate the effect of S_k^{\ominus} : only $a_{7,k}$ was perturbed by an absolute value of +0.01; thus, the S_k^{\ominus} values were shifted by a constant +0.08314 J / (mol K), independent of temperature.

Since absolute perturbations were applied in the case of thermodynamic parameters, it is more meaningful to write equation (25) in a slightly different manner because the perturbation factor is not characteristic in this case. The sensitivity coefficients were calculated for the thermodynamic quantities at $T_0 = 300$ K. For species molar heat capacity and molar enthalpy parameters ($a_{1,k}$ and $a_{7,k}$) at 300 K, and, the following formula was used:

$$sn_{ij} = \frac{q_j}{R} \cdot \frac{1}{Y_i} \cdot s_{ij} = \frac{q_j}{R} \cdot \frac{1}{Y_i} \cdot \frac{Y'_i - Y_i}{d}, \quad (31)$$

where q_j is the original value of the thermodynamic quantity, ($c_{p,k}^{\ominus}(300 \text{ K})$ and $S_k^{\ominus}(300 \text{ K})$, respectively, calculated according to the corresponding original NASA polynomials), and $d = +0.01$ in both cases. Note, that $T_0 = 300$ K was chosen arbitrarily as the temperature of the investigations; any other temperature (within the range of validity of the NASA coefficients) could have been chosen. In equation (32), the d value characterizes the perturbation, unlike in equation (25), in which f_{pert} plays this role. Then, the scaled normalized (\tilde{sn}_{ij}) sensitivity coefficients were computed according to equation (26).

In the case of the species enthalpies ($a_{6,k}$) at 300 K, the full normalization of the sensitivity coefficients cannot be utilized because the various species may have enthalpies of different signs and orders of magnitude, which would result in biased results. Consequently, in this case, the so-called *semi-normalized sensitivity coefficients* (ssn_{ij}) were calculated as follows:

$$ssn_{ij} = \frac{1}{R} \cdot \frac{1}{Y_i} \cdot s_{ij} = \frac{1}{R} \cdot \frac{1}{Y_i} \cdot \frac{Y'_i - Y_i}{d}, \quad (32)$$

where $d = +3$ K. Hence, the semi-normalized sensitivity coefficients have a unit of ($\text{J}^{-1} \text{ mol}$). The *scaled semi-normalized sensitivity coefficients* (\widetilde{ssn}_{ij}) were computed in a similar way to equation (26):

$$\widetilde{ssn}_{ij} = \frac{ssn_{ij}}{\max_j \{|\widetilde{ssn}_{ij}|\}}. \quad (33)$$

In this case, criterion (27) was adapted as follows:

$$|\widetilde{ssn}_{ij}| \geq 0.1 \quad (34)$$

5. Results and discussion

5.1. The comparison of syngas/NO_x combustion mechanisms

The simulations were carried out with *OpenSMOKE++*. All simulations were successful, so no data point needed to be omitted for this reason. The reactor models and the corresponding settings used in the simulations with *OpenSMOKE++* are shown in Table 8.

Table 8. The reactor models applied in the simulations using *OpenSMOKE++*.







Experiment type	Solver	Reactor settings
JSR	Perfectly-Stirred-Reactor	isotherm–isobar
ST-IDT	Batch-Reactor	adiabatic–isochor
FR ($c-t$)	Batch-Reactor	adiabatic–isobar
FR (c_{out})	Plug-Flow-Reactor	isotherm–isobar
BSF	PremixedLaminarFlame1D	Gradient = 0.015, Curvature = 0.15

The comparison of the performance of the mechanisms was based on the following principle: *the mechanisms are compared based on the same set of data points*. It was not possible, however, to use all data points for the comparison, because some points had very large (several thousand or ten thousand) E_{ij} values for some mechanisms, which resulted in artificially high overall E values for the models. A very high E_{ij} value can have several reasons, for example, an important missing reaction path in the mechanism, or a wrong standard deviation assignment that does not consider the large systematic error of the measurement. From our investigations, it does not turn out which one of these explanations is the real reason, but we need to exclude these data points from the calculations to make the comparison unbiased. For this, I applied a two-step filtering process for the data points.

I chose four mechanisms as references: Zhang-2017_mod, Glarborg-2018, Shrestha-2019, Wang-2020. The first three can be considered reliable based on the comparative work of Kovács et al. [106] (H₂/O₂/NO_x systems) and that of Kawka et al. [108] (NH₃ oxidation and pyrolysis), so it is relatively unlikely that an important reaction pathway is missing from these mechanisms. Wang-2020 is an update of Zhang-2017_mod, so it should be at least as reliable as Zhang-2017_mod. When the E_{ij} value of a data point was higher than 100 for *each of the four reference mechanisms*, the point was omitted from the calculations.

After the first filtration step, however, some data points with very high E_{ij} values (several thousand) for one or a few mechanisms remained in the set of data points. These experimental data are probably not erroneous because at least one of the three reference mechanisms reproduced them well, but their inclusion in the investigations biases the overall E value of the mechanisms significantly towards large E values. Therefore, in the second filtration step, every data point was excluded from the calculations for which the E_{ij} value of *any of the investigated mechanisms* was greater than 1000. The number of data points with $E_{ij} > 1000$ in the second filtration step for each mechanism is also indicative of the reliability of the respective model, so besides the E values themselves, these numbers can also be used for comparison.

The performance of the mechanisms is compared for each experiment type, and then, their overall performance is discussed. The E values are summarized in tables in each case. To facilitate the visual interpretation of the tables, the following color codes are used for the different E values in the tables:

	$E < 9$
	$9 \leq E < 16$
	$16 \leq E < 25$
	$25 \leq E < 36$
	$36 \leq E < 49$
	$49 \leq E < 64$
	$64 \leq E < 81$
	$81 \leq E < 100$
	$100 \leq E$

5.1.1. Jet stirred reactor simulations

In the JSR measurements, 19 data points needed to be excluded in the first filtration step (10% of all data points), and further two data points (1%) were omitted in the second step, which means that the simulation results do not deviate very much from the experimental data, overall. As seen in Table 9, several models have an E_{JSR} value around 15–18. These models did not have a data point with an E_{ij} value of more than 1000 in the second filtration step. The results suggest that changing the preexponential factor of (R16) in Zhang-2017 does not affect the predictions of the JSR experiments. The E_i values by datasets are summarized in Table A5 for each mechanism.

Table 9. The overall error function values for JSR measurements (E_{JSR}) and the number of data points with a very high E_{ij} value ($E_{ij} > 1000$) for each mechanism. The percentages for the points omitted in step 2 are calculated as compared to the number of points included after step 1. The simulations were performed using *OpenSMOKE++*.

Mechanism	E_{JSR}	$E_{ij} > 1000$ (Step 2)
GRI3.0-1999	34.15	2 (1.2%)
SanDiego-2004	21.80	2 (1.2%)
Tian-2009	16.80	0 (0.0%)
Konnov-2009	46.18	1 (0.6%)
POLIMI-2014	23.62	0 (0.0%)
GDFKin-2016	17.34	0 (0.0%)
Zhang-2017	19.34	0 (0.0%)
Zhang-2017_mod	19.34	0 (0.0%)
SanDiego-2018	24.10	1 (0.6%)
Okafor-2018	28.33	2 (1.2%)
Glarborg-2018	17.03	0 (0.0%)
Shrestha 2019	16.49	0 (0.0%)
POLIMI-2019	15.43	0 (0.0%)
Han-2020	25.54	0 (0.0%)
Wang-2020	16.22	0 (0.0%)
Konnov-2021	33.59	1 (0.6%)

Total number of XMLs: **5**
Total number of datasets: **17**
Total number of data points: **183**
Included data points: **162**
Points omitted in step 1: **19 (10.4%)**
Points omitted in step 2: **2 (1.2%)**

5.1.2. Shock tube simulations

In the case of shock tube simulations, no data point needed to be omitted in either the first or the second filtration step, so these experimental data can be considered reliable, and none of the mechanisms performed very poorly on this kind of experiment. The E values and the number of omitted points can be seen in Table 10. The Zhang-2017, Zhang-2017_mod, and the Wang-2020 models have the best performance for this experiment type with $E_{\text{ST-IDT}} = 6.24$ and 6.11, respectively, which means that they can reproduce the experimental data within their $\pm 3\sigma$ uncertainty limits, on average. Besides that, the Konnov-2021 model also provides relatively good results with an $E_{\text{ST-IDT}}$ value of 22.28. The E_i values by datasets are summarized in Table A6 for each mechanism.

Table 10. The overall error function values for ST-IDT measurements ($E_{\text{ST-IDT}}$) and the number of data points with a very high E_{ij} value ($E_{ij} > 1000$) for each mechanism. The percentages for the points omitted in step 2 are calculated as compared to the number of points included after step 1. The simulations were carried out using *OpenSMOKE++*.

Mechanism	$E_{\text{ST-IDT}}$	$E_{ij} > 1000$ (Step 2)	
GRI3.0-1999	45.60	0 (0%)	
SanDiego-2004	55.33	0 (0%)	
Tian-2009	35.16	0 (0%)	
Konnov-2009	61.97	0 (0%)	Total number of XMLs: 6
POLIMI-2014	41.27	0 (0%)	Total number of datasets: 6
GDFKin-2016	40.42	0 (0%)	Total number of data points: 80
Zhang-2017	6.43	0 (0%)	
Zhang-2017_mod	6.24	0 (0%)	Included data points: 80
SanDiego-2018	57.75	0 (0%)	Points omitted in step 1: 0 (0%)
Okafor-2018	40.32	0 (0%)	
Glarborg-2018	37.98	0 (0%)	Points omitted in step 2: 0 (0%)
Shrestha-2019	47.15	0 (0%)	
POLIMI-2019	41.07	0 (0%)	
Han-2020	37.80	0 (0%)	
Wang-2020	6.20	0 (0%)	
Konnov-2021	22.28	0 (0%)	

5.1.3. Flow reactor simulations

Approximately 10% of the FR data points needed to be excluded in the first filtration step, and 8% of the remaining points in the second step. After all these exclusions, ca. 81% of the data points were included in the comparison. Table 11 shows the average error function values for the FR measurements. Four mechanisms, Zhang-2017, Zhang-2017_mod, POLIMI-2019, and Wang-2020 have an E_{FR} value of less than 9 – they are the best-performing models for this kind of experimental data, with Wang-2020 being the best. These models have only a few data points excluded in the second step as well. The E_i values by datasets are summarized in Table A7 for each mechanism.

Table 11. The overall error function values for FR measurements (E_{FR}) and the number of data points with a very high E_{ij} value ($E_{ij} > 1000$) for each mechanism. The percentages for the points omitted in step 2 are calculated as compared to the number of points included after step 1. All simulations were carried out by *OpenSMOKE++*.

Mechanism	E_{FR}	$E_{ij} > 1000$ (Step 2)	
GRI3.0-1999	43.59	36 (3.3%)	
SanDiego-2004	50.52	63 (5.8%)	
Tian-2009	25.79	10 (0.9%)	Total number of XMLs: 46
Konnov-2009	38.70	34 (3.1%)	Total number of datasets: 93
POLIMI-2014	13.79	4 (0.4%)	Total number of data points: 1210
GDFKin-2016	27.65	6 (0.5%)	Included data points: 1006
Zhang-2017	7.50	1 (0.1%)	Points omitted in step 1: 117 (9.7%)
Zhang-2017_mod	7.50	1 (0.1%)	Points omitted in step 2: 87 (8.0%)
SanDiego-2018	47.91	58 (5.3%)	
Okafor-2018	34.62	42 (3.8%)	
Glarborg-2018	16.97	2 (0.2%)	
Shrestha-2019	25.21	7 (0.6%)	
POLIMI-2019	8.63	8 (0.7%)	
Han-2020	25.07	3 (0.3%)	
Wang-2020	5.97	7 (0.6%)	
Konnov-2021	43.07	34 (3.1%)	

5.1.4. Burner stabilized flame simulations

In the case of the flow reactor measurements, approximately 9% of the data points were excluded in the first filtration step; however, in the second filtration step, almost 20% of the points needed to be omitted. As can be seen in Table 12, there is a great difference between the number of points having an E_{ij} value of more than 1000 for the various mechanisms. The two worst-performing models were the SanDiego-2004 and SanDiego-2018 mechanisms: they had an E_{ij} value of more than 1000 for ca. 15% of the data points. In addition, GRI3.0-1999, POLIMI-2014, Okafor-2018, Han-2020 also had much more $E_{ij} > 1000$ results after the first filtration step than other mechanisms. It is worth noting that none of the mechanisms have an E_{BSF} value of less than 30, which shows that there is a large deviation between the experimental and simulation results of BSF experiments. The E_i values by datasets are summarized in Table A8 for each mechanism.

Table 12. The overall error function values for BSF measurements (E_{BSF}) and the number of data points with a very high E_{ij} value ($E_{ij} > 1000$) for each mechanism. The percentages for the points omitted in step 2 are calculated as compared to the number of points included after step 1.

Mechanism	E_{BSF}	$E_{ij} > 1000$ (Step 2)	
GRI3.0-1999	72.80	31 (9.4%)	
SanDiego-2004	207.62	50 (15.2%)	
Tian-2009	33.00	2 (0.6%)	Total number of XMLs: 4
Konnov-2009	32.84	1 (0.3%)	Total number of datasets: 29
POLIMI-2014	71.01	31 (9.4%)	Total number of data points: 361
GDFKin-2016	40.83	2 (0.6%)	Included data points: 266
Zhang-2017	35.91	6 (1.8%)	Points omitted in step 1: 31 (8.6%)
Zhang-2017_mod	35.91	6 (1.8%)	Points omitted in step 2: 64 (19.4%)
SanDiego-2018	216.59	50 (15.2%)	
Okafor-2018	65.61	31 (9.4%)	
Glarborg-2018	34.98	2 (0.6%)	
Shrestha-2019	30.28	0 (0.0%)	
POLIMI-2019	33.31	2 (0.6%)	
Han-2020	139.79	21 (6.4%)	
Wang-2020	35.91	6 (1.8%)	
Konnov-2021	30.19	1 (0.3%)	

5.2. The comparison of the results with *FlameMaster* and *OpenSMOKE++*

FlameMaster and *OpenSMOKE++* are combustion simulation packages that solve the kinetic system of differential equations numerically, and they use the same subroutine (CVODE [127]) to solve the initial value problem. To consider the simulation results reliable and reproducible, it is expected that the two solvers provide almost identical results for the same experiment (small deviations are allowed due to the numerical integration, especially in the case of 1D computations). To explore this, I chose four mechanisms, the Zhang-2017_mod, Glarborg-2018, Shrestha-2019, and POLIMI-2019 models (the last one was also found to be relatively reliable in Section 5.1). I performed the same simulations with both solver packages, and the average error function values were calculated for both cases (Table 13). Note, that the E_{BSF_OS} values of Glarborg-2018 and Shrestha-2019 differ from those in Section 5.1 because several data points could not be simulated by FM; therefore, these points had to be excluded from this comparison. Also, in the case of FR experiments, adiabatic reactor settings were used for the simulations because the isotherm settings are not applicable in the case of *FlameMaster*. Hence, the overall error function values obtained with OS in this section differ from those in Section 5.1. This is also true for the number of included data points. Table 14 summarizes the results of the pointwise comparison of the simulation results obtained by the two solvers for the four reference mechanisms. It shows the percentage of the data points for which the two kinds of simulation results deviated significantly (“suspicious points”). I refer to the caption of Table 14 to the definition of suspicious points.

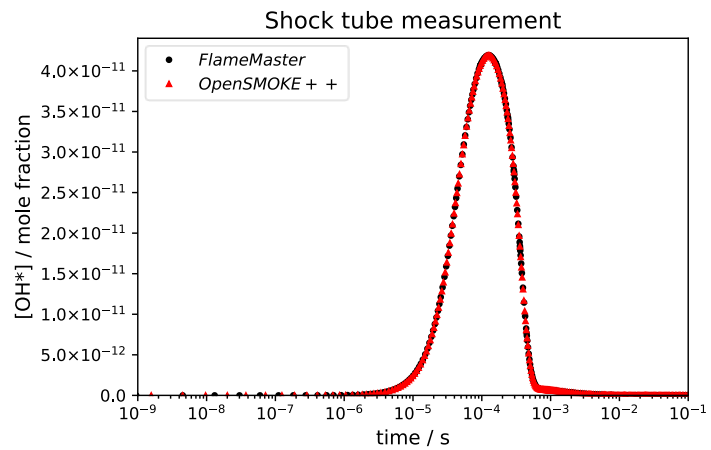


Figure 9. Comparison of the computed OH* (excited OH) profiles by *FlameMaster* and *OpenSMOKE++* during a ST-IDT experiment using the Zhang-2017_mod mechanism. Initial gas composition (in mole fractions): 0.03 CO, 0.0005 H₂, 0.01 N₂O, 0.9595 Ar; temperature and pressure behind the reflected shock wave: 1838 K, 1.4 atm. These conditions refer to point 12 of x10401000.xml (see Table A2).

Table 13. Error function values of four selected mechanisms calculated by the *FlameMaster* and *OpenSMOKE++* solvers, respectively. Δ was calculated as $(E_{OS} - E_{FM}) / \text{average}(E_{OS}; E_{FM})$.

	Zhang-2017_mod	Glarborg-2018	Shrestha-2019	POLIMI-2019
<i>E</i> _{JSR} : 162 data points ✓				
FM	19.34	17.03	16.49	15.43
OS	19.34	17.03	16.49	15.43
$\Delta\%$	0.0%	0.0%	0.0%	0.0%
<i>E</i> _{ST-IDT} : 80 data points ✓				
FM	6.16	37.95	46.77	41.07
OS	6.24	37.98	47.16	41.19
$\Delta\%$	+1.3%	+0.1%	+0.8%	-0.3%
<i>E</i> _{FR} : 1049 data points ^a ✓				
FM	26.63	39.14	65.05	19.08
OS	26.60	39.02	64.91	18.93
$\Delta\%$	-0.1%	-0.3%	-0.2%	-0.8%
<i>E</i> _{BSF} : 266/106 data points ^b ✗				
FM	32.90	36.66	23.94	34.41
OS	35.91	38.45	21.48	33.31
$\Delta\%$	+8.8%	+4.8%	-10.8%	-3.2%

^a: Different reactor settings were applied as in Section 5.1; therefore, the number of included points is also different.

^b: In the case of Glarborg-2018 and Shrestha-2019, not all BSF simulations could be performed by FM; therefore, only 107 data points were included in the comparison in those cases.

Table 14. The pointwise comparison of the simulation results of *FlameMaster* and *OpenSMOKE++*. A data point was considered suspicious if the relative deviation between the simulation results obtained by the two solvers was more than 1% and the absolute deviation was more than 10 ppm in the case of the zero-dimensional concentration measurements (JSR, FR) and more than 3 μ s in the case of the ST-IDT measurements. These limits were 5% and 20 ppm for the BSF experiments (one-dimensional simulations).

	Zhang-2017_mod	Glarborg-2018	Shrestha-2019	POLIMI-2019
JSR				
Investigated points:	183	183	183	183
Suspicious points:	0 (0%) ✓	0 (0%) ✓	0 (0%) ✓	0 (0%) ✓
ST-IDT				
Investigated points:	80	80	80	80
Suspicious points:	0 (0%) ✓	0 (0%) ✓	0 (0%) ✓	0 (0%) ✓
FR				
Investigated points:	1210	1210	1210	1210
Suspicious points:	0 (0%) ✓	0 (0%) ✓	0 (0%) ✓	2 (0.2%) ✓
BSF				
Investigated points:	361	186	186	361
Suspicious points:	175 (48%) ✗	79 (43%) ✗	58 (31%) ✗	209 (58%) ✗

As can be seen in Table 13 and Table 14, the results of the JSR, ST-IDT, and FR computations agree excellently; therefore, these simulation data can be considered reliable. In Section 5.1.2, the results of OS were used for the mechanism comparison because the simulations with OS are faster than with FM, in general. To demonstrate the excellent agreement between the solutions of the two solvers, the computed OH* concentration profiles during an ST-IDT experiment are plotted together in Figure 9. The ignition delay time was determined based on the OH* concentration profile in this experiment.

In the case of BSF measurements, the deviation between the simulation results of the two solvers is much more significant than in the previous cases (Table 13 and Table 14). This is not surprising because in the case of one-dimensional simulations, a greater numerical error can be expected, although a maximum of ca. 5% deviation would be satisfactory. It can also be seen that in some cases, FM provides somewhat lower average E values (Zhang-2017_mod, Glarborg-2018), but in other cases, the OS better reproduces the experimental data, on average (Shrestha-2019, POLIMI-2019). However, as shown in Table 14, a very large fraction of the data points can be considered “suspicious” (30–60%). It means, for example, that even though the E_{BSF} values of POLIMI-2019 differ only by 0.3%, it is because the pointwise large deviations between the simulation results to either direction compensate each other, which results in the very similar average E_{BSF} values. Note, that there are several suspicious points in all XMLs for each mechanism, so these points do not belong to only one or a few experiments. In Section 5.1.4, the results of OS were used because in that case, all simulations were successful, whereas FM failed to simulate at least one experiment for several mechanisms. This way, no data point needed to be omitted due to failed simulations.

Figure 10 shows the profiles of some physical–chemical properties computed in a burner stabilized flame by the two solvers. The experimental temperature values are usually published for BSF measurements at certain distances from the burner plate, and this information is stored in the XML file. The solvers use this experimental temperature profile for the computations, and they calculate the temperature values between the distances where they were experimentally measured by linear interpolation. Therefore, the computed temperature profiles of the two solvers agree well (top left graph). However, as shown for CO and OH, the computed concentration profiles do not coincide satisfactorily. One possible reason for the disagreement is the fact that even though the number of grid points is approximately equal in the two cases, the two solvers distribute the grid points in different ways along the distance axis (see Figure 10), which may cause deviations in the simulation

results. It can be concluded that the BSF simulation results obtained with either or both of the utilized solvers may not be reliable; therefore, mechanism comparison and development should not be based on these experimental data.

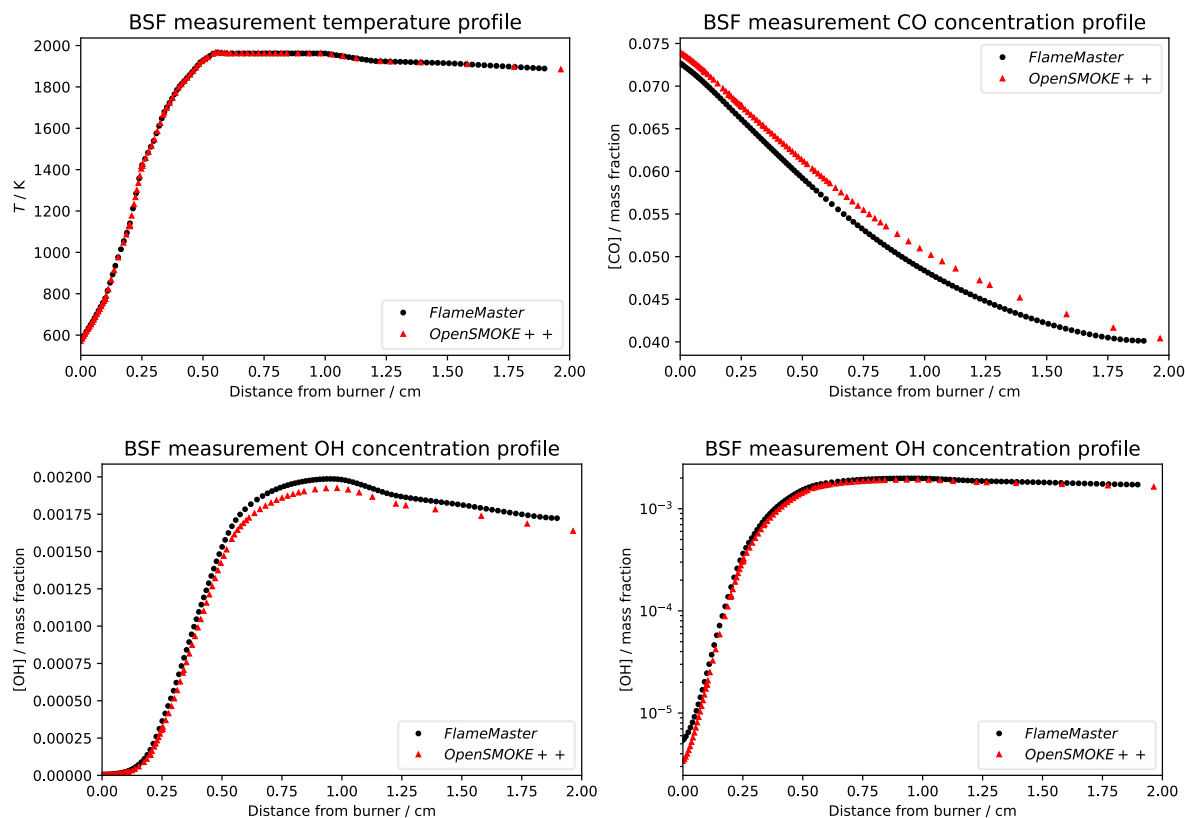


Figure 10. Comparison of the computed temperature and some concentration profiles by *FlameMaster* and *OpenSMOKE++* during a BSF experiment using the Zhang-2017_mod mechanism. Note the different scaling of the OH concentration axes in the two graphs at the bottom: they are used to highlight the concentration differences at small OH concentrations (log scale) and large OH concentrations (linear scale). Initial (unburnt) gas composition (in mole fractions): 0.082 CO, 0.258 H₂, 0.284 N₂O, 0.376 Ar; unburnt gas pressure: 30 Torr, temperature: 300 K, initial flow rate: 83 cm / s. These conditions refer to x60401000.xml (see Table A4). The flame front is at around 1 cm from the burner plate on this distance scale.

5.3. Overview of mechanism performance comparisons

Table 15 shows the calculated error function values by experiment type and the overall error function values (E_{overall}), highlighted in bold in the rightmost block of the table, for each mechanism. As described in Section 5.2, the results of the BSF simulations were found to be unreliable; therefore, these experiments were excluded from the overall E calculation, and they are not shown in the table. Hence, E_{overall} was calculated by considering only the JSR, ST-IDT, and FR data. Altogether, 1239 data points were included in the final comparison which is 84.1% of the total number of data points (1473). As seen, the Zhang-2017, Zhang-2017_mod, and Wang-2020 models have the best overall performance, with an E_{overall} value of less than 9. There is no difference between the performance Zhang-2017 and Zhang-2017_mod models in any of the experiment types. These mechanisms have a common development history: Zhang-2017 was used as the initial mechanism for the development of

Table 15. Summary of the comparison of mechanism performance. The percentages for the points omitted in step 2 are calculated as compared to the number of points included after step 1.

Mechanism	E_{JSR}	$E_{\text{ST-IDT}}$	E_{FR}	$E_{\text{overall}}^{\text{a}}$
XML/Ds./Dp. ^b :	5/17/183	6/6/80	46/93/1210	57/116/1473
Step 1 excl. ^c :	19 (10.4%)	0 (0%)	117 (9.7%)	136 (9.2%)
Step 2 excl. ^d :	2 (1.2%)	0 (0%)	87 (8.0%)	89 (6.7%)
Included ^e :	162 (88.5%)	80 (100.0%)	1006 (83.1%)	1248 (84.7%)
GRI3.0-1999	34.15	45.60	43.59	42.95
SanDiego-2004	21.80	55.33	50.52	48.44
Tian-2009	16.80	35.16	25.79	26.00
Konnov-2009	46.18	61.97	38.70	41.92
POLIMI-2014	23.62	41.27	13.79	17.68
GDFKin-2016	17.34	40.42	27.65	28.11
Zhang-2017	19.34	6.43	7.50	8.46
Zhang-2017_mod	19.34	6.24	7.50	8.46
SanDiego-2018	24.10	57.75	47.91	46.82
Okafor-2018	28.33	40.32	34.62	34.67
Glarborg-2018	17.03	37.98	16.97	19.27
Shrestha-2019	16.49	47.15	25.21	26.81
POLIMI-2019	15.43	41.07	8.63	12.79
Han-2020	25.54	37.80	25.07	26.50
Wang-2020	16.22	6.20	5.97	6.93
Konnov-2021	33.59	22.28	43.07	40.00

^a: BSF measurements were not included in the overall E calculation, based on the arguments presented in Section 5.2.

^b: Total number of XMLs/Total number of datasets/Total number of data points.

^c: Number of excluded points in step 1.

^d: Number of excluded points in step 2.

^e: Number of points included in the E value calculation.

Wang-2020. Accordingly, Wang-2020 performs slightly better ($E_{\text{overall}} = 5.54$) than Zhang-2017 and Zhang-2017_mod ($E_{\text{overall}} = 6.36$). Therefore, Wang-2020 was chosen as the starting point for further mechanism analysis and development.

The Chemical Kinetics Laboratory at ELTE Eötvös Loránd University [21] already developed optimized reaction mechanisms for various combustion systems. One of these was a syngas combustion mechanism developed in 2016 by Varga et al. [11] who used the Kèromnés et al. [7] syngas oxidation model (published in 2013) as a starting point for mechanism optimization. The optimization was performed on a very large set of experimental data, and the rate parameters of 18 reactions were optimized. This optimized mechanism

Table 16. The comparison of the structure of the ELTE-2016 syngas combustion mechanism and that of the H₂/CO oxidation sub-mechanism of Wang-2020.

Species	ELTE-2016	Wang-2020	Comment
Noble gases			
Ar	✓	✓	—
He	✓	✓	—
N ₂	✓	✓	—
H/O species			
H	✓	✓	—
H ₂	✓	✓	—
H ₂ O	✓	✓	—
H ₂ O ₂	✓	✓	—
HO ₂	✓	✓	—
O	✓	✓	—
O ₂	✓	✓	—
OH	✓	✓	—
OH*	✓	✓	—
C/O species			
CO	✓	✓	—
CO ₂	✓	✓	—
H/C/O species			
HCO	✓	✗	HCO sub-mechanism in ELTE-2016; may be important in larger hydrocarbon combustion
HOCO	✗	✓	HOCO sub-mechanism in Wang-2020; may be important at high pressures
OCHO	✗	✓	only one reaction: H + CO ₂ = OCHO
CH ₃	✗	✓	only one reaction: HOCO + CH ₃ = CO ₂ + CH ₄
CH ₄	✗	✓	only two reactions: OH* + CH ₄ = OH + CH ₄ , HOCO + CH ₃ = CO ₂ + CH ₄ ; and third body collider

(denoted by ELTE-2016) can be considered the best existing model for syngas oxidation; for instance, it was used as the H₂/CO sub-mechanism in the Han-2020 mechanism. The H₂/CO sub-mechanisms of both Zhang-2017_mod and Wang-2020 are also based on the syngas combustion model of Kèromnés et al. [7], but in those cases no optimization was performed.

Table 16 summarizes the similarities and the differences between the ELTE-2016 syngas combustion mechanism and the H₂/CO oxidation sub-mechanism of Wang-2020 by listing the species present in each model. It can be seen that the noble gases and the H/O and C/O species are identical in the two mechanisms, but there are differences in the included H/C/O species.

The Kèromnés et al. [7] mechanism was validated against a large set of experimental data on H₂/CO oxidation which included ignition delay time measurements, concentration profiles in JSRs and FRs, and laminar burning velocity measurements. Although H₂/CO oxidation was found to be insensitive to the HCO sub-mechanism by Kèromnés et al. [7], the authors included it in their model, considering the work of Li et al. [9] which showed that HCO chemistry is important in the modeling of the flames of larger hydrocarbons. To follow the strategy of hierarchical mechanism development, Varga et al. [11] also included the reactions of the HCO radical in their optimized model, however, they are not present in the Wang-2020 model because these mechanisms aimed to model only syngas/NO_x systems. Since our research group also applies the hierarchical mechanism development strategy, the reactions of HCO from the ELTE-2016 model should be included in the initial mechanism.

According to Nilsson and Konnov [128], the model predictions of IDT, LBV, FR, and JSR experiments on syngas combustion are practically identical with and without the HOCO chemistry. They found that the HOCO reactions were among the 20 most sensitive reactions in the case of syngas mixtures with a high CO content at low temperatures, but still, they were not influential enough to alter the model predictions significantly. However, Nilsson and Konnov [128] also suggested that HOCO reactions should be included in H₂/CO combustion mechanisms to facilitate the hierarchical mechanism development approach because these reactions are important in the combustion of small oxygenated fuels such as formic acid [129] and ethyl propionate [130]. Note, that Nilsson and Konnov did not investigate high-pressure experiments such as those of Rasmussen et al [14], based on which Zhang et al. [77] showed that HOCO chemistry promotes the CO → CO₂ conversion at $T > 700$ K at high pressures ($p > 50$ atm). Therefore, HOCO chemistry should be included in the initial model of the mechanism analysis.

Considering the previous arguments, I combined Wang-2020 with the ELTE-2016 mechanism as follows:

- All (H₂/CO) reactions in Wang-2020 that are present in ELTE-2016 were replaced by the corresponding reactions of ELTE-2016 because the rate parameters of ELTE-2016 are considered better for these reactions.
- All the other H₂/CO reactions in Wang-2020 that are not present in ELTE-2016 were kept; these are the reactions of HOCO, OCHO, CH₃, CH₄.
- Reactions of ELTE-2016 that are not present in Wang-2020 were added to the model; these are the reactions of HCO.
- The N-chemistry of Wang-2020 was kept.

Let us denote this mechanism by “Wang-2020+ELTE-2016”.

Furthermore, Kovács et al. [106] recently optimized the rate coefficients of nine H/N/O reactions starting from the Glarborg-2018 model using a very large set of H/N/O experimental data (ca. 2000 data points). These reactions and their optimized rate coefficients are listed in Table 17 – they are all included in the Wang-2020 model. Therefore, I prepared a third mechanism: the rate parameters of (R17)–(R25) in Wang-2020+ELTE-2016 were replaced by the rate coefficients optimized by Kovács et al. [106] (Table 17). Let us call this mechanism “Wang-2020+ELTE-2020”.

However, some comments are noteworthy regarding the pressure-dependent reactions (R18), (R21), and (R25) in Table 17. In all cases, only the low-pressure (LP) limit rate coefficients were optimized by Kovács et al. [106], because the high-pressure limits were not found to be important in the investigated H/N/O experiments. In the case of (R18), Kovács et

Table 17. The H/N/O reactions whose rate parameters were optimized by Kovács et al. [106] and the optimized Arrhenius parameters. In the case of pressure-dependent rate coefficients, the data refer to Ar as third body: the third body coefficient of Ar is $m(\text{Ar}) = 1$. Other third body coefficients are as follows: $m(\text{N}_2)_{(\text{R18})} = 1.7$, $m(\text{O}_2)_{(\text{R18})} = 1.4$, $m(\text{H}_2\text{O})_{(\text{R18})} = 12$, $m(\text{N}_2)_{(\text{R21})} = 1.6$.

Nr.	Reaction	p dependence	A^a	n	$(E/R)/K$
(R17)	$\text{NO}_2 + \text{H} = \text{NO} + \text{OH}$	–	$1.574 \cdot 10^{14}$	0	144.84
(R18) – LP ^b	$\text{N}_2\text{O} + \text{M} = \text{N}_2 + \text{O} + \text{M}$	Lindemann	$1.810 \cdot 10^{29}$	–3.962	34 809
(R19)	$\text{N}_2\text{O} + \text{H} = \text{N}_2 + \text{OH}$	–	$1.577 \cdot 10^2$	3.278	3096.6
(R20)	$\text{NO} + \text{HO}_2 = \text{NO}_2 + \text{OH}$	–	$4.553 \cdot 10^{13}$	–0.433	–94.969
(R21) – LP ^b	$\text{NO} + \text{H} + \text{M} = \text{HNO} + \text{M}$	Troe	$7.950 \cdot 10^{21}$	–2.093	492.17
(R22)	$\text{NH} + \text{NO} = \text{N}_2\text{O} + \text{H}$	–	$2.713 \cdot 10^{14}$	–0.575	–359.92
(R23)	$\text{NH} + \text{OH} = \text{HNO} + \text{H}$	–	$4.951 \cdot 10^{11}$	0.476	–452.80
(R24)	$\text{HNO} + \text{H} = \text{NO} + \text{H}_2$	–	$2.817 \cdot 10^{16}$	–0.938	1332.6
(R25) – LP ^b	$\text{NO} + \text{OH} + \text{M} = \text{HONO} + \text{M}$	Troe	$5.582 \cdot 10^{24}$	–2.974	47.473

^a: Unit of A is $\text{cm}^3 \text{mol}^{-1} \text{s}^{-1}$ or $\text{cm}^6 \text{mol}^{-2} \text{s}^{-1}$.

^b: Low-pressure limit.

al. used different rate coefficients for the starting point of the optimization from the ones included in Wang-2020: Kovács et al. optimized the LP rate coefficient of Johnsson et al. [131] and the HP limit in Glarborg-2018 was of Baulch et al. [132], while Wang et al. used the LP limit of Javoy et al. [26] and the HP limit of Zuev and Starikovskii [133] in Wang-2020. As Kovács et al. optimized only the LP limit, only that was replaced in Wang-2020 with the optimized parameters of Kovács et al., and the HP limit of Wang-2020 was kept. Note, that since the pressure dependence of the reaction is parameterized by the Lindemann formalism, this should not cause any problem. Also, the HP limits of Baulch et al. and Zuev and Starikovskii are relatively close to each other: they agree within a factor of 2 in the investigated temperature range (700–3600 K). The third body coefficients of Ar, N₂, O₂, and H₂O were the same in Wang-2020 as the ones Kovács et al. suggested, but Wang-2020 also provided the coefficients for NO and N₂O, so these values were kept in Wang-2020+ELTE-2020.

The HP (Tsang and Herron [134]) and LP (Riley et al. [135]) limits and the Troe parameters of (R21) were the same in Wang-2020 and Glarborg-2018 (the starting point of the optimization of Kovács et al.); therefore, the LP limit in Wang-2020 was replaced with the optimized rate coefficient of Kovács et al. and the HP limit and the Troe parameters were left unchanged. The third body coefficient of N₂ was 1.6 in both cases, however, Kovács et al. reported unity coefficient for Ar, while it was 0.75 in Wang-2020 based on the Konnov-2009 model. The disagreement stems from the fact that Konnov et al. [61] used the rate coefficient of Glarborg et al. [136] (1998) for the LP limit which was determined using N₂ as the bath gas (consequently, the third body coefficient of N₂ was unity in Konnov-2009), while the rate coefficient of Riley et al. [135] was measured using Ar as the bath gas and Riley et al. suggested a third body coefficient of 1.6 for N₂. Therefore, the correct third body coefficient for Ar would have been unity in Wang-2020, so this value was used in the Wang-2020+ELTE-2020 model. In addition, the third body coefficients of H₂O, O₂, H₂, and CO₂ were provided in Wang-2020, but these were not included in Wang-2020+ELTE-2020 because they were not computed for Ar bath gas.

Reaction (R25) was implemented in Wang-2020 according to the results of a recent (2019) theoretical rate coefficient determination of Chen et al. [137]. The pressure dependence of this rate coefficient was given according to the PLOG formalism. In contrast, Kovács et al. optimized the LP of the Troe parameterized rate coefficient of Fulle et al. [138]. As the two kinds of formalism cannot easily be converted to each other, I completely replaced

the rate parameters in Wang-2020 with the Troe parameterized rate coefficient from Glarborg-2018 with the optimized LP limit of Kovács et al.

Having the aforementioned three mechanisms, I tested the performance of Wang-2020+ELTE-2016 and Wang-2020+ELTE-2020 and compared it to that of the original Wang-2020 model. Table 18 summarizes the average error function values obtained by the original Wang-2020 model and its two modified versions.

In the table, two different overall E values are shown (these are calculated based on all experiment types except for BSF measurements) which were obtained by two different filtering methods. One of them was the same point exclusion procedure as applied in Section 5.1 for the calculation of E_{overall} (here, denoted by “ E_{old} ”). In contrast, in the calculation of “ E_{new} ”, only those data points were excluded from the ones that were filtered out in step 1 in Section 5.1 for which $E_{ij} > 100$ using the Wang-2020+ELTE-2016 and Wang-2020+ELTE-2020 models as well. This resulted in 5 points to include that had previously been excluded in step 1 (these points are all FR measurements). In step 2 of the filtering procedure, those data points were excluded whose E value was higher than 100 for any of the three mechanisms; there were 8 such points. Hence, altogether 139 points were excluded in the new filtering procedure, which resulted in 1334 included data points. Since the data points that were used for the calculation of E_{new} will be used for further mechanism development, the average E values are also shown in Table 18 for each experiment type using that data filtering method ($E_{\text{new}}^{\text{JSR}}$, $E_{\text{new}}^{\text{ST-IDT}}$, $E_{\text{new}}^{\text{FR}}$). Table A9 of the Appendix shows the error function values by datasets for each mechanism using the new filtering method.

Table 18 shows that the replacement of the H_2/CO sub-mechanism in Wang-2020 deteriorated the performance of the mechanism, overall and for each experiment type as well. Note, that this does not mean that the Varga et al. [11] syngas combustion mechanism is worse than the H_2/CO sub-mechanism of Wang-2020. It may often happen that a mechanism that is composed of sub-mechanisms of different sources and has never been fully validated and optimized against experiments on a certain kind of system has worse performance than

Table 18. The effect of the choice of H_2/CO sub-mechanism on the average error function values in the Wang-2020 model.

Mechanism	E_{old}	$E_{\text{new}}^{\text{JSR}}$	$E_{\text{new}}^{\text{ST-IDT}}$	$E_{\text{new}}^{\text{FR}}$	E_{new}
Data points:	1248	164	80	1090	1334
Wang-2020	6.93	18.46	6.20	10.14	10.47
Wang-2020+ELTE-2016	12.95	20.48	6.37	19.14	17.87
Wang-2020+ELTE-2020	12.66	39.22	4.73	16.52	17.30

the full original mechanism that has been developed and validated against a large set of experimental data on that kind of system (like Wang-2020).

It is interesting to observe that the replacement of the rate parameters of the nine N-chemistry reactions by the ones optimized by Kovács et al. [106] improved the mechanism performance for ST-IDT measurements but the E value became much higher in the case of JSR measurements. Table A9 shows that the extremely high $E_{\text{new}}^{\text{JSR}}$ value of Wang-2020+ELTE-2020 is mainly due to only one dataset, the NO concentration profile of XML x00201004. For this dataset, the E_i value of Wang-2020+ELTE-2020 is 364.93, while it is 13.06–13.06 for the other two models. If this dataset was completely excluded, the $E_{\text{new}}^{\text{JSR}}$ values of the models would be 19.39, 21.43, 23.49, respectively (in the order as in Table 18). This means that at least one of the reactions optimized by Kovács et al. [106] have a large influence on the NO predictions in XML x00201004, and we should consider reoptimizing these rate parameters including the present JSR experiments as well. The FR predictions of Wang-2020+ELTE-2020 are better than those of Wang-2020+ELTE-2016, but they are worse than those of the original Wang-2020 model.

The overall E value of Wang-2020+ELTE-2020 is somewhat lower than that of Wang-2020+ELTE-2016, but it is greater than that of Wang-2020.

This part of the work aimed to select a mechanism to be the starting point of further mechanism development. For this purpose, I was looking for the existing mechanism having the best performance on syngas/NO_x indirect experiments. This mechanism was found to be the Wang-2020 model. However, the syngas combustion mechanism of Varga et al. [11] and the N-chemistry rate parameters of Kovács et al. [106] were optimized based on a very large set of experimental data; therefore, these results are considered the best rate parameters for these reactions. Both works were carried out in the Chemical Kinetics Laboratory at Eötvös Loránd University (ELTE) [21]. Hence, to follow the hierarchical mechanism development strategy of the research group, I chose the Wang-2020+ELTE-2020 mechanism for further mechanism development. This mechanism contains the rate parameters optimized by our research group previously.

5.4. Results of the sensitivity analysis

Local sensitivity analysis was carried out on the Wang2020-ELTE2020 mechanism according to the method described in Section 4.5 using the 1343 indirect experimental data points specified in Section 5.3. The sensitivities of both the kinetic parameters (see Section 3.3.1.2) and the thermodynamic parameters (see Section 3.3.1.1) of the model were investigated.

Parameter j was considered influential for data point i (in other words, data point i was *sensitive* to parameter j) if either criterion (27) (for kinetic, heat capacity, and entropy parameters) or criterion (34) (for enthalpy parameters) was true, that is, $|\tilde{s}n_{ij}| \geq 0.1$ and $|\tilde{s}sn_{ij}| \geq 0.1$, respectively. Using either of these conditions, the ratio of the number of experimental data points that were sensitive to parameter j and the total number of points was computed for each parameter; these values are called “frequency” in this section. This way, it could be explored which parameters influence the syngas/NO_x combustion systems the most. This kind of investigation is important because we can identify the reactions and thermodynamic quantities whose parameters should be optimized on this combustion system.

5.4.1. Kinetic parameters

In the case of kinetic parameters (see Section 3.3.1.2), the local sensitivity coefficients, s_{ij} , were computed for each preexponential factor. (A , see equation (8)) and for each experimental data point using $f_{\text{pert}} = 0.05$ as the perturbation factor. The investigated model contained altogether 26 pressure-dependent reactions, and the rate coefficients of 3 of them were parameterized with the Lindemann formalism, 11 with the Troe formalism, and 12 with the PLOG formalism. The preexponential factors of both the high-pressure and low-pressure limits of Lindemann and Troe parameterized reactions and each preexponential factor of the PLOG reactions were perturbed one by one. The normalized (sn_{ij}) and scaled normalized ($\tilde{s}n_{ij}$) sensitivity coefficients were computed according to equations (25) and (26), respectively.

Table 19 shows the 20 most important reactions in the case of the ST-IDT experiments. The reactions were ordered based on the number of data points that are sensitive to the corresponding reaction according to condition (27). There are four reactions (1–4) to which most data points are sensitive (>80%), however, the rate coefficients of these reactions had already been optimized by either Varga et al. [11] or Kovács et al. [106], which confirms the hierarchical structure of combustion mechanisms. These previously optimized reactions are written in gray fonts in the table. As shown in Table 2, the fuel was H₂/CO and the oxidizer was N₂O in all ST-IDT experiments, and no other NO_x species was present in the initial gas mixtures. Therefore, it is not surprising that seven of the 20 reactions are a reaction of N₂O, and the most important reaction that has not yet been optimized in our research group is the direct reaction between N₂O and CO (5). This reaction is also an example of the direct

Table 19. The 20 most important reactions in the case of the ST-IDT measurements based on the frequency values.

ST-IDT: 80 data points					
Nr.	Reaction	Count ^a	Frequency ^b	$ \overline{\tilde{n}_{ij}} $ ^c	System ^d
1	O + H ₂ = H + OH	79	98.8%	0.561	syngas
2	N ₂ O + H = N ₂ + OH	76	95.0%	0.599	H/N/O
3	N ₂ O + M = N ₂ + O + M (LP)	75	93.8%	0.695	H/N/O
4	CO + OH = CO ₂ + H	66	82.5%	0.550	syngas
5	N₂O + CO = N₂ + CO₂	48	60.0%	0.247	p. w.
6	H + O ₂ = O + OH	37	46.3%	0.123	syngas
7	NH + NO = N ₂ O + H	32	40.0%	0.145	H/N/O
8	OH + H ₂ = H + H ₂ O	24	30.0%	0.113	syngas
9	NH + O = NO + H	22	27.5%	0.090	p. w.
10	N₂O + O = NO + NO	17	21.3%	0.088	p. w.
11	N₂O + M = N₂ + O + M	16	20.0%	0.078	p. w.
12	N + OH = NO + H	13	16.3%	0.049	p. w.
13	N₂O + O = N₂ + O₂	13	16.3%	0.066	p. w.
14	NH + H = N + H₂	13	16.3%	0.052	p. w.
15	N + NO = N₂ + O	7	8.8%	0.035	p. w.
16	H + NO ₂ = OH + NO	6	7.5%	0.024	H/N/O
17	CO + O + M = CO₂ + M (LP)	6	7.5%	0.038	p. w.
18	OH* + CO = OH + CO	4	5.0%	0.019	p. w.
19	NH + OH = N + H₂O	3	3.8%	0.024	p. w.
20	NO + O + M = NO₂ + M (LP)	3	3.8%	0.015	p. w.

^a: Number of data points for which the reaction has $|\tilde{n}_{ij}| \geq 0.1$.

^b: The 'Count' value normalized by the total number of ST-IDT data points.

^c: The average of the $|\tilde{n}_{ij}|$ values for all ST-IDT data points for each reaction.

^d: Syngas: the rate parameters of this reaction were optimized by Varga et al. [11], H/N/O: the rate parameters of this reaction were optimized by Kovács et al. [106], p. w.: the rate coefficient of this reaction could be optimized using the experiments investigated in the present work.

coupling of the C and N chemistry. As the ignition delay time was defined based on the OH* concentration profile in several experiments, one reaction of OH* – its de-excitation by CO (18) – is among the 20 most important reactions.

Table 20 shows the sensitivity analysis results for the concentration profile measurements, separately for JSR and FR experiments. As shown in Table 2, the gas mixtures investigated in most of these experiments contain NO (and sometimes NO₂) as nitrogen species, O₂ is usually the oxidizer, and CO is always present in the fuel. In many FR experiments, hydrogen comes from the water vapor content of the initial gas mixture. Therefore, it is not surprising that the reactions of N₂O are not among the most important ones, contrary to the ST-IDT measurements. Also, the reactions of OH* are missing from the list. Many previously optimized reactions can be found among the 20 most important reactions in these cases as well. The most important, previously not optimized rate coefficient is the low-pressure limit of the NO oxidation reaction to NO₂ by the O radical (8 and 5, respectively) in both cases. The importance of the coupling of C and N chemistry is represented by the reaction of NO₂ and CO in the case of FR experiments (10).

Table 20. The 20 most important reactions in the case of the concentration profiles measured in JSR and FR, respectively, based on the frequency values.

	JSR <i>c</i> -profiles: 164 data points					FR <i>c</i> -profiles: 1090 data points				
Nr.	Reaction	Count ^a	Frequency ^b	$\overline{ \widetilde{sn}_{ij} }$ ^c	System ^d	Reaction	Count ^a	Frequency ^b	$\overline{ \widetilde{sn}_{ij} }$ ^c	System ^d
1	H + O ₂ = O + OH	150	91.5%	0.491	syngas	H + O ₂ + M = HO ₂ + M (LP)	807	74.0%	0.543	syngas
2	CO + OH = CO ₂ + H	147	89.6%	0.734	syngas	CO + OH = CO ₂ + H	719	66.0%	0.463	syngas
3	OH + H ₂ = H + H ₂ O	132	80.5%	0.335	syngas	H + NO ₂ = OH + NO	561	51.5%	0.320	H/N/O
4	NO + H + M = HNO + M (LP)	128	78.0%	0.440	H/N/O	H + O ₂ = O + OH	503	46.1%	0.227	syngas
5	HNO + H = NO + H ₂	106	64.6%	0.313	H/N/O	NO + O + M = NO₂ + M (LP)	491	45.0%	0.155	p. w.
6	O + H ₂ = H + OH	100	61.0%	0.179	syngas	NO₂ + O = NO + O₂	416	38.2%	0.145	p. w.
7	H + O ₂ + M = HO ₂ + M (LP)	99	60.4%	0.211	syngas	OH + OH = O + H ₂ O	408	37.4%	0.176	syngas
8	NO + O + M = NO₂ + M (LP)	99	60.4%	0.160	p. w.	NO + HO ₂ = NO ₂ + OH	366	33.6%	0.140	H/N/O
9	NH + OH = HNO + H	87	53.0%	0.334	H/N/O	HO ₂ + OH = H ₂ O + O ₂	357	32.8%	0.138	syngas
10	H + OH + M = H ₂ O + M	35	21.3%	0.075	syngas	NO₂ + CO = NO + CO₂	222	20.4%	0.130	p. w.
11	H + H + M = H ₂ + M	19	11.6%	0.028	syngas	HONO + OH = NO₂ + H₂O	172	15.8%	0.054	p. w.
12	NO + HO ₂ = NO ₂ + OH	14	8.5%	0.035	H/N/O	NO₂ + NO₂ → NO + NO + O₂	140	12.8%	0.087	p. w.
13	HNO + O = NO + OH	14	8.5%	0.057	p. w.	NO + H + M = HNO + M (LP)	137	12.6%	0.092	H/N/O
14	NH + O = NO + H	13	7.9%	0.030	p. w.	HNO + H = NO + H ₂	132	12.1%	0.078	H/N/O
15	HONO + OH = NO₂ + H₂O	11	6.7%	0.023	p. w.	H + HONO = H₂ + NO₂	127	11.7%	0.073	p. w.
16	NH + NO = N ₂ O + H	10	6.1%	0.025	H/N/O	NH + OH = HNO + H	126	11.6%	0.091	H/N/O
17	HO ₂ + OH = H ₂ O + O ₂	9	5.5%	0.026	syngas	H + OH + M = H ₂ O + M	119	10.9%	0.054	syngas
18	H + NO ₂ = OH + NO	8	4.9%	0.015	H/N/O	OH + H ₂ = H + H ₂ O	101	9.3%	0.052	syngas
19	NO + OH + M = HONO + M (LP)	7	4.3%	0.024	H/N/O	N + NO = N₂ + O	75	6.9%	0.030	p. w.
20	HNO + O₂ = NO + HO₂	6	3.7%	0.014	p. w.	N + OH = NO + H	74	6.8%	0.022	p. w.

^a: Number of data points for which the reaction has $|\tilde{s}n_{ij}| \geq 0.1$.

^b: The 'Count' value normalized by the total number of JSR/FR data points.

^c: The average of the $|\tilde{s}n_{ij}|$ values for all JSR/FR data points for each reaction.

^d: Syngas: the rate parameters of this reaction were optimized by Varga et al. [11], H/N/O: the rate parameters of this reaction were optimized by Kovács et al. [106], p. w.: the rate coefficient of this reaction could be optimized using the experiments investigated in the present work.

Table 21 shows the sensitivity analysis results computed for all investigated indirect experiments (1343 data points). The table lists all reactions whose frequency value is above 5%, which is true for only 26 preexponential factors of the 354 investigated. This accords with the fact that the outputs of detailed kinetic combustion mechanisms are usually sensitive to only a few parameters. In Table 21, only 9 reactions are listed whose rate coefficient had not been optimized previously by our research group. These rate parameters may be the primary targets of parameter optimization to be performed on this experimental dataset. The complete list of reactions according to the order of the frequency values can be found in Table A10.

Table 21. Reactions whose frequency value is greater than 5% for all investigated indirect measurements.

All experiments: 1334 data points					
Nr.	Reaction	Count ^a	Frequency ^b	$ \overline{\tilde{n}_{ij}} $ ^c	System ^d
1	$\text{CO} + \text{OH} = \text{CO}_2 + \text{H}$	932	69.9%	0.502	syngas
2	$\text{H} + \text{O}_2 + \text{M} = \text{HO}_2 + \text{M} \text{ (LP)}$	906	67.9%	0.469	syngas
3	$\text{H} + \text{O}_2 = \text{O} + \text{OH}$	690	51.7%	0.253	syngas
4	$\text{NO} + \text{O} + \text{M} = \text{NO}_2 + \text{M} \text{ (LP)}$	593	44.5%	0.147	p. w.
5	$\text{H} + \text{NO}_2 = \text{OH} + \text{NO}$	575	43.1%	0.265	H/N/O
6	$\text{NO}_2 + \text{O} = \text{NO} + \text{O}_2$	421	31.6%	0.120	p. w.
7	$\text{OH} + \text{OH} = \text{O} + \text{H}_2\text{O}$	412	30.9%	0.150	syngas
8	$\text{NO} + \text{HO}_2 = \text{NO}_2 + \text{OH}$	380	28.5%	0.119	H/N/O
9	$\text{HO}_2 + \text{OH} = \text{H}_2\text{O} + \text{O}_2$	366	27.4%	0.116	syngas
10	$\text{NO} + \text{H} + \text{M} = \text{HNO} + \text{M} \text{ (LP)}$	265	19.9%	0.130	H/N/O
11	$\text{OH} + \text{H}_2 = \text{H} + \text{H}_2\text{O}$	257	19.3%	0.090	syngas
12	$\text{HNO} + \text{H} = \text{NO} + \text{H}_2$	238	17.8%	0.102	H/N/O
13	$\text{NO}_2 + \text{CO} = \text{NO} + \text{CO}_2$	222	16.6%	0.106	p. w.
14	$\text{NH} + \text{OH} = \text{HNO} + \text{H}$	215	16.1%	0.116	H/N/O
15	$\text{O} + \text{H}_2 = \text{H} + \text{OH}$	208	15.6%	0.063	syngas
16	$\text{HONO} + \text{OH} = \text{NO}_2 + \text{H}_2\text{O}$	183	13.7%	0.047	p. w.
17	$\text{H} + \text{OH} + \text{M} = \text{H}_2\text{O} + \text{M}$	155	11.6%	0.054	syngas
18	$\text{NO}_2 + \text{NO}_2 \rightarrow \text{NO} + \text{NO} + \text{O}_2$	140	10.5%	0.071	p. w.
19	$\text{H} + \text{HONO} = \text{H}_2 + \text{NO}_2$	127	9.5%	0.060	p. w.
20	$\text{N}_2\text{O} + \text{M} = \text{N}_2 + \text{O} + \text{M} \text{ (LP)}$	116	8.7%	0.063	H/N/O
21	$\text{N}_2\text{O} + \text{H} = \text{N}_2 + \text{OH}$	91	6.8%	0.043	H/N/O
22	$\text{NH} + \text{O} = \text{NO} + \text{H}$	90	6.7%	0.024	p. w.
23	$\text{N} + \text{OH} = \text{NO} + \text{H}$	87	6.5%	0.021	p. w.
24	$\text{N} + \text{NO} = \text{N}_2 + \text{O}$	82	6.1%	0.028	p. w.
25	$\text{NH} + \text{NO} = \text{N}_2\text{O} + \text{H}$	73	5.5%	0.020	H/N/O
26	$\text{H} + \text{H} + \text{M} = \text{H}_2 + \text{M}$	70	5.2%	0.014	syngas

^a: Number of data points for which the reaction has $|\tilde{n}_{ij}| \geq 0.1$.

^b: The 'Count' value normalized by the total number of data points.

^c: The average of the $|\tilde{n}_{ij}|$ values for all data points for each reaction.

^d: Syngas: the rate parameters of this reaction were optimized by Varga et al. [11], H/N/O: the rate parameters of this reaction were optimized by Kovács et al. [106], p. w.: the rate coefficient of this reaction could be optimized using the experiments investigated in the present work.

5.4.2. Thermodynamic parameters

Table 22 summarizes the results of the sensitivity analysis for the thermodynamic quantities for each experiment type (ST-IDT, JSR, FR) and overall. The 10 most sensitive species are included in this table for each case. The species are ordered according to the frequency values (see in the caption of the table) of the corresponding thermodynamic parameters. The complete list containing all 44 species of the Wang2020-ELTE2020 mechanism for each thermodynamic parameter using all experimental data points (1295) can be found in Table A11 of the Appendix.

From the overall results (rightmost block of the table, highlighted in bold), it can be seen that the most sensitive species are very similar for each thermodynamic parameter. The reactive H/O radicals (OH, O, H), H₂O, and NO are among the five most sensitive species in all cases. The most sensitive N-containing radical is HONO, and the CO, H₂, O₂, and NO₂ molecules also show a significant influence on the simulation results.

The results obtained for each experiment type separately do not deviate significantly from the overall result, only small differences can be observed. In the case of ST-IDT measurements, N₂O is the most sensitive species for two thermodynamic parameters. This is probably because N₂O was in the initial gas mixture in significant amounts in all ST-IDT measurements (see Table 2), while in the other experiments, only trace amounts of it were formed during the reaction.

The results of the JSR measurements show relatively large sensitivity to the thermodynamic parameters of CO₂, while NO₂ is not in any of the JSR lists. This observation may be explained by the fact that in all JSR experiments, the concentration of CO₂ was recorded, while that of NO₂ was not measured in any of the experiments.

Table 22. The 10 most sensitive species in the Wang2020-ELTE2020 model for each experiment type (JSR, FR, ST-IDT) and overall, and for each investigated thermodynamic parameter (heat capacity, enthalpy, entropy) based on the frequency values (see below).

ST-IDT: 80 data points			JSR: 164 data points			FR: 1090 data points			All: 1334 data points		
Sp. ^a	Freq. ^b	$ \overline{\widetilde{sn}}_{ij} ^c$	Sp. ^a	Freq. ^b	$ \overline{\widetilde{sn}}_{ij} ^c$	Sp. ^a	Freq. ^b	$ \overline{\widetilde{sn}}_{ij} ^c$	Sp. ^a	Freq. ^b	$ \overline{\widetilde{sn}}_{ij} ^c$
Standard (constant pressure) molar heat capacity at 300 K											
N ₂ O	87.5%	0.403	OH	96.3%	0.774	OH	84.9%	0.716	OH	86.3%	0.724
OH	85.0%	0.735	H ₂ O	79.9%	0.477	H ₂ O	72.0%	0.362	H ₂ O	72.0%	0.368
O ₂	82.5%	0.479	H	78.0%	0.267	O	58.5%	0.192	O	54.6%	0.184
NO	80.0%	0.293	HNO	73.8%	0.384	NO	45.6%	0.232	NO	46.2%	0.229
O	78.8%	0.294	NH	70.1%	0.301	HONO	39.0%	0.221	H	44.6%	0.173
H	73.8%	0.213	H ₂	54.3%	0.321	H	37.4%	0.156	HONO	35.3%	0.203
NH	72.5%	0.278	O ₂	48.2%	0.179	NO ₂	33.7%	0.229	H ₂	30.4%	0.183
H ₂	60.0%	0.137	CO ₂	47.6%	0.258	CO	27.7%	0.127	O ₂	30.2%	0.127
H ₂ O	55.0%	0.229	CO	39.6%	0.209	H ₂	24.7%	0.165	CO	29.4%	0.139
CO ₂	38.8%	0.195	NO	33.5%	0.181	O ₂	23.7%	0.093	NO ₂	27.9%	0.188
Standard molar enthalpy at 300 K ($\overline{\widetilde{sn}}_{ij}$ values instead of \widetilde{sn}_{ij} values)											
O ₂	90.0%	0.486	OH	96.3%	0.807	OH	82.9%	0.709	OH	84.9%	0.716
OH	87.5%	0.624	H	83.5%	0.406	H ₂ O	71.6%	0.339	H ₂ O	70.5%	0.339
H	85.0%	0.437	H ₂ O	79.9%	0.461	O	63.7%	0.267	O	59.7%	0.247
NO	85.0%	0.504	HNO	73.2%	0.362	NO	45.0%	0.247	H	51.4%	0.266
N ₂ O	81.3%	0.500	NH	70.1%	0.315	H	44.1%	0.232	NO	46.1%	0.257
O	80.0%	0.279	H ₂	54.3%	0.353	HONO	34.5%	0.168	HONO	31.3%	0.154
NH	77.5%	0.507	O ₂	49.4%	0.182	NO ₂	28.5%	0.187	O ₂	31.3%	0.129
H ₂	67.5%	0.144	CO ₂	43.9%	0.237	CO	26.6%	0.144	H ₂	29.9%	0.205
CO ₂	38.8%	0.180	CO	39.6%	0.238	O ₂	24.2%	0.094	CO	28.9%	0.158
CO	37.5%	0.181	NO	34.8%	0.199	H ₂	23.5%	0.187	NO ₂	23.5%	0.154
Standard molar entropy at 300 K											
N ₂ O	91.3%	0.477	OH	96.3%	0.776	OH	83.8%	0.705	OH	85.2%	0.708
NO	88.8%	0.459	H ₂ O	79.9%	0.464	H ₂ O	71.2%	0.338	H ₂ O	70.2%	0.339
O ₂	85.0%	0.515	H	77.4%	0.246	O	62.5%	0.231	O	57.9%	0.214
OH	81.3%	0.618	HNO	74.4%	0.410	NO	48.8%	0.257	NO	49.9%	0.263
NH	76.3%	0.390	NH	69.5%	0.298	HONO	37.2%	0.202	H	42.5%	0.152
O	72.5%	0.237	H ₂	49.4%	0.251	H	35.6%	0.133	HONO	34.0%	0.186
H	65.0%	0.206	CO ₂	48.8%	0.257	NO ₂	32.0%	0.224	O ₂	32.1%	0.137
H ₂	46.3%	0.088	O ₂	48.2%	0.206	CO	28.3%	0.142	CO	30.7%	0.156
H ₂ O	37.5%	0.087	CO	44.5%	0.240	O ₂	25.8%	0.098	H ₂	27.3%	0.134
CO ₂	36.3%	0.180	NO	38.4%	0.206	H ₂	22.6%	0.120	NO ₂	26.3%	0.184

^a: Chemical formula of the species.

^b: The number of data points for which the species has $|\widetilde{sn}_{ij}| \geq 0.1$ or $|\overline{\widetilde{sn}}_{ij}| \geq 0.1$ divided by the total number of data points.

^c: The average of the $|\widetilde{sn}_{ij}|$ or $|\overline{\widetilde{sn}}_{ij}|$ values for the data points for each species.

6. Conclusions and outlook

In this work, a large set of indirect experimental data on the combustion of syngas/ NO_x systems was collected, and the experimental data were digitized into XML files that can be used for numerical simulations using the *Optima++* framework [94]. The data included JSR, ST-IDT, FR, and BSF experiments. The standard deviations of the collected datasets were also estimated using the computer program Minimal Spline Fit [112, 113], and an overall standard deviation was assigned to each of them using the estimated and the reported experimental errors.

16 detailed combustion mechanisms were utilized from the literature that can be used for the modeling of syngas/ NO_x combustions systems. The performance of these models was assessed against the investigated indirect experiments. The performance comparison was done by the evaluation of an error function that considers also the standard deviation of the data points. This error function allows the quantitative comparison of several mechanisms on large experimental datasets. It was found that the mechanism of Wang et al. [87] had the best overall performance.

From the comparison of two numerical solver packages, it was found that the simulations of BSF experiments are unreliable; therefore, these experiments were excluded from further mechanism development.

The syngas submechanism of the Wang et al. [87] model was partly replaced by the optimized syngas combustion model of Varga et al. [11], and the rate parameters of nine reactions were replaced by the optimized parameters of Kovács et al. [106]. The mechanism obtained this way contained 44 species and 259 reactions.

Local sensitivity analysis was performed on the kinetic and thermodynamic parameters of the model. It was found that many of the most important rate parameters had already been optimized by the ELTE Chemical Kinetics Research Group. The two most sensitive reactions whose rate parameters were not optimized by our research group were reactions $\text{NO} + \text{O} + \text{M} = \text{NO}_2 + \text{M}$ (LP) and $\text{NO}_2 + \text{O} = \text{NO} + \text{O}_2$. The direct C/N coupling reaction $\text{NO}_2 + \text{CO} = \text{NO} + \text{CO}_2$ was also found to be important in 16.6% of the investigated data points. The results showed that model predictions are the most sensitive to the thermochemical parameters of the reactive H/O radicals (OH, O, H), H_2O , and NO, followed by the HONO radical. These parameters may be the primary targets of model parameter optimization, which is our goal in the future.

Appendix

Table A1. Concentration profile measurements in jet stirred reactors: experimental details by XMLs and standard deviations by datasets.

Reference	XML ID	T / K	p / atm	Φ	Fuel	Ox. ^a	$x_{\text{dopant}}^{\text{b}}$	$x_{\text{diluent}}^{\text{b}}$	Meas. ^c	Dp. ^d	Error type	σ
Dagaut (2003) [34]	x00201000	851–1200	1	0.10	H ₂ /CO	O ₂	0.001 NO	0.975 N ₂	H ₂	8	relative	0.210
									CO	8	relative	0.042
									CO ₂	8	relative	0.108
Dagaut (2003) [34]	x00201001	849–1399	1	0.93	H ₂ /CO	O ₂	0.00095 NO	0.97955 N ₂	H ₂	9	relative	0.154
									CO	9	relative	0.120
									CO ₂	9	relative	0.069
Dagaut (2003) [34]	x00201002	901–1326	1	1.75	H ₂ /CO	O ₂	0.001 NO	0.981875 N ₂	H ₂	12	absolute	0.033
									CO	12	relative	0.027
									CO ₂	12	relative	0.108
Dagaut (2003) [33]	x00201003	1100	1	0.48–2.10	H ₂ /CO	O ₂	0.001 NO	0.973–0.983 N ₂	NO	12	relative	0.025
									CO	12	relative	0.027
									CO ₂	12	relative	0.028
									H ₂	12	relative	0.062
Dagaut (2003) [33]	x00201004	1400	1	0.48–2.10	H ₂ /CO	O ₂	0.001 NO	0.973–0.983 N ₂	NO	12	relative	0.026
									CO	12	relative	0.034
									CO ₂	12	relative	0.048
									H ₂	12	relative	0.032

^a: Oxidizer, ^b: in mole fraction, ^c: Measured species ^d: Number of data points in the dataset.

Table A2. Shock tube ignition delay time measurements: experimental details and standard deviations by datasets.

Reference	XML ID	T / K	p / atm	Φ	Fuel	Oxidizer	$x_{\text{dopant}}^{\text{a}}$	$x_{\text{diluent}}^{\text{a}}$	Dp. ^b	Error type	σ
Kopp (2012) [47]	x10401000	1712–2202	1.40	3.05	H ₂ /CO	N ₂ O	–	0.9595 Ar	18	relative	0.151
Kopp (2012) [47]	x10401001	1654–2221	10.40	3.05	H ₂ /CO	N ₂ O	–	0.9595 Ar	15	relative	0.157
Dean (1978) [46]	x10401002	1930–2765	1.15-1.90	3.01	H ₂ /CO	N ₂ O	–	0.9595 Ar	13	relative	0.193
Dean (1978) [46]	x10401003	1930–2765	1.15-1.90	3.01	H ₂ /CO	N ₂ O	–	0.9595 Ar	12	relative	0.227
Dean (1978) [46]	x10401004	2030–2845	1.37-2.21	11.6	H ₂ /CO	N ₂ O	–	0.8691 Ar	11	relative	0.269
Dean (1978) [46]	x10401005	2030–2845	1.37-2.21	11.6	H ₂ /CO	N ₂ O	–	0.8691 Ar	11	relative	0.111

^a: in mole fraction, ^b: Number of data points in the dataset.

Table A3. Concentration profile measurements in flow reactors: experimental details by XMLs and standard deviations by datasets.

Reference	XML ID	T / K	p / atm	Φ	Fuel	Ox.^a	x_{dopant}^b	x_{diluent}^b	Meas. ^c	Dp. ^d	Error type	σ
Hulgaard (1993) [48]	x30401000	1071–1367	1.04	9.09	CO	N_2O	–	0.998 N_2	NO	6	relative	0.025
									N_2O	6	relative	0.083
Hulgaard (1993) [48]	x30401001	1071–1369	1.04	0.04	CO	$\text{N}_2\text{O}/\text{O}_2$	–	0.973 N_2	NO	6	relative	0.025
									N_2O	6	relative	0.057
Roesler (1995) [49]	x30201048	1007	1.00	0.92	CO	O_2	0.00017 NO, 0.0059 H_2O	0.979 N_2	CO	19	relative	0.030
Roesler (1995) [49]	x30201049	1000	1.00	0.10	CO	O_2	0.000175 NO, 0.0059 H_2O	0.934325 N_2	CO	19	relative	0.029
Glarborg (1995) [50]	x30201016	781–1288	1.05	0.01	CO	O_2	0.00522 NO, 0.054 H_2O	0.902948 N_2	CO	21	relative	0.025
									CO_2	21	relative	0.025
									NO	21	relative	0.025
									NO_2	21	relative	0.1
Glarborg (1995) [50]	x30201017	917–1253	1.05	0.01	CO	O_2	0.000102 NO, 0.009 H_2O	0.952399 N_2	CO	17	relative	0.025
									NO	17	relative	0.025
Glarborg (1995) [50]	x30201018	811–1176	1.05	0.01	CO	O_2	0.001187 NO, 0.01 H_2O	0.947362 N_2	CO	15	relative	0.025
Glarborg (1995) [50]	x30201019	883–1199	1.05	0.01	CO	O_2	0.000108 NO, 0.093 H_2O	0.864418 N_2	CO	13	relative	0.025
									NO	13	relative	0.025
Glarborg (1995) [50]	x30201020	837–1202	1.05	0.01	CO	O_2	0.001119 NO, 0.103 H_2O	0.855429 N_2	CO	15	relative	0.025
Glarborg (1995) [50]	x30201021	1173–1396	1.05	0.02	CO	O_2	0.01 NO, 0.01 H_2O	0.969534 N_2	CO	10	relative	0.033
Glarborg (1995) [50]	x30301003	890–1256	1.05	0.01	CO	O_2	0.001384 NO, 0.00013 NO_2 , 0.01 H_2O	0.944983 N_2	CO	12	relative	0.029
									NO	12	relative	0.025
Glarborg (1995) [50]	x30301004	891–1257	1.05	0.01	CO	O_2	$3 \cdot 10^{-6}$ NO, $2.8 \cdot 10^{-5}$ NO_2 ,	0.946489 N_2	CO	12	relative	0.101
									NO	12	relative	0.025

0.01 H ₂ O												
Glarborg (1995) [50]	x30301005	889–1256	1.05	0.01	CO	O ₂	1 · 10 ⁻⁵ NO,	0.946385 N ₂	CO	12	relative	0.025
							1.05 · 10 ⁻⁴ NO ₂ ,		NO	12	relative	0.211
0.01 H ₂ O												
Glarborg (1995) [50]	x30301006	890–1257	1.05	0.01	CO	O ₂	1.04 · 10 ⁻⁴ NO,	0.945803 N ₂	CO	12	relative	0.025
							6.22 · 10 ⁻⁴ NO ₂ ,		NO	12	relative	0.025
0.01 H ₂ O												
Glarborg (1996) [39]	x30201033	916–1253	1.05	0.01	CO	O ₂	0.000102 NO,	0.952399 N ₂	CO	17	relative	0.035
0.009 H ₂ O												
Glarborg (1996) [39]	x30201034	883–1200	1.05	0.01	CO	O ₂	0.000108 NO,	0.864418 N ₂	CO	13	relative	0.030
0.093 H ₂ O												
Glarborg (1996) [39]	x30201035	811–1175	1.05	0.01	CO	O ₂	0.001414 NO,	0.947135 N ₂	CO	15	relative	0.074
0.01 H ₂ O												
Glarborg (1996) [39]	x30201036	838–2000	1.05	0.01	CO	O ₂	0.00143 NO,	0.855118 N ₂	CO	15	relative	0.036
0.103 H ₂ O												
Alzueta (1997) [51]	x30201063	938–1396	1.00	1.03	CO	O ₂	0.00093 NO	0.99213 N ₂	CO ₂	22	relative	0.025
									CO	22	relative	0.047
									NO	22	relative	0.025
Mueller (1999) [15]	x30201022	950	10.00	0.34	CO	O ₂	0.000107 NO,	0.982293 N ₂	CO	18	relative	0.025
							0.0049 H ₂ O		NO	18	relative	0.025
									NO ₂	18	relative	0.025
Mueller (1999) [15]	x30201023	950	1.20	0.35	CO	O ₂	0.000107 NO,	0.982093 N ₂	CO	15	relative	0.025
							0.0049 H ₂ O		NO	15	relative	0.035
									NO ₂	15	relative	0.025
Mueller (1999) [15]	x30201024	954	3.00	0.34	CO	O ₂	0.000107 NO,	0.982493 N ₂	CO	18	relative	0.025
							0.0048 H ₂ O		NO	18	relative	0.035
									NO ₂	18	relative	0.025
Mueller (1999) [15]	x30201025	952	6.50	0.33	CO	O ₂	0.000108 NO,	0.982292 N ₂	CO	19	relative	0.025
							0.0049 H ₂ O		NO	19	relative	0.025
									NO ₂	19	relative	0.025
Mueller (1999) [15]	x30201026	950	3.00	0.33	CO	O ₂	5.4 · 10 ⁻⁵ NO,	0.982346 N ₂	CO	19	relative	0.025

0.005 H ₂ O												
Mueller (1999) [15]	x30201027	950	3.00	0.34	CO	O ₂	0.000139 NO, 0.0049 H ₂ O	0.982161 N ₂	CO	19	relative	0.025
Mueller (1999) [15]	x30201028	950	3.00	0.33	CO	O ₂	0.000508 NO, 0.0049 H ₂ O	0.981992 N ₂	CO	19	relative	0.025
Mueller (1999) [15]	x30201029	950	3.00	0.33	CO	O ₂	0.000222 NO, 0.0048 H ₂ O	0.982578 N ₂	CO	19	relative	0.025
Mueller (1999) [15]	x30201030	1010	10.00	0.35	CO	O ₂	4.1 · 10 ⁻⁵ NO, 0.005 H ₂ O	0.982059 N ₂	CO	16	relative	0.045
									NO	16	relative	0.025
Mueller (1999) [15]	x30201031	950	10.00	0.36	CO	O ₂	4.1 · 10 ⁻⁵ NO, 0.0048 H ₂ O	0.982359 N ₂	CO	19	relative	0.025
									NO	19	relative	0.025
Mueller (1999) [15]	x30201032	980	10.00	0.36	CO	O ₂	4.1 · 10 ⁻⁵ NO, 0.005 H ₂ O	0.982059 N ₂	CO	19	relative	0.025
									NO	19	relative	0.025
Glarborg (2000) [52]	x30201050	938–1397	1.00	1.01	CO	O ₂	0.000927 NO, 0.0185H ₂ O	0.973573 N ₂	CO	23	relative	0.046
									CO ₂	23	relative	0.025
									NO	23	relative	0.025
Glarborg (2000) [52]	x30201051	1406–1547	1.00	5.60	CO	O ₂	0.000297 NO, 0.047 H ₂ O	0.931503 N ₂	NO	4	relative	0.025
Glarborg (2000) [52]	x30201052	1406–1547	1.00	3.63	CO	O ₂	0.000292 NO, 0.04 H ₂ O	0.938008 N ₂	NO	4	relative	0.025
Glarborg (2000) [52]	x30201053	1406–1547	1.00	2.14	CO	O ₂	0.000281 NO, 0.045 H ₂ O	0.931919 N ₂	NO	4	relative	0.025
Glarborg (2000) [52]	x30201054	1473–1773	1.00	0.12	CO	O ₂	0.0009 NO, 0.06 H ₂ O	0.9141 N ₂	CO	4	relative	0.025
									NO	4	relative	0.029
Glarborg (2000) [52]	x30201055	1473–1773	1.00	0.24	CO	O ₂	0.0009 NO, 0.06 H ₂ O	0.9091 N ₂	CO	4	relative	0.025
									NO	4	relative	0.029
Glarborg (2000) [52]	x30201056	1473–1773	1.00	1.22	CO	O ₂	0.0009 NO, 0.06 H ₂ O	0.8691 N ₂	CO	4	relative	0.029
									NO	4	relative	0.025
Glarborg (2000) [52]	x30201057	1473–1773	1.00	2.44	CO	O ₂	0.0009 NO, 0.06 H ₂ O	0.8191 N ₂	CO	4	relative	0.025
									NO	4	relative	0.025

Glarborg (2000) [52]	x30201058	1473–1773	1.00	4.89	CO	O ₂	0.0009 NO, 0.06 H ₂ O	0.7191 N ₂	CO NO	4 4	relative relative	0.029 0.035
Glarborg (2000) [52]	x30201059	1473–1773	1.00	2.39	CO	O ₂	0.0009 NO, 0.06 H ₂ O	0.8791 N ₂	CO NO	4 4	relative relative	0.029 0.025
Glarborg (2000) [52]	x30201060	1473–1773	1.00	9.57	CO	O ₂	0.0009 NO, 0.06 H ₂ O	0.7291 N ₂	CO NO	4 4	relative relative	0.029 0.025
Glarborg (2000) [52]	x30201061	1473–1773	1.00	0.50	CO	O ₂	0.0009 NO, 0.06 H ₂ O	0.8391 N ₂	CO NO	4 4	relative relative	0.025 0.029
Glarborg (2000) [52]	x30201062	1473–1773	1.00	1.98	CO	O ₂	0.0009 NO, 0.06 H ₂ O	0.6891 N ₂	CO NO	4 4	relative relative	0.025 0.025
Rasmussen (2008) [14]	x30301000	600–898	19.74	0.03	H ₂ /CO	O ₂	0.000113 NO, 3.6 · 10 ⁻⁵ NO ₂	0.98358 N ₂	CO CO ₂ NO NO ₂ O ₂	13 13 13 13 13	relative relative relative relative relative	0.029 0.038 0.025 0.025 0.025
Rasmussen (2008) [14]	x30301001	600–898	49.35	0.03	H ₂ /CO	O ₂	2.6 · 10 ⁻⁵ NO, 0.000125 NO ₂	0.983485 N ₂	CO CO ₂ NO NO ₂ O ₂	13 13 13 13 13	relative relative relative relative relative	0.025 0.035 0.025 0.025 0.025
Rasmussen (2008) [14]	x30301002	601–898	98.69	0.03	H ₂ /CO	O ₂	6 · 10 ⁻⁶ NO, 0.000145 NO ₂	0.984107 N ₂	CO CO ₂ NO NO ₂ O ₂	13 13 13 13 13	relative relative relative relative relative	0.025 0.025 0.025 0.025 0.025

^a: Oxidizer, ^b: in mole fraction, ^c: Measured species, ^d: Number of data points in the dataset.

Table A4. Concentration profile measurements in burner stabilized flames: experimental details by XMLs and standard deviations by datasets.

Reference	XML ID	T_u / K^a	p / atm^b	Φ	Fuel	Oxidizer	x_{dopant}	x_{diluent}^c	Meas. ^d	Dp. ^e	Error type	σ
Vandooren (1997) [43]	x60401000	300	0.04	1.20	H_2/CO	N_2O	–	0.376 Ar	N_2O	10	relative	0.056
									H	22	relative	0.141
									NO	24	relative	0.098
									CO	23	relative	0.069
									CO_2	15	relative	0.059
									O_2	12	relative	0.094
									N_2	14	relative	0.069
									H_2	14	relative	0.083
									H_2O	14	relative	0.051
									O	9	relative	0.107
									OH	18	relative	0.131
Dindi (1991) [53]	x60401001	298	0.07	1.00	CO	N_2O	–	–	CO	9	relative	0.072
									N_2O	9	relative	0.090
									CO_2	9	relative	0.094
									NO	9	relative	0.354
									N_2	9	relative	0.085
									O_2	9	relative	0.214
Dindi (1991) [53]	x60401002	298	0.07	1.32	CO	N_2O	–	–	CO	13	relative	0.027
									N_2O	13	relative	0.061
									CO_2	13	relative	0.103
									NO	13	relative	0.165
									N_2	13	relative	0.054
									O_2	13	relative	0.220
Dindi (1991) [53]	x60401003	298	0.07	1.50	CO	N_2O	–	–	CO	9	relative	0.041
									N_2O	9	relative	0.120
									CO_2	9	relative	0.029
									NO	9	relative	0.243
									N_2	9	relative	0.106
									O_2	9	relative	0.119

^a: Unburnt gas temperature, ^b: Unburnt gas pressure, ^c: in mole fraction, ^d: Measured species, ^e: Number of data points in the dataset.

Table A5. Error function values by dataset (E_i) for the JSR measurements for each mechanism.

XML ID	Profile	All data points	Included points	Excluded points	GRI3.0-1999	SanDiego-2004	Tian-2009	Konnov-2009	POLIMI-2014	GDFKin-2016	Zhang-2017	Zhang-2017_mod	SanDiego-2018	Okafor-2018	Glarborg-2018	Shrestha-2019	POLIMI-2019	Han-2020	Wang-2020	Konnov-2021
x00201000	H ₂	8	6	2	65.51	31.77	36.31	51.44	49.96	35.30	43.69	43.69	34.59	55.97	37.38	32.80	40.81	54.99	44.51	30.02
x00201000	CO	8	8	0	71.76	119.73	32.66	11.62	5.84	39.28	8.32	8.32	132.27	94.55	32.38	36.50	10.72	2.89	10.97	50.33
x00201000	CO ₂	8	7	1	19.20	18.10	0.24	1.07	0.27	0.80	0.12	0.12	20.64	20.12	0.25	2.08	0.25	1.38	1.79	1.94
x00201001	H ₂	9	9	0	4.81	1.66	1.64	9.13	2.30	2.29	1.45	1.45	2.88	4.25	1.61	1.99	2.05	2.85	1.63	5.85
x00201001	CO	9	9	0	1.81	0.70	0.76	4.84	1.09	0.92	1.01	1.01	1.45	1.93	0.77	0.87	0.96	1.32	0.78	2.42
x00201001	CO ₂	9	8	1	4.78	6.18	4.16	14.69	3.46	32.93	3.96	3.96	1.56	4.20	6.19	2.10	1.40	1.05	3.00	6.26
x00201002	H ₂	12	12	0	93.02	27.14	48.71	188.08	105.09	34.54	72.27	72.27	45.31	80.77	44.24	51.27	50.81	120.69	40.81	115.76
x00201002	CO	12	12	0	24.59	0.88	6.29	53.68	17.38	1.53	13.04	13.04	4.87	18.00	5.29	4.38	4.68	18.95	3.95	29.60
x00201002	CO ₂	12	10	2	32.52	2.43	11.08	55.40	25.41	3.45	18.11	18.11	9.80	26.55	8.67	8.43	9.72	27.52	7.31	37.53
x00201003	NO	12	12	0	26.47	3.10	4.17	59.80	2.52	4.95	1.81	1.81	3.27	4.22	3.00	4.82	4.01	5.14	1.84	44.19
x00201003	CO	12	12	0	39.29	6.11	21.97	83.67	71.60	13.46	50.03	50.03	12.01	24.03	19.92	19.93	36.15	80.47	38.28	36.80
x00201003	CO ₂	12	12	0	27.21	9.03	5.82	69.09	28.32	5.96	15.40	15.40	4.48	18.34	4.68	4.74	5.82	26.25	5.91	36.28
x00201003	H ₂	12	8	4	18.81	25.81	23.14	7.86	6.68	36.34	10.79	10.79	16.18	24.46	27.81	20.47	13.25	6.89	17.40	15.06
x00201004	NO	12	12	0	43.64	12.45	2.39	63.34	1.39	0.55	4.03	4.03	9.47	3.40	7.48	3.26	1.21	1.17	13.06	57.01
x00201004	CO	12	9	3	39.19	33.55	33.94	44.72	33.79	30.49	35.87	35.87	36.10	35.37	36.92	33.70	30.91	33.10	35.96	45.02
x00201004	CO ₂	12	12	0	1.46	1.39	0.98	2.34	0.99	1.25	1.22	1.22	1.11	0.92	1.08	1.09	1.10	1.09	1.13	1.61
x00201004	H ₂	12	4	8	62.98	66.40	54.49	72.87	46.04	52.39	51.62	51.62	61.50	47.37	57.23	54.62	54.21	47.76	57.74	62.86

Table A6. Error function values by dataset (E_i) for the ST-IDT measurements for each mechanism.

XML ID	All data points	Included points	Excluded points	GRI3.0-1999	SanDiego-2004	Tian-2009	Konnov-2009	POLIMI-2014	GDFKin-2016	Zhang-2017	Zhang-2017_mod	SanDiego-2018	Okafor-2018	Glarborg-2018	Shrestha-2019	POLIMI-2019	Han-2020	Wang-2020	Konnov-2021
x10401000	18	18	0	152.98	179.88	121.42	156.03	131.50	140.98	4.12	3.98	179.91	136.69	125.68	4.82	140.94	121.39	3.83	3.82
x10401001	15	15	0	106.48	122.37	75.61	92.97	81.29	89.33	7.19	7.15	127.63	92.79	88.01	11.78	91.19	70.23	7.22	5.59
x10401002	13	13	0	4.05	5.84	0.52	6.10	14.05	3.25	16.29	15.27	9.44	3.86	1.56	27.43	0.65	24.73	15.12	5.38
x10401003	12	12	0	4.70	8.17	1.63	2.33	9.19	3.47	2.86	2.46	5.66	4.01	1.91	7.45	1.98	3.66	2.46	2.47
x10401004	11	11	0	2.17	5.56	3.19	40.31	2.76	1.13	2.02	1.65	17.86	1.63	3.04	55.39	4.55	3.64	1.65	42.30
x10401005	11	11	0	3.22	10.18	8.62	74.10	8.85	4.34	6.13	6.93	6.01	2.92	7.66	176.08	7.11	3.16	6.93	77.49

Table A7. Error function values by datasets (E_i) for the FR measurements for each mechanism.

XML ID	Profile	All data points	Included points	Excl. points	GRI3.0-1999	SanDiego-2004	Tian-2009	Konnov-2009	POLIMI-2014	GDFKin-2016	Zhang-2017	Zhang-2017_mod	SanDiego-2018	Okafor-2018	Glarborg-2018	Shrestha-2019	POLIMI-2019	Han-2020	Wang-2020	Konnov-2021
x30201016	CO	21	17	4	24.75	85.04	8.56	0.10	2.42	17.49	2.40	2.40	74.18	56.75	3.97	21.19	2.71	28.92	3.81	5.16
x30201016	CO ₂	21	17	4	20.47	68.60	3.76	0.02	1.93	10.83	1.07	1.07	54.96	50.39	1.33	13.35	1.68	29.41	2.59	1.61
x30201016	NO	21	21	0	1.15	0.96	0.09	0.03	0.05	0.14	0.02	0.02	0.83	1.63	0.08	0.12	0.05	0.11	0.02	0.15
x30201016	NO ₂	21	21	0	5.98	6.07	0.83	0.77	0.77	1.47	0.74	0.74	5.26	8.43	0.69	1.33	0.50	1.23	0.57	0.90
x30201017	CO	17	17	0	22.68	105.39	34.92	5.38	14.15	11.23	1.09	1.09	100.55	1.96	14.24	29.60	4.12	70.75	0.64	47.52
x30201017	NO	17	17	0	0.42	1.14	0.34	0.46	0.41	0.37	0.53	0.53	1.11	0.36	0.35	0.58	0.43	0.57	0.45	0.36
x30201018	CO	15	11	4	25.88	127.03	23.13	4.66	0.17	43.68	0.49	0.49	121.98	74.54	20.52	50.85	0.27	22.71	0.62	25.02
x30201019	CO	13	13	0	32.00	48.82	24.97	3.30	61.32	49.34	8.07	8.07	43.75	4.69	6.28	21.41	8.07	107.88	4.41	11.17
x30201019	NO	13	13	0	1.21	2.15	0.96	1.93	1.68	0.81	3.04	3.04	2.04	1.24	1.59	2.16	0.85	4.90	0.93	2.29
x30201020	CO	15	11	4	76.93	160.86	9.76	0.40	3.01	34.54	3.54	3.54	129.37	128.76	3.52	36.32	1.40	45.66	6.16	2.91
x30201021	CO	10	6	4	68.36	272.81	114.34	47.02	11.46	153.74	5.29	5.29	280.73	163.98	121.33	256.75	2.22	5.33	8.06	120.49
x30201022	CO	18	16	2	49.49	295.49	47.17	16.72	29.81	15.13	2.65	2.65	295.48	10.22	19.34	68.28	2.80	80.28	2.09	24.72
x30201022	NO	18	18	0	11.46	31.80	14.64	9.79	0.41	0.56	0.92	0.92	31.58	12.28	9.53	18.64	0.26	0.44	0.22	14.40
x30201022	NO ₂	18	18	0	4.60	32.31	15.80	10.08	0.44	0.60	1.07	1.07	32.11	5.45	10.82	19.62	0.23	0.49	0.21	11.21
x30201023	CO	15	15	0	41.96	0.68	16.93	19.25	20.35	6.39	1.59	1.59	0.44	11.14	2.03	6.29	2.14	48.31	1.34	21.67
x30201023	NO	15	15	0	1.14	0.33	0.14	1.13	0.07	0.20	0.10	0.10	0.34	0.67	0.10	0.21	0.10	0.09	0.09	2.01
x30201023	NO ₂	15	15	0	0.06	0.43	0.32	0.46	0.22	0.31	0.30	0.30	0.42	0.08	0.31	0.37	0.26	0.21	0.27	0.48
x30201024	CO	18	18	0	30.37	22.59	50.59	34.86	29.04	13.54	0.30	0.30	7.95	2.50	15.12	52.32	1.09	63.56	0.29	35.66
x30201024	NO	18	18	0	4.90	0.44	0.91	6.64	0.02	0.03	0.03	0.03	0.44	4.44	0.40	1.15	0.01	0.02	0.01	12.51
x30201024	NO ₂	18	18	0	0.24	0.55	0.93	1.03	0.02	0.07	0.13	0.13	0.53	0.27	0.45	1.26	0.03	0.05	0.05	0.99
x30201025	CO	19	14	5	46.14	288.07	41.60	22.03	51.55	23.53	0.94	0.94	288.07	6.93	17.56	58.79	9.93	97.53	0.95	30.56
x30201025	NO	19	19	0	8.46	12.15	5.34	9.35	0.10	0.17	0.33	0.33	11.53	8.59	3.39	6.55	0.09	0.20	0.09	16.65
x30201025	NO ₂	19	19	0	2.89	10.08	4.55	3.14	0.06	0.02	0.08	0.08	9.60	3.19	2.87	5.39	0.02	0.06	0.01	3.74

x30201026	CO	19	0	19	excl.	excl.	excl.	excl.	excl.	excl.	excl.	excl.	excl.	excl.	excl.	excl.	excl.	excl.	excl.	excl.
x30201027	CO	19	19	0	11.10	45.52	49.63	50.40	22.68	4.79	1.96	1.96	12.17	3.28	27.62	73.38	1.43	54.61	2.62	55.06
x30201028	CO	19	0	19	excl.	excl.	excl.	excl.	excl.	excl.	excl.	excl.	excl.	excl.	excl.	excl.	excl.	excl.	excl.	excl.
x30201029	CO	19	18	1	0.34	246.91	21.22	44.08	61.86	2.88	3.33	3.33	246.91	26.52	22.62	67.68	51.35	109.92	0.44	52.43
x30201030	CO	16	8	8	16.62	11.58	204.11	50.08	2.35	6.76	3.93	3.93	15.38	9.18	25.62	89.68	9.37	13.74	1.51	89.18
x30201030	NO	16	16	0	5.77	0.97	0.12	0.41	0.11	0.27	0.04	0.04	0.97	5.97	0.07	0.24	0.14	0.39	0.11	0.99
x30201031	CO	19	0	19	excl.	excl.	excl.	excl.	excl.	excl.	excl.	excl.	excl.	excl.	excl.	excl.	excl.	excl.	excl.	excl.
x30201031	NO	19	19	0	1.92	5.28	1.47	1.43	1.93	1.43	2.18	2.18	5.43	2.01	0.79	4.27	1.06	0.60	1.14	0.70
x30201032	CO	19	16	3	99.47	9.65	141.81	46.37	15.61	44.97	1.17	1.17	6.10	64.62	7.41	77.64	2.63	73.80	2.98	78.88
x30201032	NO	19	19	0	3.33	2.66	7.99	5.99	0.71	0.61	0.50	0.50	2.62	3.56	0.20	7.46	0.19	0.38	0.26	7.14
x30201033	CO	17	17	0	15.96	76.23	28.56	3.38	9.71	10.08	0.97	0.97	72.65	1.85	12.42	20.40	3.07	46.60	0.65	38.35
x30201034	CO	13	13	0	27.88	47.12	25.26	2.06	48.68	41.03	6.26	6.26	41.96	4.53	4.52	20.82	7.28	82.17	3.84	9.20
x30201035	CO	15	15	0	16.92	151.65	8.36	0.62	0.74	29.28	0.31	0.31	133.24	53.05	7.17	38.15	0.77	13.58	0.21	9.18
x30201036	CO	15	11	4	38.03	98.05	1.47	3.11	6.96	10.93	0.09	0.09	67.20	77.78	0.19	10.52	0.84	46.37	0.22	0.18
x30201048	CO	19	19	0	35.97	66.94	92.42	73.61	1.41	276.73	23.13	23.13	106.37	55.30	108.18	53.16	26.89	9.78	21.14	230.52
x30201049	CO	19	12	7	22.01	105.70	145.93	29.13	1.53	40.78	18.84	18.84	104.58	1.42	103.99	30.34	33.21	19.21	19.77	254.58
x30201050	CO	23	23	0	9.69	31.91	9.44	37.96	11.05	19.80	17.01	17.02	9.96	10.36	13.98	6.54	11.20	19.69	22.75	18.61
x30201050	CO ₂	23	19	4	0.78	25.39	1.96	5.91	0.76	14.59	3.17	3.17	3.14	0.23	2.93	0.42	4.13	1.54	17.16	1.97
x30201050	NO	23	23	0	4.75	0.72	1.22	17.07	1.86	1.54	1.14	1.14	0.81	4.74	0.72	1.13	1.37	1.79	0.56	16.56
x30201051	NO	4	3	1	49.77	17.06	26.40	86.77	35.28	26.32	21.11	21.12	18.89	8.40	16.86	20.20	24.83	33.09	12.19	6.74
x30201052	NO	4	4	0	27.09	40.66	56.62	46.16	70.65	55.22	50.14	50.15	43.38	32.68	41.03	45.22	53.95	67.68	33.94	17.22
x30201053	NO	4	3	1	8.23	23.03	34.29	15.64	43.23	33.09	28.43	28.44	24.44	19.72	22.96	26.87	32.25	41.55	17.33	7.86
x30201054	CO	4	4	0	0.38	0.38	0.38	0.38	0.37	0.37	0.38	0.38	0.38	0.38	0.38	0.38	0.38	0.38	0.38	0.38
x30201054	NO	4	4	0	0.04	0.03	0.04	0.04	0.05	0.05	0.04	0.04	0.04	0.04	0.04	0.04	0.04	0.05	0.04	0.04
x30201055	CO	4	4	0	1.79	1.79	1.79	1.79	1.73	1.74	1.79	1.79	1.79	1.79	1.79	1.79	1.79	1.79	1.79	1.79
x30201055	NO	4	4	0	0.05	0.03	0.05	0.05	0.06	0.06	0.05	0.05	0.03	0.05	0.04	0.05	0.05	0.08	0.03	0.05
x30201056	CO	4	3	1	8.28	9.59	10.19	8.45	9.84	9.49	9.94	9.95	9.56	9.26	9.66	9.64	9.80	10.50	9.38	9.02
x30201056	NO	4	4	0	19.11	5.26	11.23	24.13	11.94	7.12	8.32	8.34	5.01	3.82	5.11	5.22	6.79	15.31	3.83	8.54
x30201057	CO	4	4	0	0.52	0.46	0.45	0.51	0.47	0.48	0.45	0.45	0.46	0.50	0.46	0.47	0.47	0.45	0.46	0.49
x30201057	NO	4	3	1	492.12	15.10	37.12	448.12	19.70	8.79	23.45	23.45	15.80	161.60	16.81	3.07	6.15	53.37	7.35	226.39

x30201058	CO	4	4	0	0.23	0.20	0.20	0.22	0.21	0.21	0.20	0.20	0.20	0.22	0.20	0.21	0.21	0.21	0.20	0.22
x30201058	NO	4	1	3	858.24	18.07	45.07	675.81	0.02	0.87	27.90	27.88	20.37	634.48	23.39	8.01	4.30	68.27	7.30	402.49
x30201059	CO	4	3	1	0.54	1.09	1.15	0.54	1.05	0.97	1.10	1.10	1.08	0.82	1.10	1.06	1.09	1.22	1.02	0.70
x30201059	NO	4	4	0	254.71	13.07	27.59	271.40	27.68	15.85	19.15	19.15	13.97	14.37	13.61	9.84	14.38	36.89	7.02	54.80
x30201060	CO	4	4	0	0.02	0.03	0.03	0.02	0.02	0.02	0.03	0.03	0.03	0.02	0.03	0.02	0.03	0.03	0.02	0.02
x30201060	NO	4	0	4	excl.	excl.	excl.	excl.	excl.	excl.	excl.	excl.	excl.	excl.	excl.	excl.	excl.	excl.	excl.	excl.
x30201061	CO	4	4	0	27.33	27.34	27.38	27.38	26.53	26.59	27.38	27.38	27.33	27.38	27.44	27.38	27.38	27.44	27.38	27.42
x30201061	NO	4	4	0	1.14	0.48	1.00	1.22	0.81	0.74	0.74	0.74	0.42	0.94	0.68	0.58	0.62	1.58	0.63	1.08
x30201062	CO	4	4	0	0.23	0.39	0.42	0.24	0.36	0.36	0.39	0.39	0.39	0.25	0.40	0.37	0.38	0.44	0.38	0.24
x30201062	NO	4	4	0	568.01	40.94	76.06	507.95	29.55	20.41	43.11	43.12	39.66	352.00	43.12	10.77	13.36	104.78	21.18	428.67
x30201063	CO ₂	22	0	22	excl.	excl.	excl.	excl.	excl.	excl.	excl.	excl.	excl.	excl.	excl.	excl.	excl.	excl.	excl.	excl.
x30201063	CO	22	3	19	32.07	32.07	32.07	32.07	32.07	32.07	32.07	32.07	32.07	32.07	32.07	32.07	32.07	32.07	32.07	32.07
x30201063	NO	22	22	0	3.58	3.68	3.69	3.60	3.60	3.61	3.68	3.68	3.68	3.59	3.69	3.61	3.60	3.65	3.68	3.69
x30301000	CO	13	13	0	39.80	70.53	5.10	44.18	8.11	147.19	0.79	0.79	70.04	40.51	1.14	4.04	10.29	10.05	8.14	51.98
x30301000	CO ₂	13	8	5	7.06	0.00	0.01	0.01	0.30	24.07	0.03	0.03	0.00	0.00	0.03	0.02	0.01	0.01	0.01	0.00
x30301000	NO	13	13	0	74.30	50.42	1.36	28.05	25.29	73.48	4.86	4.86	49.35	5.09	5.74	7.94	1.17	2.72	0.74	35.20
x30301000	NO ₂	13	13	0	72.71	50.40	1.16	28.62	24.38	70.66	4.48	4.48	49.34	5.01	5.28	7.61	1.10	2.40	0.71	35.58
x30301000	O ₂	13	13	0	1.49	2.13	1.46	1.89	1.20	0.92	1.36	1.36	2.13	1.69	1.34	1.41	1.52	1.45	1.52	1.97
x30301001	CO	13	9	4	77.31	84.06	15.42	72.04	3.59	62.87	1.39	1.39	84.01	80.11	3.45	9.00	44.36	18.47	40.03	72.46
x30301001	CO ₂	13	8	5	74.71	89.67	10.91	73.18	3.82	205.48	7.51	7.51	89.63	87.30	13.86	8.40	37.10	11.31	30.87	73.57
x30301001	NO	13	13	0	5.31	8.63	5.58	48.41	32.84	23.38	6.69	6.69	8.55	6.03	4.08	8.79	1.53	3.44	1.71	53.35
x30301001	NO ₂	13	13	0	6.56	8.32	5.01	43.72	29.37	21.52	5.81	5.81	8.26	6.73	3.59	7.77	1.27	4.02	1.66	48.19
x30301001	O ₂	13	13	0	1.54	1.68	0.86	1.51	0.80	0.57	0.75	0.75	1.68	1.56	0.73	0.83	1.07	0.86	1.03	1.57
x30301002	CO	13	7	6	52.83	53.63	5.67	44.08	9.99	229.19	9.09	9.09	53.54	52.80	37.43	5.72	23.58	7.84	21.13	43.95
x30301002	CO ₂	13	5	8	0.80	1.15	0.17	0.41	2.83	244.98	4.99	4.99	1.14	1.05	11.49	0.11	0.20	0.03	0.17	0.41
x30301002	NO	13	11	2	2.32	2.04	26.93	63.01	49.70	45.92	29.06	29.06	2.06	2.20	24.44	29.66	10.35	1.08	9.34	69.82
x30301002	NO ₂	13	11	2	12.28	11.82	18.49	36.81	28.94	28.65	19.79	19.79	11.86	12.19	16.01	20.03	8.56	8.43	10.71	41.43
x30301002	O ₂	13	13	0	0.12	0.12	0.15	0.13	0.15	0.40	0.21	0.21	0.12	0.11	0.23	0.15	0.10	0.18	0.12	0.16
x30301003	CO	12	10	2	1.46	8.53	30.91	0.78	0.67	41.53	9.79	9.79	8.38	11.53	24.98	5.80	0.60	19.74	9.14	37.43
x30301003	NO	12	12	0	0.39	1.04	0.16	0.15	0.24	0.15	0.63	0.63	0.96	0.20	0.16	0.17	0.26	0.69	0.61	0.16
x30301004	CO	12	12	0	5.87	4.51	20.48	5.84	0.11	9.45	1.10	1.10	4.61	2.55	16.61	2.93	3.08	6.41	1.14	38.46

x30301004	NO	12	12	0	1.11	0.67	1.04	1.81	0.36	0.13	0.10	0.10	0.55	0.14	1.10	0.63	0.35	0.87	0.10	2.27
x30301005	CO	12	8	4	1.41	3.56	0.59	0.42	0.30	0.22	0.41	0.41	2.35	0.34	0.37	0.10	0.17	5.30	0.39	3.42
x30301005	NO	12	12	0	7.43	15.56	2.19	1.11	0.27	1.94	1.56	1.56	14.31	3.01	0.53	0.15	0.26	5.30	1.48	10.74
x30301006	CO	12	12	0	11.34	25.57	3.23	0.89	0.84	1.95	0.36	0.36	24.02	5.98	7.89	1.15	2.54	3.97	0.34	23.59
x30301006	NO	12	10	2	100.96	194.48	12.18	66.08	73.73	12.72	1.49	1.49	181.24	85.59	12.28	3.70	14.66	2.51	1.46	158.21
x30401000	NO	6	6	0	0.10	0.05	0.03	0.11	0.10	0.05	0.05	0.05	0.09	0.10	0.04	0.07	0.14	0.17	0.05	0.06
x30401000	N₂O	6	6	0	28.40	54.92	20.15	32.55	22.23	19.25	15.31	15.31	55.22	28.38	21.24	61.90	11.45	29.93	15.31	29.07
x30401001	NO	6	6	0	0.16	0.37	0.25	0.17	0.16	0.19	0.19	0.19	0.45	0.16	0.22	0.40	0.15	0.61	0.19	0.19
x30401001	N₂O	6	6	0	31.82	58.55	22.54	36.13	25.38	21.57	17.52	17.52	58.86	31.80	23.65	61.12	13.46	33.40	17.52	32.68

Table A8. Error function values by datasets (E_i) for the BSF measurements for each mechanism.

XML ID	Profile	All data points	Included points	Excluded points	GRI3.0-1999	SanDiego-2004	Tian-2009	Konnov-2009	POLIMI-2014	GDFKin-2016	Zhang-2017	Zhang-2017_mod	SanDiego-2018	Okafor-2018	Glarborg-2018	Shrestha-2019	POLIMI-2019	Han-2020	Wang-2020	Konnov-2021
x60401000	N ₂ O	10	7	3	18.29	36.10	4.97	13.12	3.04	13.29	3.92	3.92	40.88	4.88	8.56	8.70	3.23	3.79	3.92	7.26
x60401000	H	22	18	4	37.00	51.47	30.05	32.18	27.20	34.64	29.40	29.40	108.23	31.02	31.07	51.34	28.80	38.28	29.40	28.86
x60401000	NO	24	24	0	10.64	30.00	5.72	6.77	4.72	3.94	4.91	4.91	70.35	7.18	10.29	8.60	9.16	6.62	4.91	4.56
x60401000	CO	23	23	0	14.44	20.70	5.45	14.32	6.61	13.33	10.26	10.26	22.50	5.58	8.58	2.08	7.01	7.61	10.26	9.64
x60401000	CO ₂	15	13	2	142.99	248.12	45.26	136.98	57.09	125.36	96.52	96.52	266.63	46.69	74.61	17.91	58.09	71.00	96.52	97.25
x60401000	O ₂	12	10	2	84.80	28.84	29.61	57.76	13.85	147.88	66.35	66.35	338.42	12.75	61.09	249.35	27.76	28.08	66.35	81.74
x60401000	N ₂	14	12	2	6.98	6.79	17.06	8.58	14.21	7.60	11.40	11.40	6.33	17.38	9.38	10.09	13.70	14.97	11.40	9.09
x60401000	H ₂	14	14	0	9.41	15.40	3.54	8.64	3.91	7.74	4.61	4.61	23.00	4.10	6.35	8.58	5.21	2.72	4.61	5.61
x60401000	H ₂ O	14	13	1	8.27	14.46	4.66	6.22	4.83	8.02	4.74	4.74	13.28	4.57	5.80	7.99	4.08	5.67	4.74	11.14
x60401000	O	9	9	0	101.90	181.33	30.21	80.28	24.38	119.04	48.52	48.52	263.25	21.34	39.58	214.62	33.64	14.64	48.52	44.63
x60401000	OH	18	17	1	35.25	52.57	6.13	22.02	5.42	30.37	18.12	18.12	67.77	4.66	14.77	44.19	7.67	4.32	18.12	18.37
x60401001	CO	9	9	0	77.95	91.16	37.41	31.40	79.81	38.11	43.64	43.64	91.44	77.86	37.55	6.23	40.11	57.56	43.64	32.69
x60401001	N ₂ O	9	8	1	60.74	139.37	45.79	28.84	74.94	46.61	21.50	21.50	139.75	60.65	45.30	4.36	35.53	82.70	21.50	20.87
x60401001	CO ₂	9	0	9	excl.	excl.	excl.	excl.	excl.	excl.	excl.	excl.	excl.	excl.	excl.	excl.	excl.	excl.	excl.	excl.
x60401001	NO	9	9	0	14.27	13.98	11.17	10.47	12.70	10.67	15.58	15.58	13.78	15.26	10.76	5.87	10.54	417.34	15.58	12.67
x60401001	N ₂	9	7	2	83.78	514.06	34.30	25.53	105.46	33.82	27.52	27.52	518.42	83.91	32.50	48.95	28.75	83.94	27.51	24.31
x60401001	O ₂	9	8	1	30.35	526.03	11.54	19.76	25.78	10.92	22.16	22.16	503.20	30.35	14.64	6.41	19.64	73.63	22.16	18.29
x60401002	CO	13	12	1	235.86	292.70	82.69	67.32	245.09	84.58	98.43	98.43	292.67	235.37	82.69	62.91	89.80	166.55	98.41	70.86
x60401002	N ₂ O	13	9	4	55.78	107.69	38.60	30.42	66.43	39.08	25.50	25.50	107.73	55.63	38.33	30.42	33.74	69.96	25.50	26.68
x60401002	CO ₂	13	0	13	excl.	excl.	excl.	excl.	excl.	excl.	excl.	excl.	excl.	excl.	excl.	excl.	excl.	excl.	excl.	excl.
x60401002	NO	13	0	13	excl.	excl.	excl.	excl.	excl.	excl.	excl.	excl.	excl.	excl.	excl.	excl.	excl.	excl.	excl.	excl.
x60401002	N ₂	13	0	13	excl.	excl.	excl.	excl.	excl.	excl.	excl.	excl.	excl.	excl.	excl.	excl.	excl.	excl.	excl.	excl.
x60401002	O ₂	13	12	1	48.40	552.31	25.01	32.06	42.96	25.10	35.95	35.95	524.94	48.47	27.21	24.11	34.00	96.81	35.95	31.65

x60401003	CO	9	9	0	139.19	172.76	50.29	41.28	144.70	51.46	58.95	58.95	172.75	138.50	50.30	10.81	54.29	99.80	58.95	43.11
x60401003	N₂O	9	9	0	93.62	203.92	68.64	49.58	113.99	69.36	43.80	43.80	203.94	91.16	68.81	24.21	56.42	133.42	43.79	30.22
x60401003	CO₂	9	0	9	excl.	excl.	excl.	excl.	excl.	excl.	excl.	excl.	excl.	excl.	excl.	excl.	excl.	excl.	excl.	excl.
x60401003	NO	9	7	2	40.35	36.43	23.21	20.48	35.25	23.05	35.26	35.26	36.30	41.49	20.66	3.30	22.08	855.54	35.26	27.40
x60401003	N₂	9	7	2	53.68	361.54	12.20	7.61	70.49	13.00	10.40	10.40	361.47	53.30	11.40	5.41	10.39	59.36	10.39	7.37
x60401003	O₂	9	0	9	excl.	excl.	excl.	excl.	excl.	excl.	excl.	excl.	excl.	excl.	excl.	excl.	excl.	excl.	excl.	excl.

Table A9. Error function values by dataset for the mechanisms investigated in Section 5.3 of the main text.

XML ID	Profile	All points	Included points	Excl. points	Wang-2020	Wang-2020+ ELTE-2016	Wang-2020+ ELTE-2020
x00201000	H ₂	8	6	2	44.51	51.69	51.04
x00201000	CO	8	8	0	10.97	5.41	5.11
x00201000	CO ₂	8	8	0	33.55	25.91	10.42
x00201001	H ₂	9	9	0	1.63	2.15	1.65
x00201001	CO	9	9	0	0.78	0.80	0.75
x00201001	CO ₂	9	9	0	4.93	13.22	9.14
x00201002	H ₂	12	12	0	40.81	51.39	37.77
x00201002	CO	12	12	0	3.95	5.10	13.42
x00201002	CO ₂	12	10	2	7.31	10.10	12.48
x00201003	NO	12	12	0	1.84	1.89	4.71
x00201003	CO	12	12	0	38.28	56.93	55.92
x00201003	CO ₂	12	12	0	5.91	6.93	9.86
x00201003	H ₂	12	8	4	17.40	13.70	8.90
x00201004	NO	12	12	0	13.06	13.06	364.93
x00201004	CO	12	9	3	35.96	36.65	63.63
x00201004	CO ₂	12	12	0	1.13	1.16	3.86
x00201004	H ₂	12	4	8	57.74	58.30	83.63
x10401000	-	18	18	0	3.83	4.36	4.99
x10401001	-	15	15	0	7.22	7.84	8.40
x10401002	-	13	13	0	15.12	15.25	5.95
x10401003	-	12	12	0	2.46	2.32	2.22
x10401004	-	11	11	0	1.65	1.66	0.83
x10401005	-	11	11	0	6.93	6.76	5.97
x30201016	CO	21	21	0	7.12	1.32	2.12
x30201016	CO ₂	21	21	0	6.91	1.59	4.40
x30201016	NO	21	21	0	0.02	0.02	0.04
x30201016	NO ₂	21	21	0	0.57	0.63	0.98

x30201017	CO	17	17	0	0.64	44.47	43.12
x30201017	NO	17	17	0	0.45	0.44	0.59
x30201018	CO	15	15	0	2.24	2.63	2.76
x30201019	CO	13	13	0	4.41	56.57	55.34
x30201019	NO	13	13	0	0.93	1.55	3.34
x30201020	CO	15	15	0	6.64	0.97	1.74
x30201021	CO	10	10	0	9.42	4.96	5.17
x30201022	CO	18	18	0	2.86	55.15	46.13
x30201022	NO	18	18	0	0.22	0.10	0.98
x30201022	NO ₂	18	18	0	0.21	0.11	1.09
x30201023	CO	15	15	0	1.34	42.46	42.29
x30201023	NO	15	15	0	0.09	0.07	0.10
x30201023	NO ₂	15	15	0	0.27	0.17	0.25
x30201024	CO	18	18	0	0.29	49.30	43.85
x30201024	NO	18	18	0	0.01	0.01	0.03
x30201024	NO ₂	18	18	0	0.05	0.01	0.10
x30201025	CO	19	19	0	1.12	69.86	61.05
x30201025	NO	19	19	0	0.09	0.07	0.34
x30201025	NO ₂	19	19	0	0.01	0.17	0.10
x30201026	CO	19	0	19	excl.	excl.	excl.
x30201027	CO	19	19	0	2.62	33.07	27.24
x30201028	CO	19	0	19	excl.	excl.	excl.
x30201029	CO	19	19	0	0.50	39.42	26.29
x30201030	CO	16	13	3	13.99	87.78	70.37
x30201030	NO	16	16	0	0.11	0.69	0.16
x30201031	CO	19	0	19	excl.	excl.	excl.
x30201031	NO	19	19	0	1.14	0.36	1.57
x30201032	CO	19	19	0	3.44	112.30	91.87
x30201032	NO	19	19	0	0.26	0.37	0.71
x30201033	CO	17	17	0	0.65	29.31	28.48
x30201034	CO	13	13	0	3.84	43.84	42.34
x30201035	CO	15	15	0	0.21	3.34	3.29
x30201036	CO	15	15	0	0.57	6.50	7.37

x30201048	CO	19	19	0	21.14	8.55	6.24
x30201049	CO	19	17	2	57.26	35.14	36.88
x30201050	CO	23	23	0	22.75	22.73	30.40
x30201050	CO ₂	23	20	3	20.17	20.52	11.27
x30201050	NO	23	23	0	0.56	0.57	2.14
x30201051	NO	4	4	0	34.85	37.84	15.20
x30201052	NO	4	4	0	33.94	36.53	16.06
x30201053	NO	4	4	0	42.44	44.94	20.49
x30201054	CO	4	4	0	0.38	0.38	0.38
x30201054	NO	4	4	0	0.04	0.04	0.04
x30201055	CO	4	4	0	1.79	1.79	1.79
x30201055	NO	4	4	0	0.03	0.03	0.03
x30201056	CO	4	3	1	9.38	9.48	9.07
x30201056	NO	4	4	0	3.83	4.29	6.44
x30201057	CO	4	4	0	0.46	0.46	0.45
x30201057	NO	4	4	0	8.06	10.10	30.73
x30201058	CO	4	4	0	0.20	0.20	0.21
x30201058	NO	4	4	0	7.73	11.68	23.17
x30201059	CO	4	3	1	1.02	1.05	0.87
x30201059	NO	4	4	0	7.02	9.85	6.58
x30201060	CO	4	4	0	0.02	0.03	0.02
x30201060	NO	4	4	0	0.60	24.08	25.08
x30201061	CO	4	4	0	27.38	27.38	27.38
x30201061	NO	4	4	0	0.63	0.61	0.56
x30201062	CO	4	4	0	0.38	0.39	0.35
x30201062	NO	4	4	0	21.18	33.72	8.84
x30201063	CO ₂	22	0	22	excl.	excl.	excl.
x30201063	CO	22	3	19	32.07	32.07	32.07
x30201063	NO	22	22	0	3.68	3.67	3.67
x30301000	CO	13	13	0	8.14	13.44	13.86
x30301000	CO ₂	13	13	0	9.47	19.33	21.01
x30301000	NO	13	13	0	0.74	0.20	2.02
x30301000	NO ₂	13	13	0	0.71	0.13	2.06
x30301000	O ₂	13	13	0	1.52	1.54	1.57
x30301001	CO	13	11	2	96.92	129.06	114.08

x30301001	CO ₂	13	13	0	139.68	176.17	150.01
x30301001	NO	13	13	0	1.71	1.25	2.09
x30301001	NO ₂	13	13	0	1.66	1.31	1.95
x30301001	O ₂	13	13	0	1.03	1.06	1.03
x30301002	CO	13	11	2	89.26	110.22	102.25
x30301002	CO ₂	13	12	1	109.74	127.37	116.68
x30301002	NO	13	11	2	9.34	8.72	10.05
x30301002	NO ₂	13	11	2	10.71	10.39	10.92
x30301002	O ₂	13	13	0	0.12	0.11	0.11
x30301003	CO	12	10	2	9.14	17.96	20.42
x30301003	NO	12	12	0	0.61	0.78	0.83
x30301004	CO	12	12	0	1.14	4.20	4.57
x30301004	NO	12	12	0	0.10	0.71	0.76
x30301005	CO	12	11	1	25.44	73.02	83.82
x30301005	NO	12	12	0	1.48	4.52	4.75
x30301006	CO	12	12	0	0.34	2.37	2.41
x30301006	NO	12	12	0	2.95	1.35	1.33
x30401000	NO	6	6	0	0.05	0.05	0.08
x30401000	N ₂ O	6	6	0	15.31	15.31	11.81
x30401001	NO	6	6	0	0.19	0.19	0.17
x30401001	N ₂ O	6	6	0	17.52	17.47	13.86

Table A10. Results of the local sensitivity analysis performed on the kinetic parameters (preexponential factors) of the Wang2020-ELTE2020 model. Reactions are ordered according to their frequency values (see below). The “LP” in parentheses after a reaction refers to the low-pressure limit Arrhenius parameters of pressure-dependent falloff reactions. The “PLOGXX” in parentheses after a reaction refers to pressure-dependent rate coefficients described by the PLOG formalism where “XX” is the number of the parameter set in ascending pressure order for the corresponding reaction.

All experiments: 1334 data points					
Nr.	Reaction	Count ^a	Frequency ^b	$ \widetilde{sn}_{ij} ^c$	System ^d
1	CO + OH = CO ₂ + H	932	69.9%	0.502	syngas
2	H + O ₂ + M = HO ₂ + M (LP)	906	67.9%	0.469	syngas
3	H + O ₂ = O + OH	690	51.7%	0.253	syngas
4	NO + O + M = NO₂ + M (LP)	593	44.5%	0.147	p. w.
5	H + NO ₂ = OH + NO	575	43.1%	0.265	H/N/O
6	NO₂ + O = NO + O₂	421	31.6%	0.120	p. w.
7	OH + OH = O + H ₂ O	412	30.9%	0.150	syngas
8	NO + HO ₂ = NO ₂ + OH	380	28.5%	0.119	H/N/O
9	HO ₂ + OH = H ₂ O + O ₂	366	27.4%	0.116	syngas
10	NO + H + M = HNO + M (LP)	265	19.9%	0.130	H/N/O
11	OH + H ₂ = H + H ₂ O	257	19.3%	0.090	syngas
12	HNO + H = NO + H ₂	238	17.8%	0.102	H/N/O
13	NO₂ + CO = NO + CO₂	222	16.6%	0.106	p. w.
14	NH + OH = HNO + H	215	16.1%	0.116	H/N/O
15	O + H ₂ = H + OH	208	15.6%	0.063	syngas
16	HONO + OH = NO₂ + H₂O	183	13.7%	0.047	p. w.
17	H + OH + M = H ₂ O + M	155	11.6%	0.054	syngas
18	NO₂ + NO₂ → NO + NO + O₂	140	10.5%	0.071	p. w.
19	H + HONO = H₂ + NO₂	127	9.5%	0.060	p. w.
20	N ₂ O + M = N ₂ + O + M (LP)	116	8.7%	0.063	H/N/O
21	N ₂ O + H = N ₂ + OH	91	6.8%	0.043	H/N/O
22	NH + O = NO + H	90	6.7%	0.024	p. w.
23	N + OH = NO + H	87	6.5%	0.021	p. w.
24	N + NO = N₂ + O	82	6.1%	0.028	p. w.
25	NH + NO = N ₂ O + H	73	5.5%	0.020	H/N/O
26	H + H + M = H ₂ + M	70	5.2%	0.014	syngas
27	HNO + O = NO + OH	64	4.8%	0.022	p. w.
28	N₂O + CO = N₂ + CO₂	63	4.7%	0.023	p. w.
29	NH + H = N + H₂	58	4.3%	0.014	p. w.
30	CO + O ₂ = CO ₂ + O	50	3.7%	0.026	syngas
31	NO₂ + HO₂ = HNO₂ + O₂	49	3.7%	0.014	p. w.
32	HOCO = CO + OH (PLOG10)	49	3.7%	0.011	p. w.
33	HNO₂ + OH = NO₂ + H₂O	48	3.6%	0.014	p. w.
34	N₂O + O = NO + NO	42	3.1%	0.019	p. w.
35	NO + HO₂ + M = HNO₃ + M	34	2.5%	0.008	p. w.
36	NO + OH + M = HONO + M (LP)	34	2.5%	0.013	H/N/O
37	HOCO + O₂ = CO₂ + HO₂	33	2.5%	0.008	p. w.
38	NO₂ + O + M = NO₃ + M (LP)	33	2.5%	0.012	p. w.

39	$\text{HO}_2 + \text{O} = \text{OH} + \text{O}_2$	31	2.3%	0.008	p. w.
40	$\text{NO}_2 + \text{HO}_2 = \text{HONO} + \text{O}_2$	30	2.2%	0.005	p. w.
41	$\text{OH} + \text{NO} = \text{HNO}_2$ (PLOG08)	30	2.2%	0.006	p. w.
42	$\text{CO} + \text{O} + \text{M} = \text{CO}_2 + \text{M}$	29	2.2%	0.012	p. w.
43	$\text{CO} + \text{O} + \text{M} = \text{CO}_2 + \text{M}$ (LP)	29	2.2%	0.009	p. w.
44	$\text{N}_2\text{O} + \text{O} = \text{N}_2 + \text{O}_2$	28	2.1%	0.006	p. w.
45	$\text{HOCO} + \text{NO}_2 = \text{CO}_2 + \text{HONO}$	23	1.7%	0.005	p. w.
46	$\text{HO}_2 + \text{H} = \text{OH} + \text{OH}$	20	1.5%	0.009	syngas
47	$\text{HCO} + \text{H} = \text{CO} + \text{H}_2$	20	1.5%	0.006	syngas
48	$\text{N} + \text{O}_2 = \text{NO} + \text{O}$	17	1.3%	0.005	p. w.
49	$\text{N}_2\text{O} + \text{M} = \text{N}_2 + \text{O} + \text{M}$	17	1.3%	0.007	p. w.
50	$\text{NH} + \text{OH} = \text{N} + \text{H}_2\text{O}$	17	1.3%	0.004	p. w.
51	$\text{HNO} + \text{O}_2 = \text{NO} + \text{HO}_2$	17	1.3%	0.007	p. w.
52	$\text{NH} + \text{NO} = \text{N}_2 + \text{OH}$	16	1.2%	0.005	p. w.
53	$\text{OH} + \text{NO} = \text{HNO}_2$ (PLOG07)	16	1.2%	0.003	p. w.
54	$\text{HOCO} = \text{CO} + \text{OH}$ (PLOG09)	13	1.0%	0.004	p. w.
55	$\text{NNH} + \text{O} = \text{NH} + \text{NO}$	10	0.7%	0.004	p. w.
56	$\text{NO}_2 + \text{NO}_2 = \text{NO}_3 + \text{NO}$	9	0.7%	0.003	p. w.
57	$\text{NO}_3 + \text{NO}_2 \rightarrow \text{NO} + \text{NO}_2 + \text{O}_2$	8	0.6%	0.002	p. w.
58	$\text{HON} + \text{H} = \text{NH} + \text{OH}$	7	0.5%	0.005	p. w.
59	$\text{NNH} + \text{O}_2 = \text{N}_2 + \text{HO}_2$	6	0.4%	0.003	p. w.
60	$\text{NNH} + \text{O}_2 \rightarrow \text{N}_2 + \text{H} + \text{O}_2$	6	0.4%	0.003	p. w.
61	$\text{NH} + \text{O}_2 = \text{HNO} + \text{O}$	5	0.4%	0.002	p. w.
62	$\text{HCO} + \text{M} = \text{H} + \text{CO} + \text{M}$ (LP)	5	0.4%	0.003	p. w.
63	$\text{H} + \text{O}_2 + \text{M} = \text{HO}_2 + \text{M}$	4	0.3%	0.010	p. w.
64	$\text{H} + \text{HO}_2 = \text{H}_2 + \text{O}_2$	4	0.3%	0.009	syngas
65	$\text{OH}^* + \text{CO} = \text{OH} + \text{CO}$	4	0.3%	0.001	p. w.
66	$\text{NNH} + \text{O} = \text{N}_2\text{O} + \text{H}$	4	0.3%	0.001	p. w.
67	$\text{NNH} = \text{N}_2 + \text{H}$	3	0.2%	0.001	p. w.
68	$\text{O} + \text{H} + \text{M} = \text{OH} + \text{M}$	2	0.1%	0.003	p. w.
69	$\text{OH}^* + \text{CO}_2 = \text{OH} + \text{CO}_2$	2	0.1%	0.001	p. w.
70	$\text{NO} + \text{O} + \text{M} = \text{NO}_2 + \text{M}$	2	0.1%	0.007	p. w.
71	$\text{NH}_2 + \text{H} = \text{NH} + \text{H}_2$	2	0.1%	0.001	p. w.
72	$\text{DUP}_2\text{NH}_2 + \text{O} = \text{NH} + \text{OH}$	2	0.1%	0.001	p. w.
73	$\text{NH}_2 + \text{O} = \text{HNO} + \text{H}$	2	0.1%	0.003	p. w.
74	$\text{NH}_2 + \text{NH}_2 = \text{N}_2\text{H}_3 + \text{H}$	2	0.1%	0.000	p. w.
75	$\text{N}_2\text{H}_2 + \text{O} = \text{NNH} + \text{OH}$	2	0.1%	0.001	p. w.
76	$\text{HOCO} = \text{CO} + \text{OH}$ (PLOG06)	2	0.1%	0.001	p. w.
77	$\text{O} + \text{O} + \text{M} = \text{O}_2 + \text{M}$	1	0.1%	0.001	p. w.
78	$\text{DUP}_1\text{HO}_2 + \text{HO}_2 = \text{H}_2\text{O}_2 + \text{O}_2$	1	0.1%	0.001	syngas
79	$\text{H}_2\text{O}_2 + \text{H} = \text{H}_2\text{O} + \text{OH}$	1	0.1%	0.001	p. w.
80	$\text{H}_2\text{O}_2 + \text{H} = \text{H}_2 + \text{HO}_2$	1	0.1%	0.001	syngas
81	$\text{H}_2\text{O}_2 + \text{O} = \text{OH} + \text{HO}_2$	1	0.1%	0.000	p. w.
82	$\text{DUP}_2\text{H}_2\text{O}_2 + \text{OH} = \text{H}_2\text{O} + \text{HO}_2$	1	0.1%	0.002	p. w.
83	$\text{CO} + \text{HO}_2 = \text{CO}_2 + \text{OH}$	1	0.1%	0.002	syngas
84	$\text{HCO} + \text{M} = \text{H} + \text{CO} + \text{M}$	1	0.1%	0.000	syngas

85	$\text{HCO} + \text{O}_2 = \text{CO} + \text{HO}_2$	1	0.1%	0.001	p. w.
86	$\text{HCO} + \text{O} = \text{CO}_2 + \text{H}$	1	0.1%	0.000	p. w.
87	$\text{HCO} + \text{HO}_2 \rightarrow \text{CO}_2 + \text{H} + \text{OH}$	1	0.1%	0.000	p. w.
88	$\text{H} + \text{CO}_2 = \text{OCHO}$	1	0.1%	0.000	p. w.
89	$\text{HOCO} + \text{O} = \text{CO}_2 + \text{OH}$	1	0.1%	0.000	p. w.
90	$\text{DUP}_1\text{HOCO} + \text{OH} = \text{CO}_2 + \text{H}_2\text{O}$	1	0.1%	0.000	p. w.
91	$\text{HOCO} + \text{HO}_2 = \text{CO}_2 + \text{H}_2\text{O}_2$	1	0.1%	0.000	p. w.
92	$\text{HOCO} + \text{NO} = \text{CO}_2 + \text{HNO}$	1	0.1%	0.000	p. w.
93	$\text{NO}_2 + \text{NO} = \text{N}_2\text{O} + \text{O}_2$	1	0.1%	0.000	p. w.
94	$\text{N}_2\text{O} + \text{H} = \text{OH}^* + \text{N}_2$	1	0.1%	0.000	p. w.
95	$\text{N}_2\text{O} + \text{OH} = \text{HNO} + \text{NO}$	1	0.1%	0.000	p. w.
96	$\text{NO}_2 + \text{O} + \text{M} = \text{NO}_3 + \text{M}$	1	0.1%	0.001	p. w.
97	$\text{NO}_3 + \text{O} = \text{NO}_2 + \text{O}_2$	1	0.1%	0.000	p. w.
98	$\text{NO}_3 + \text{OH} = \text{NO}_2 + \text{HO}_2$	1	0.1%	0.000	p. w.
99	$\text{HON} + \text{H} = \text{HNO} + \text{H}$	1	0.1%	0.001	p. w.
100	$\text{HON} + \text{O} = \text{NO} + \text{OH}$	1	0.1%	0.001	p. w.
101	$\text{HON} + \text{OH} = \text{HONO} + \text{H}$	1	0.1%	0.000	p. w.
102	$\text{HONO} + \text{NH}_2 = \text{NO}_2 + \text{NH}_3$	1	0.1%	0.000	p. w.
103	$\text{HONO} + \text{HONO} \rightarrow \text{NO} + \text{NO}_2 + \text{H}_2\text{O}$	1	0.1%	0.000	p. w.
104	$\text{HNO}_2 + \text{O} = \text{NO}_2 + \text{OH}$	1	0.1%	0.000	p. w.
105	$\text{HNO}_3 + \text{H} = \text{NO}_2 + \text{H}_2\text{O}$	1	0.1%	0.000	p. w.
106	$\text{HNO}_3 + \text{H} = \text{HONO} + \text{OH}$	1	0.1%	0.000	p. w.
107	$\text{NH}_3 + \text{O} = \text{NH}_2 + \text{OH}$	1	0.1%	0.000	p. w.
108	$\text{DUP}_1\text{NH}_2 + \text{O} = \text{NH} + \text{OH}$	1	0.1%	0.001	p. w.
109	$\text{NH}_2 + \text{OH} = \text{NH} + \text{H}_2\text{O}$	1	0.1%	0.000	p. w.
110	$\text{NH}_2 + \text{N} \rightarrow \text{N}_2 + \text{H} + \text{H}$	1	0.1%	0.000	p. w.
111	$\text{NH}_2 + \text{NO}_2 = \text{H}_2\text{NO} + \text{NO}$	1	0.1%	0.000	p. w.
112	$\text{NH} + \text{O}_2 = \text{HNO}_2$	1	0.1%	0.000	p. w.
113	$\text{NNH} + \text{OH} = \text{N}_2 + \text{H}_2\text{O}$	1	0.1%	0.000	p. w.
114	$\text{NNH} + \text{NH} = \text{N}_2 + \text{NH}_2$	1	0.1%	0.000	p. w.
115	$\text{NNH} + \text{NO} = \text{N}_2 + \text{HNO}$	1	0.1%	0.001	p. w.
116	$\text{H}_2\text{NO} + \text{M} = \text{H}_2 + \text{NO} + \text{M}$	1	0.1%	0.000	p. w.
117	$\text{H}_2\text{NO} + \text{M} = \text{HNO} + \text{H} + \text{M}$	1	0.1%	0.001	p. w.
118	$\text{H}_2\text{NO} + \text{H} = \text{NH}_2 + \text{OH}$	1	0.1%	0.001	p. w.
119	$\text{H}_2\text{NO} + \text{HO}_2 = \text{HNO} + \text{H}_2\text{O}_2$	1	0.1%	0.000	p. w.
120	$\text{NH}_2\text{OH} + \text{O} = \text{HNOH} + \text{OH}$	1	0.1%	0.000	p. w.
121	$\text{NH}_2\text{OH} + \text{NH}_2 = \text{H}_2\text{NO} + \text{NH}_3$	1	0.1%	0.000	p. w.
122	$\text{HNOH} + \text{NH}_2 = \text{HNO} + \text{NH}_3$	1	0.1%	0.000	p. w.
123	$\text{N}_2\text{H}_3 + \text{O} = \text{N}_2\text{H}_2 + \text{OH}$	1	0.1%	0.000	p. w.
124	$\text{N}_2\text{H}_3 + \text{O} = \text{NH}_2 + \text{HNO}$	1	0.1%	0.000	p. w.
125	$\text{N}_2\text{H}_3 + \text{O} \rightarrow \text{NH}_2 + \text{NO} + \text{H}$	1	0.1%	0.000	p. w.
126	$\text{N}_2\text{H}_3 + \text{OH} = \text{H}_2\text{NN} + \text{H}_2\text{O}$	1	0.1%	0.000	p. w.
127	$\text{N}_2\text{H}_3 + \text{HO}_2 = \text{N}_2\text{H}_2 + \text{H}_2\text{O}_2$	1	0.1%	0.000	p. w.
128	$\text{N}_2\text{H}_2 + \text{H} = \text{NNH} + \text{H}_2$	1	0.1%	0.000	p. w.
129	$\text{N}_2\text{H}_2 + \text{O} = \text{NH}_2 + \text{NO}$	1	0.1%	0.000	p. w.
130	$\text{N}_2\text{H}_2 + \text{NO} = \text{N}_2\text{O} + \text{NH}_2$	1	0.1%	0.000	p. w.

131	$\text{H}_2\text{NN} + \text{NH}_2 = \text{NNH} + \text{NH}_3$	1	0.1%	0.000	p. w.
132	$\text{H} + \text{HNO}_2 = \text{H}_2 + \text{NO}_2$	1	0.1%	0.003	p. w.
133	$\text{NH}_3 + \text{H} = \text{NH}_2 + \text{H}_2$	1	0.1%	0.000	p. w.
134	$\text{NH}_2 + \text{NO} = \text{NNH} + \text{OH}$	1	0.1%	0.001	p. w.
135	$\text{HNO} + \text{NO}_2 = \text{NO} + \text{HONO}$	1	0.1%	0.001	p. w.
136	$\text{NH}_2 + \text{H} + \text{M} = \text{NH}_3 + \text{M} \text{ (LP)}$	1	0.1%	0.000	p. w.
137	$\text{HOCO} = \text{CO} + \text{OH} \text{ (PLOG07)}$	1	0.1%	0.001	p. w.
138	$\text{HOCO} = \text{CO}_2 + \text{H} \text{ (PLOG07)}$	1	0.1%	0.001	p. w.
139	$\text{HNO}_2 = \text{HONO} \text{ (PLOG04)}$	1	0.1%	0.000	p. w.
140	$\text{HNO} + \text{OH} = \text{H} + \text{HONO} \text{ (PLOG04)}$	1	0.1%	0.002	p. w.
141	$\text{HNO} + \text{OH} = \text{NO} + \text{H}_2\text{O} \text{ (PLOG04)}$	1	0.1%	0.001	p. w.
142	$\text{H} + \text{HNO}_2 = \text{NO} + \text{H}_2\text{O} \text{ (PLOG04)}$	1	0.1%	0.000	p. w.
143	$\text{H} + \text{HNO}_2 = \text{HNO} + \text{OH} \text{ (PLOG04)}$	1	0.1%	0.000	p. w.
144	$\text{N}_2\text{H}_2 = \text{NNH} + \text{H} \text{ (PLOG02)}$	1	0.1%	0.000	p. w.
145	$\text{DUP}_2\text{HO}_2 + \text{HO}_2 = \text{H}_2\text{O}_2 + \text{O}_2$	0	0.0%	0.001	p. w.
146	$\text{OH} + \text{OH} + \text{M} = \text{H}_2\text{O}_2 + \text{M}$	0	0.0%	0.000	p. w.
147	$\text{DUP}_1\text{H}_2\text{O}_2 + \text{OH} = \text{H}_2\text{O} + \text{HO}_2$	0	0.0%	0.001	p. w.
148	$\text{HCO} + \text{O} = \text{CO} + \text{OH}$	0	0.0%	0.000	p. w.
149	$\text{HCO} + \text{OH} = \text{CO} + \text{H}_2\text{O}$	0	0.0%	0.001	p. w.
150	$\text{HCO} + \text{HCO} \rightarrow \text{H}_2 + \text{CO} + \text{CO}$	0	0.0%	0.000	p. w.
151	$\text{H} + \text{O} + \text{M} = \text{OH}^* + \text{M}$	0	0.0%	0.000	p. w.
152	$\text{OH}^* + \text{H}_2\text{O} = \text{OH} + \text{H}_2\text{O}$	0	0.0%	0.000	p. w.
153	$\text{OH}^* + \text{H}_2 = \text{OH} + \text{H}_2$	0	0.0%	0.000	p. w.
154	$\text{OH}^* + \text{N}_2 = \text{OH} + \text{N}_2$	0	0.0%	0.000	p. w.
155	$\text{OH}^* + \text{OH} = \text{OH} + \text{OH}$	0	0.0%	0.000	p. w.
156	$\text{OH}^* + \text{H} = \text{OH} + \text{H}$	0	0.0%	0.000	p. w.
157	$\text{OH}^* + \text{Ar} = \text{OH} + \text{AR}$	0	0.0%	0.000	p. w.
158	$\text{OH}^* = \text{OH}$	0	0.0%	0.000	p. w.
159	$\text{OH}^* + \text{O}_2 = \text{OH} + \text{O}_2$	0	0.0%	0.000	p. w.
160	$\text{OH}^* + \text{CH}_4 = \text{OH} + \text{CH}_4$	0	0.0%	0.000	p. w.
161	$\text{HOCO} + \text{H} = \text{CO}_2 + \text{H}_2$	0	0.0%	0.000	p. w.
162	$\text{DUP}_2\text{HOCO} + \text{OH} = \text{CO}_2 + \text{H}_2\text{O}$	0	0.0%	0.000	p. w.
163	$\text{HOCO} + \text{CH}_3 = \text{CO}_2 + \text{CH}_4$	0	0.0%	0.000	p. w.
164	$\text{N}_2 + \text{M} = \text{N} + \text{N} + \text{M}$	0	0.0%	0.000	p. w.
165	$\text{N} + \text{O} + \text{M} = \text{NO} + \text{M}$	0	0.0%	0.000	p. w.
166	$\text{NO}_2 + \text{N} = \text{N}_2\text{O} + \text{O}$	0	0.0%	0.000	p. w.
167	$\text{N}_2\text{O} + \text{OH} = \text{HO}_2 + \text{N}_2$	0	0.0%	0.000	p. w.
168	$\text{N}_2\text{O} + \text{N} = \text{N}_2 + \text{NO}$	0	0.0%	0.000	p. w.
169	$\text{N}_2\text{O} + \text{NO} = \text{NO}_2 + \text{N}_2$	0	0.0%	0.000	p. w.
170	$\text{NO}_3 + \text{H} = \text{NO}_2 + \text{OH}$	0	0.0%	0.000	p. w.
171	$\text{NO}_3 + \text{HO}_2 \rightarrow \text{NO}_2 + \text{O}_2 + \text{OH}$	0	0.0%	0.000	p. w.
172	$\text{HNO} + \text{N} = \text{NO} + \text{NH}$	0	0.0%	0.000	p. w.
173	$\text{HNO} + \text{HNO} = \text{N}_2\text{O} + \text{H}_2\text{O}$	0	0.0%	0.000	p. w.
174	$\text{HON} + \text{M} = \text{NO} + \text{H} + \text{M}$	0	0.0%	0.001	p. w.
175	$\text{HON} + \text{O}_2 = \text{NO}_2 + \text{OH}$	0	0.0%	0.000	p. w.
176	$\text{HONO} + \text{O} = \text{NO}_2 + \text{OH}$	0	0.0%	0.001	p. w.

177	$\text{HONO} + \text{NO}_2 = \text{HONO}_2 + \text{NO}$	0	0.0%	0.000	p. w.
178	$\text{NO}_2 + \text{OH} + \text{M} = \text{HONO}_2 + \text{M}$	0	0.0%	0.000	p. w.
179	$\text{HONO}_2 + \text{H} = \text{NO}_3 + \text{H}_2$	0	0.0%	0.000	p. w.
180	$\text{HONO}_2 + \text{H} = \text{NO}_2 + \text{H}_2\text{O}$	0	0.0%	0.000	p. w.
181	$\text{HONO}_2 + \text{H} = \text{HONO} + \text{OH}$	0	0.0%	0.000	p. w.
182	$\text{HONO}_2 + \text{OH} = \text{NO}_3 + \text{H}_2\text{O}$	0	0.0%	0.000	p. w.
183	$\text{HNO}_3 + \text{H} = \text{NO}_3 + \text{H}_2$	0	0.0%	0.000	p. w.
184	$\text{HNO}_3 + \text{OH} = \text{NO}_3 + \text{H}_2\text{O}$	0	0.0%	0.000	p. w.
185	$\text{NH}_3 + \text{HO}_2 = \text{NH}_2 + \text{H}_2\text{O}_2$	0	0.0%	0.000	p. w.
186	$\text{NH}_2 + \text{O}_2 = \text{H}_2\text{NO} + \text{O}$	0	0.0%	0.000	p. w.
187	$\text{NH}_2 + \text{O}_2 = \text{HNO} + \text{OH}$	0	0.0%	0.000	p. w.
188	$\text{NH}_2 + \text{NH}_2 = \text{NH}_3 + \text{NH}$	0	0.0%	0.000	p. w.
189	$\text{NH}_2 + \text{NH}_2 = \text{N}_2\text{H}_2 + \text{H}_2$	0	0.0%	0.000	p. w.
190	$\text{NH}_2 + \text{NH}_2 = \text{H}_2\text{NN} + \text{H}_2$	0	0.0%	0.000	p. w.
191	$\text{NH}_2 + \text{NH} = \text{NH}_3 + \text{N}$	0	0.0%	0.000	p. w.
192	$\text{NH}_2 + \text{NH} = \text{N}_2\text{H}_2 + \text{H}$	0	0.0%	0.000	p. w.
193	$\text{NH}_2 + \text{NO}_2 = \text{N}_2\text{O} + \text{H}_2\text{O}$	0	0.0%	0.000	p. w.
194	$\text{NH} + \text{O}_2 = \text{NO} + \text{OH}$	0	0.0%	0.001	p. w.
195	$\text{NH} + \text{O}_2 = \text{HONO}$	0	0.0%	0.000	p. w.
196	$\text{NH} + \text{NH} = \text{NH}_2 + \text{N}$	0	0.0%	0.000	p. w.
197	$\text{NH} + \text{N} = \text{N}_2 + \text{H}$	0	0.0%	0.000	p. w.
198	$\text{NH} + \text{HONO} = \text{NH}_2 + \text{NO}_2$	0	0.0%	0.000	p. w.
199	$\text{NH} + \text{NO}_2 = \text{HNO} + \text{NO}$	0	0.0%	0.000	p. w.
200	$\text{NH} + \text{NO}_2 = \text{N}_2\text{O} + \text{OH}$	0	0.0%	0.000	p. w.
201	$\text{NNH} + \text{H} = \text{N}_2 + \text{H}_2$	0	0.0%	0.000	p. w.
202	$\text{NNH} + \text{O} = \text{N}_2 + \text{OH}$	0	0.0%	0.000	p. w.
203	$\text{NNH} + \text{NH}_2 = \text{N}_2 + \text{NH}_3$	0	0.0%	0.000	p. w.
204	$\text{H}_2\text{NO} + \text{M} = \text{HNOH} + \text{M}$	0	0.0%	0.000	p. w.
205	$\text{H}_2\text{NO} + \text{H} = \text{HNO} + \text{H}_2$	0	0.0%	0.000	p. w.
206	$\text{H}_2\text{NO} + \text{O} = \text{HNO} + \text{OH}$	0	0.0%	0.000	p. w.
207	$\text{H}_2\text{NO} + \text{OH} = \text{HNO} + \text{H}_2\text{O}$	0	0.0%	0.000	p. w.
208	$\text{H}_2\text{NO} + \text{NO} = \text{HNO} + \text{HNO}$	0	0.0%	0.000	p. w.
209	$\text{H}_2\text{NO} + \text{NH}_2 = \text{HNO} + \text{NH}_3$	0	0.0%	0.000	p. w.
210	$\text{H}_2\text{NO} + \text{NO}_2 = \text{HONO} + \text{HNO}$	0	0.0%	0.000	p. w.
211	$\text{NH}_2\text{OH} + \text{M} = \text{NH}_2 + \text{OH} + \text{M}$	0	0.0%	0.000	p. w.
212	$\text{NH}_2\text{OH} + \text{H} = \text{HNOH} + \text{H}_2$	0	0.0%	0.000	p. w.
213	$\text{NH}_2\text{OH} + \text{H} = \text{H}_2\text{NO} + \text{H}_2$	0	0.0%	0.000	p. w.
214	$\text{NH}_2\text{OH} + \text{O} = \text{H}_2\text{NO} + \text{OH}$	0	0.0%	0.000	p. w.
215	$\text{NH}_2\text{OH} + \text{OH} = \text{HNOH} + \text{H}_2\text{O}$	0	0.0%	0.000	p. w.
216	$\text{NH}_2\text{OH} + \text{OH} = \text{H}_2\text{NO} + \text{H}_2\text{O}$	0	0.0%	0.000	p. w.
217	$\text{NH}_2\text{OH} + \text{HO}_2 = \text{HNOH} + \text{H}_2\text{O}_2$	0	0.0%	0.000	p. w.
218	$\text{NH}_2\text{OH} + \text{HO}_2 = \text{H}_2\text{NO} + \text{H}_2\text{O}_2$	0	0.0%	0.000	p. w.
219	$\text{NH}_2\text{OH} + \text{NH}_2 = \text{HNOH} + \text{NH}_3$	0	0.0%	0.000	p. w.
220	$\text{NH}_2\text{OH} + \text{NH} = \text{HNOH} + \text{NH}_2$	0	0.0%	0.000	p. w.
221	$\text{NH}_2\text{OH} + \text{NH} = \text{H}_2\text{NO} + \text{NH}_2$	0	0.0%	0.000	p. w.
222	$\text{HNOH} + \text{M} = \text{HNO} + \text{H} + \text{M}$	0	0.0%	0.000	p. w.

223	$\text{HNOH} + \text{H} = \text{NH}_2 + \text{OH}$	0	0.0%	0.000	p. w.
224	$\text{HNOH} + \text{H} = \text{HNO} + \text{H}_2$	0	0.0%	0.000	p. w.
225	$\text{DUP}_1\text{-HNOH} + \text{O} = \text{HNO} + \text{OH}$	0	0.0%	0.000	p. w.
226	$\text{DUP}_2\text{-HNOH} + \text{O} = \text{HNO} + \text{OH}$	0	0.0%	0.000	p. w.
227	$\text{HNOH} + \text{OH} = \text{HNO} + \text{H}_2\text{O}$	0	0.0%	0.000	p. w.
228	$\text{HNOH} + \text{HO}_2 = \text{HNO} + \text{H}_2\text{O}_2$	0	0.0%	0.000	p. w.
229	$\text{HNOH} + \text{O}_2 = \text{HNO} + \text{HO}_2$	0	0.0%	0.000	p. w.
230	$\text{HNOH} + \text{NH}_2 = \text{N}_2\text{H}_3 + \text{OH}$	0	0.0%	0.000	p. w.
231	$\text{HNOH} + \text{NO}_2 = \text{HNO} + \text{HONO}$	0	0.0%	0.000	p. w.
232	$\text{NH}_2 + \text{NH}_2 + \text{M} = \text{N}_2\text{H}_4 + \text{M}$	0	0.0%	0.000	p. w.
233	$\text{N}_2\text{H}_4 + \text{H} = \text{N}_2\text{H}_3 + \text{H}_2$	0	0.0%	0.000	p. w.
234	$\text{N}_2\text{H}_4 + \text{O} = \text{N}_2\text{H}_3 + \text{OH}$	0	0.0%	0.000	p. w.
235	$\text{N}_2\text{H}_4 + \text{O} = \text{N}_2\text{H}_2 + \text{H}_2\text{O}$	0	0.0%	0.000	p. w.
236	$\text{N}_2\text{H}_4 + \text{OH} = \text{N}_2\text{H}_3 + \text{H}_2\text{O}$	0	0.0%	0.000	p. w.
237	$\text{N}_2\text{H}_4 + \text{NH}_2 = \text{N}_2\text{H}_3 + \text{NH}_3$	0	0.0%	0.000	p. w.
238	$\text{N}_2\text{H}_3 + \text{H} = \text{N}_2\text{H}_2 + \text{H}_2$	0	0.0%	0.000	p. w.
239	$\text{N}_2\text{H}_3 + \text{OH} = \text{N}_2\text{H}_2 + \text{H}_2\text{O}$	0	0.0%	0.000	p. w.
240	$\text{N}_2\text{H}_3 + \text{OH} = \text{NH}_3 + \text{HNO}$	0	0.0%	0.000	p. w.
241	$\text{N}_2\text{H}_3 + \text{HO}_2 = \text{N}_2\text{H}_4 + \text{O}_2$	0	0.0%	0.000	p. w.
242	$\text{N}_2\text{H}_3 + \text{NH}_2 = \text{N}_2\text{H}_2 + \text{NH}_3$	0	0.0%	0.000	p. w.
243	$\text{N}_2\text{H}_3 + \text{NH}_2 = \text{H}_2\text{NN} + \text{NH}_3$	0	0.0%	0.000	p. w.
244	$\text{N}_2\text{H}_3 + \text{NH} = \text{N}_2\text{H}_2 + \text{NH}_2$	0	0.0%	0.000	p. w.
245	$\text{N}_2\text{H}_2 + \text{OH} = \text{NNH} + \text{H}_2\text{O}$	0	0.0%	0.000	p. w.
246	$\text{N}_2\text{H}_2 + \text{NH}_2 = \text{NNH} + \text{NH}_3$	0	0.0%	0.000	p. w.
247	$\text{N}_2\text{H}_2 + \text{NH} = \text{NNH} + \text{NH}_2$	0	0.0%	0.000	p. w.
248	$\text{H}_2\text{NN} = \text{NNH} + \text{H}$	0	0.0%	0.000	p. w.
249	$\text{H}_2\text{NN} + \text{H} = \text{NNH} + \text{H}_2$	0	0.0%	0.000	p. w.
250	$\text{H}_2\text{NN} + \text{H} = \text{N}_2\text{H}_2 + \text{H}$	0	0.0%	0.000	p. w.
251	$\text{H}_2\text{NN} + \text{O} = \text{NNH} + \text{OH}$	0	0.0%	0.000	p. w.
252	$\text{H}_2\text{NN} + \text{O} = \text{NH}_2 + \text{NO}$	0	0.0%	0.000	p. w.
253	$\text{H}_2\text{NN} + \text{OH} = \text{NNH} + \text{H}_2\text{O}$	0	0.0%	0.000	p. w.
254	$\text{H}_2\text{NN} + \text{OH} \rightarrow \text{NH}_2 + \text{NO} + \text{H}$	0	0.0%	0.000	p. w.
255	$\text{H}_2\text{NN} + \text{HO}_2 \rightarrow \text{NH}_2 + \text{NO} + \text{OH}$	0	0.0%	0.000	p. w.
256	$\text{H}_2\text{NN} + \text{HO}_2 = \text{NNH} + \text{H}_2\text{O}_2$	0	0.0%	0.000	p. w.
257	$\text{H}_2\text{NN} + \text{O}_2 = \text{NH}_2 + \text{NO}_2$	0	0.0%	0.000	p. w.
258	$\text{N}_2\text{O}_4 + \text{M} = \text{NO}_2 + \text{NO}_2 + \text{M}$	0	0.0%	0.000	p. w.
259	$\text{N}_2\text{O}_4 + \text{O} = \text{N}_2\text{O}_3 + \text{O}_2$	0	0.0%	0.000	p. w.
260	$\text{N}_2\text{O}_3 + \text{O} = \text{NO}_2 + \text{NO}_2$	0	0.0%	0.000	p. w.
261	$\text{NO} + \text{OH} + \text{M} = \text{HONO} + \text{M}$	0	0.0%	0.001	p. w.
262	$\text{N}_2\text{O} + \text{H}_2 = \text{N}_2 + \text{H}_2\text{O}$	0	0.0%	0.000	p. w.
263	$\text{NH}_3 + \text{OH} = \text{NH}_2 + \text{H}_2\text{O}$	0	0.0%	0.000	p. w.
264	$\text{NH}_2 + \text{H} + \text{M} = \text{NH}_3 + \text{M}$	0	0.0%	0.000	p. w.
265	$\text{NO} + \text{H} + \text{M} = \text{HNO} + \text{M}$	0	0.0%	0.000	p. w.
266	$\text{NH}_2 + \text{HO}_2 = \text{H}_2\text{NO} + \text{OH}$	0	0.0%	0.000	p. w.
267	$\text{NH}_2 + \text{NO} = \text{N}_2 + \text{H}_2\text{O}$	0	0.0%	0.000	p. w.
268	$\text{H}_2\text{NO} + \text{O}_2 = \text{HNO} + \text{HO}_2$	0	0.0%	0.000	p. w.

269	$\text{NH}_2 + \text{HO}_2 = \text{NH}_3 + \text{O}_2$	0	0.0%	0.000	p. w.
270	$\text{OH} + \text{OH} + \text{M} = \text{H}_2\text{O}_2 + \text{M} \text{ (LP)}$	0	0.0%	0.001	syngas
271	$\text{NO}_2 + \text{OH} + \text{M} = \text{HONO}_2 + \text{M} \text{ (LP)}$	0	0.0%	0.000	p. w.
272	$\text{NH}_2\text{OH} + \text{M} = \text{NH}_2 + \text{OH} + \text{M} \text{ (LP)}$	0	0.0%	0.000	p. w.
273	$\text{NH}_2 + \text{NH}_2 + \text{M} = \text{N}_2\text{H}_4 + \text{M} \text{ (LP)}$	0	0.0%	0.000	p. w.
274	$\text{N}_2\text{O}_4 + \text{M} = \text{NO}_2 + \text{NO}_2 + \text{M} \text{ (LP)}$	0	0.0%	0.000	p. w.
275	$\text{HOCO} = \text{CO} + \text{OH} \text{ (PLOG01)}$	0	0.0%	0.000	p. w.
276	$\text{HOCO} = \text{CO} + \text{OH} \text{ (PLOG02)}$	0	0.0%	0.000	p. w.
277	$\text{HOCO} = \text{CO} + \text{OH} \text{ (PLOG03)}$	0	0.0%	0.000	p. w.
278	$\text{HOCO} = \text{CO} + \text{OH} \text{ (PLOG04)}$	0	0.0%	0.000	p. w.
279	$\text{HOCO} = \text{CO} + \text{OH} \text{ (PLOG05)}$	0	0.0%	0.000	p. w.
280	$\text{HOCO} = \text{CO} + \text{OH} \text{ (PLOG08)}$	0	0.0%	0.001	p. w.
281	$\text{HOCO} = \text{CO} + \text{OH} \text{ (PLOG11)}$	0	0.0%	0.000	p. w.
282	$\text{HOCO} = \text{CO} + \text{OH} \text{ (PLOG12)}$	0	0.0%	0.000	p. w.
283	$\text{HOCO} = \text{CO}_2 + \text{H} \text{ (PLOG01)}$	0	0.0%	0.000	p. w.
284	$\text{HOCO} = \text{CO}_2 + \text{H} \text{ (PLOG02)}$	0	0.0%	0.000	p. w.
285	$\text{HOCO} = \text{CO}_2 + \text{H} \text{ (PLOG03)}$	0	0.0%	0.000	p. w.
286	$\text{HOCO} = \text{CO}_2 + \text{H} \text{ (PLOG04)}$	0	0.0%	0.000	p. w.
287	$\text{HOCO} = \text{CO}_2 + \text{H} \text{ (PLOG05)}$	0	0.0%	0.000	p. w.
288	$\text{HOCO} = \text{CO}_2 + \text{H} \text{ (PLOG06)}$	0	0.0%	0.000	p. w.
289	$\text{HOCO} = \text{CO}_2 + \text{H} \text{ (PLOG08)}$	0	0.0%	0.000	p. w.
290	$\text{HOCO} = \text{CO}_2 + \text{H} \text{ (PLOG09)}$	0	0.0%	0.000	p. w.
291	$\text{HOCO} = \text{CO}_2 + \text{H} \text{ (PLOG10)}$	0	0.0%	0.000	p. w.
292	$\text{HOCO} = \text{CO}_2 + \text{H} \text{ (PLOG11)}$	0	0.0%	0.000	p. w.
293	$\text{HOCO} = \text{CO}_2 + \text{H} \text{ (PLOG12)}$	0	0.0%	0.000	p. w.
294	$\text{HOCO} = \text{CO}_2 + \text{H} \text{ (PLOG13)}$	0	0.0%	0.000	p. w.
295	$\text{HNO} + \text{NH}_2 = \text{NO} + \text{NH}_3 \text{ (PLOG01)}$	0	0.0%	0.000	p. w.
296	$\text{HNO} + \text{NH}_2 = \text{NO} + \text{NH}_3 \text{ (PLOG02)}$	0	0.0%	0.000	p. w.
297	$\text{HNO} + \text{NH}_2 = \text{NO} + \text{NH}_3 \text{ (PLOG03)}$	0	0.0%	0.000	p. w.
298	$\text{HNO} + \text{NH}_2 = \text{NO} + \text{NH}_3 \text{ (PLOG04)}$	0	0.0%	0.000	p. w.
299	$\text{HNO} + \text{NH}_2 = \text{NO} + \text{NH}_3 \text{ (PLOG05)}$	0	0.0%	0.000	p. w.
300	$\text{HNO} + \text{NH}_2 = \text{NO} + \text{NH}_3 \text{ (PLOG06)}$	0	0.0%	0.000	p. w.
301	$\text{HNO}_2 = \text{HONO} \text{ (PLOG01)}$	0	0.0%	0.000	p. w.
302	$\text{HNO}_2 = \text{HONO} \text{ (PLOG02)}$	0	0.0%	0.000	p. w.
303	$\text{HNO}_2 = \text{HONO} \text{ (PLOG03)}$	0	0.0%	0.000	p. w.
304	$\text{HNO}_2 = \text{HONO} \text{ (PLOG05)}$	0	0.0%	0.000	p. w.
305	$\text{HNO}_2 = \text{HONO} \text{ (PLOG06)}$	0	0.0%	0.000	p. w.
306	$\text{HNO}_2 = \text{HONO} \text{ (PLOG07)}$	0	0.0%	0.000	p. w.
307	$\text{HNO}_2 = \text{HONO} \text{ (PLOG08)}$	0	0.0%	0.001	p. w.
308	$\text{OH} + \text{NO} = \text{HNO}_2 \text{ (PLOG01)}$	0	0.0%	0.000	p. w.
309	$\text{OH} + \text{NO} = \text{HNO}_2 \text{ (PLOG02)}$	0	0.0%	0.000	p. w.
310	$\text{OH} + \text{NO} = \text{HNO}_2 \text{ (PLOG03)}$	0	0.0%	0.000	p. w.
311	$\text{OH} + \text{NO} = \text{HNO}_2 \text{ (PLOG04)}$	0	0.0%	0.001	p. w.
312	$\text{OH} + \text{NO} = \text{HNO}_2 \text{ (PLOG05)}$	0	0.0%	0.000	p. w.
313	$\text{OH} + \text{NO} = \text{HNO}_2 \text{ (PLOG06)}$	0	0.0%	0.001	p. w.
314	$\text{H} + \text{HONO} = \text{NO} + \text{H}_2\text{O} \text{ (PLOG01)}$	0	0.0%	0.000	p. w.

315	H + HONO = NO + H ₂ O (PLOG02)	0	0.0%	0.000	p. w.
316	H + HONO = NO + H ₂ O (PLOG03)	0	0.0%	0.000	p. w.
317	H + HONO = NO + H ₂ O (PLOG04)	0	0.0%	0.002	p. w.
318	H + HONO = NO + H ₂ O (PLOG05)	0	0.0%	0.000	p. w.
319	H + HONO = NO + H ₂ O (PLOG06)	0	0.0%	0.000	p. w.
320	H + HONO = NO + H ₂ O (PLOG07)	0	0.0%	0.000	p. w.
321	H + HONO = NO + H ₂ O (PLOG08)	0	0.0%	0.000	p. w.
322	HNO + OH = H + HONO (PLOG01)	0	0.0%	0.000	p. w.
323	HNO + OH = H + HONO (PLOG02)	0	0.0%	0.000	p. w.
324	HNO + OH = H + HONO (PLOG03)	0	0.0%	0.000	p. w.
325	HNO + OH = H + HONO (PLOG05)	0	0.0%	0.000	p. w.
326	HNO + OH = H + HONO (PLOG06)	0	0.0%	0.000	p. w.
327	HNO + OH = H + HONO (PLOG07)	0	0.0%	0.000	p. w.
328	HNO + OH = H + HONO (PLOG08)	0	0.0%	0.000	p. w.
329	HNO + OH = NO + H ₂ O (PLOG01)	0	0.0%	0.000	p. w.
330	HNO + OH = NO + H ₂ O (PLOG02)	0	0.0%	0.000	p. w.
331	HNO + OH = NO + H ₂ O (PLOG03)	0	0.0%	0.000	p. w.
332	HNO + OH = NO + H ₂ O (PLOG05)	0	0.0%	0.000	p. w.
333	HNO + OH = NO + H ₂ O (PLOG06)	0	0.0%	0.000	p. w.
334	HNO + OH = NO + H ₂ O (PLOG07)	0	0.0%	0.000	p. w.
335	HNO + OH = NO + H ₂ O (PLOG08)	0	0.0%	0.000	p. w.
336	H + HNO ₂ = NO + H ₂ O (PLOG01)	0	0.0%	0.000	p. w.
337	H + HNO ₂ = NO + H ₂ O (PLOG02)	0	0.0%	0.000	p. w.
338	H + HNO ₂ = NO + H ₂ O (PLOG03)	0	0.0%	0.000	p. w.
339	H + HNO ₂ = NO + H ₂ O (PLOG05)	0	0.0%	0.000	p. w.
340	H + HNO ₂ = NO + H ₂ O (PLOG06)	0	0.0%	0.000	p. w.
341	H + HNO ₂ = NO + H ₂ O (PLOG07)	0	0.0%	0.000	p. w.
342	H + HNO ₂ = NO + H ₂ O (PLOG08)	0	0.0%	0.000	p. w.
343	H + HNO ₂ = HNO + OH (PLOG01)	0	0.0%	0.000	p. w.
344	H + HNO ₂ = HNO + OH (PLOG02)	0	0.0%	0.000	p. w.
345	H + HNO ₂ = HNO + OH (PLOG03)	0	0.0%	0.000	p. w.
346	H + HNO ₂ = HNO + OH (PLOG05)	0	0.0%	0.000	p. w.
347	H + HNO ₂ = HNO + OH (PLOG06)	0	0.0%	0.000	p. w.
348	H + HNO ₂ = HNO + OH (PLOG07)	0	0.0%	0.000	p. w.
349	H + HNO ₂ = HNO + OH (PLOG08)	0	0.0%	0.000	p. w.
350	N ₂ H ₂ = NNH + H (PLOG01)	0	0.0%	0.000	p. w.
351	N ₂ H ₂ = NNH + H (PLOG03)	0	0.0%	0.000	p. w.
352	N ₂ H ₃ = N ₂ H ₂ + H (PLOG01)	0	0.0%	0.000	p. w.
353	N ₂ H ₃ = N ₂ H ₂ + H (PLOG02)	0	0.0%	0.000	p. w.
354	N ₂ H ₃ = N ₂ H ₂ + H (PLOG03)	0	0.0%	0.000	p. w.

^a: Number of data points for which the reaction has $|\tilde{s}\tilde{n}_{ij}| \geq 0.1$.

^b: The 'Count' value normalized by the total number of data points.

^c: The average of the $|\tilde{s}\tilde{n}_{ij}|$ values for all data points for each reaction.

^d: syngas: the rate parameters of this reaction were optimized by Varga et al. [11], H/N/O: the rate parameters of this reaction were optimized by Kovács et al. [106], p. w.: the rate coefficient of this reaction has not yet been optimized by our research group.

Table A11. Results of the local sensitivity analysis performed on the thermodynamic parameters of the Wang2020-ELTE2020 model. Species are ordered according to their frequency values (see below) for each thermodynamic quantity.

All experiments: 1343 data points														
Standard molar heat capacity at 300 K					Standard molar enthalpy at 300 K					Standard molar entropy at 300 K				
Nr.	Species	Count ^a	Frequency ^b	$ \overline{sn}_{ij} ^c$	Nr.	Species	Count ^a	Frequency ^b	$ \overline{sn}_{ij} ^c$	Nr.	Species	Count ^a	Frequency ^b	$ \overline{sn}_{ij} ^c$
1	OH	1151	86.3%	0.724	1	OH	1132	84.9%	0.716	1	OH	1136	85.2%	0.708
2	H ₂ O	960	72.0%	0.368	2	H ₂ O	941	70.5%	0.339	2	H ₂ O	937	70.2%	0.339
3	O	729	54.6%	0.184	3	O	797	59.7%	0.247	3	O	772	57.9%	0.214
4	NO	616	46.2%	0.229	4	H	686	51.4%	0.266	4	NO	666	49.9%	0.263
5	H	595	44.6%	0.173	5	NO	615	46.1%	0.257	5	H	567	42.5%	0.152
6	HONO	471	35.3%	0.203	6	HONO	418	31.3%	0.154	6	HONO	453	34.0%	0.186
7	H ₂	406	30.4%	0.183	7	O ₂	417	31.3%	0.129	7	O ₂	428	32.1%	0.137
8	O ₂	403	30.2%	0.127	8	H ₂	399	29.9%	0.205	8	CO	409	30.7%	0.156
9	CO	392	29.4%	0.139	9	CO	385	28.9%	0.158	9	H ₂	364	27.3%	0.134
10	NO ₂	372	27.9%	0.188	10	NO ₂	313	23.5%	0.154	10	NO ₂	351	26.3%	0.184
11	NH	266	19.9%	0.098	11	NH	272	20.4%	0.116	11	NH	267	20.0%	0.104
12	HNO	223	16.7%	0.095	12	HNO	226	16.9%	0.090	12	HNO	226	16.9%	0.101
13	HOCO	216	16.2%	0.082	13	CO ₂	223	16.7%	0.101	13	CO ₂	208	15.6%	0.098
14	CO ₂	207	15.5%	0.101	14	HOCO	182	13.6%	0.065	14	HOCO	203	15.2%	0.077
15	HO ₂	181	13.6%	0.051	15	HO ₂	169	12.7%	0.047	15	HO ₂	186	13.9%	0.053
16	N ₂ O	99	7.4%	0.043	16	N ₂ O	90	6.7%	0.048	16	N ₂ O	98	7.3%	0.046
17	HNO ₃	90	6.7%	0.023	17	HNO ₂	65	4.9%	0.024	17	HNO ₃	76	5.7%	0.020
18	HONO ₂	79	5.9%	0.036	18	HNO ₃	63	4.7%	0.016	18	HONO ₂	70	5.2%	0.029
19	HNO ₂	65	4.9%	0.024	19	HONO ₂	61	4.6%	0.021	19	HNO ₂	65	4.9%	0.025
20	N ₂	62	4.6%	0.027	20	HCO	50	3.7%	0.016	20	HCO	56	4.2%	0.018
21	HCO	53	4.0%	0.017	21	N ₂	34	2.5%	0.022	21	N ₂	33	2.5%	0.019
22	NO ₃	43	3.2%	0.011	22	NO ₃	30	2.2%	0.008	22	NO ₃	33	2.5%	0.008
23	HON	9	0.7%	0.005	23	N	14	1.0%	0.004	23	N	11	0.8%	0.003
24	N	9	0.7%	0.002	24	NNH	8	0.6%	0.004	24	H ₂ NO	8	0.6%	0.003
25	H ₂ NO	8	0.6%	0.003	25	H ₂ NO	6	0.4%	0.003	25	HON	8	0.6%	0.005

26	NNH	7	0.5%	0.003	26	HON	6	0.4%	0.005	26	NNH	8	0.6%	0.004
27	H ₂ O ₂	5	0.4%	0.005	27	NH ₂	2	0.1%	0.003	27	N ₂ H ₂	3	0.2%	0.001
28	Ar	4	0.3%	0.001	28	H ₂ O ₂	1	0.1%	0.005	28	N ₂ H ₃	2	0.1%	0.001
29	NH ₂	2	0.1%	0.003	29	N ₂ H ₃	1	0.1%	0.001	29	NH ₂	2	0.1%	0.003
30	HNOH	1	0.1%	0.001	30	NH ₂ OH	1	0.1%	0.001	30	H ₂ O ₂	1	0.1%	0.005
31	N ₂ H ₂	1	0.1%	0.000	31	Ar	0	0.0%	0.000	31	N ₂ H ₄	1	0.1%	0.001
32	NH ₂ OH	1	0.1%	0.001	32	CH ₃	0	0.0%	0.000	32	Ar	0	0.0%	0.000
33	OCHO	1	0.1%	0.001	33	CH ₄	0	0.0%	0.000	33	CH ₃	0	0.0%	0.000
34	CH ₃	0	0.0%	0.000	34	H ₂ NN	0	0.0%	0.000	34	CH ₄	0	0.0%	0.000
35	CH ₄	0	0.0%	0.000	35	He	0	0.0%	0.000	35	H ₂ NN	0	0.0%	0.000
36	H ₂ NN	0	0.0%	0.000	36	HNOH	0	0.0%	0.000	36	He	0	0.0%	0.000
37	He	0	0.0%	0.000	37	N ₂ H ₂	0	0.0%	0.000	37	HNOH	0	0.0%	0.000
38	N ₂ H ₃	0	0.0%	0.000	38	N ₂ H ₄	0	0.0%	0.000	38	N ₂ O ₃	0	0.0%	0.000
39	N ₂ H ₄	0	0.0%	0.000	39	N ₂ O ₃	0	0.0%	0.000	39	N ₂ O ₄	0	0.0%	0.000
40	N ₂ O ₃	0	0.0%	0.000	40	N ₂ O ₄	0	0.0%	0.000	40	NH ₂ OH	0	0.0%	0.000
41	N ₂ O ₄	0	0.0%	0.000	41	NH ₃	0	0.0%	0.000	41	NH ₃	0	0.0%	0.000
42	NH ₃	0	0.0%	0.000	42	NO*	0	0.0%	0.000	42	NO*	0	0.0%	0.000
43	NO*	0	0.0%	0.000	43	OCHO	0	0.0%	0.000	43	OCHO	0	0.0%	0.000
44	OH*	0	0.0%	0.000	44	OH*	0	0.0%	0.000	44	OH*	0	0.0%	0.000

^a: Number of data points for which the species has $|\tilde{s}\tilde{n}_{ij}| \geq 0.1$ or $|\tilde{s}\tilde{s}\tilde{n}_{ij}| \geq 0.1$.

^b: The 'Count' value normalized by the total number of data points.

^c: The average of the $|\tilde{s}\tilde{n}_{ij}|$ or $|\tilde{s}\tilde{s}\tilde{n}_{ij}|$ values for all data points for each species.

References

- [1] C. K. Westbrook, F. L. Dryer, Chemical kinetic modeling of hydrocarbon combustion, *Prog. Energy Combust. Sci.* 10 (1984) 1–57. (URL: [https://doi.org/10.1016/0360-1285\(84\)90118-7](https://doi.org/10.1016/0360-1285(84)90118-7))
- [2] B. M. Jenkins, L. L. Baxter, T. R. Miles, T. R. Miles, Combustion properties of biomass, *Fuel Process. Technol.* 54 (1998) 17–46. (URL: [https://doi.org/10.1016/S0378-3820\(97\)00059-3](https://doi.org/10.1016/S0378-3820(97)00059-3))
- [3] J. Werther, M. Saenger, E.-U. Hartge, T. Ogada, Z. Siagi, Combustion of agricultural residues, *Prog. Energy Combust. Sci.* 26 (2000) 1–27. (URL: [https://doi.org/10.1016/S0360-1285\(99\)00005-2](https://doi.org/10.1016/S0360-1285(99)00005-2))
- [4] R. Zanzi, K. Sjöström, E. Björnbom, Rapid high-temperature pyrolysis of biomass in a free-fall reactor, *Fuel* 75 (1996) 545–550. (URL: [https://doi.org/10.1016/0016-2361\(95\)00304-5](https://doi.org/10.1016/0016-2361(95)00304-5))
- [5] K. J. Whitty, H. R. Zhang, E. G. Eddings, Emissions from Syngas Combustion, *Combust. Sci. Technol.* 180 (2008) 1117–1136. (URL: <https://doi.org/10.1080/00102200801963326>)
- [6] S. G. Davis, A. V. Joshi, H. Wang, F. Egolfopoulos, An optimized kinetic model of H₂/CO combustion, *Proc. Combust. Inst.* 30 (2005) 1283–1292. (URL: <https://doi.org/10.1016/j.proci.2004.08.252>)
- [7] A. Kéromnès, W. K. Metcalfe, K. A. Heufer, N. Donohoe, A. K. Das, C.-J. Sung, J. Herzler, C. Naumann, P. Griebel, O. Mathieu, M. C. Krejci, E. L. Petersen, W. J. Pitz, H. J. Curran, An experimental and detailed chemical kinetic modeling study of hydrogen and syngas mixture oxidation at elevated pressures, *Combust. Flame* 160 (2013) 995–1011. (URL: <https://doi.org/10.1016/j.combustflame.2013.01.001>)
- [8] H. Sun, S. I. Yang, G. Jomaas, C. K. Law, High-pressure laminar flame speeds and kinetic modeling of carbon monoxide/hydrogen combustion, *Proc. Combust. Inst.* 31 (2007) 439–446. (URL: <https://doi.org/10.1016/j.proci.2006.07.193>)
- [9] J. Li, Z. Zhao, A. Kazakov, M. Chaos, F. L. Dryer, J. J. Scire, A comprehensive kinetic mechanism for CO, CH₂O, and CH₃OH combustion, *Int. J. Chem. Kinet.* 39 (2007) 109–136. (URL: <https://doi.org/10.1002/kin.20218>)
- [10] X. Li, X. You, F. Wu, C. K. Law, Uncertainty analysis of the kinetic model prediction for high-pressure H₂/CO combustion, *Proc. Combust. Inst.* 35 (2015) 617–624. (URL: <https://doi.org/10.1016/j.proci.2014.07.047>)
- [11] T. Varga, C. Olm, T. Nagy, I. G. Zsély, É. Valkó, R. Pálvölgyi, H. J. Curran, T. Turányi, Development of a Joint Hydrogen and Syngas Combustion Mechanism Based on an Optimization Approach, *Int. J. Chem. Kinet.* 48 (2016) 407–422. (URL: <https://doi.org/10.1002/kin.21006>)
- [12] J. H. Seinfeld, S. N. Pandis, Atmospheric Chemistry and Physics: From Air Pollution to Climate Change, Ed. 3, Wiley, New Jersey, USA, 1998. (ISBN: 978-1-118-94740-1)
- [13] O. Mathieu, A. Levacque, E. L. Petersen, Effects of NO₂ addition on hydrogen ignition behind reflected shock waves, *Proc. Combust. Inst.* 34 (2013) 633–640. (URL: <https://doi.org/10.1016/j.proci.2012.05.067>)

- [14] C. L. Rasmussen, J. Hansen, P. Marshall, P. Glarborg, Experimental measurements and kinetic modeling of CO/H₂/O₂/NO_x conversion at high pressure, *Int. J. Chem. Kinet.* 40 (2008) 454–480. (URL: <https://doi.org/10.1002/kin.20327>)
- [15] M. A. Mueller, R. A. Yetter, F. L. Dryer, Flow reactor studies and kinetic modeling of the H₂/O₂/NO_x and CO/H₂O/O₂/NO_x reactions, *Int. J. Chem. Kinet.* 31 (1999) 705–724. (URL: <https://onlinelibrary.wiley.com/doi/10.1002/%28SICI%291097-4601%281999%2931%3A10%3C705%3A%3AAID-JCK4%3E3.0.CO%3B2-%23>)
- [16] J.-B. Masurier, F. Foucher, G. Dayma, P. Dagaut, Investigation of iso-octane combustion in a homogeneous charge compression ignition engine seeded by ozone, nitric oxide and nitrogen dioxide, *Proc. Combust. Inst.* 35 (2015) 3125–3132. (URL: <https://doi.org/10.1016/j.proci.2014.05.060>)
- [17] F. Contino, F. Foucher, P. Dagaut, T. Lucchini, G. D’Errico, C. Mounaïm-Rousselle, Experimental and numerical analysis of nitric oxide effect on the ignition of iso-octane in a single cylinder HCCI engine, *Combust. Flame* 160 (2013) 1476–1483. (URL: <https://doi.org/10.1016/j.combustflame.2013.02.028>)
- [18] Y. Song, L. Marrodán, N. Vin, O. Herbinet, E. Assaf, C. Fittschen, A. Stagni, T. Faravelli, M. U. Alzueta, F. Battin-Leclerc, The sensitizing effects of NO₂ and NO on methane low temperature oxidation in a jet stirred reactor, *Proc. Combust. Inst.* 37 (2019) 667–675. (URL: <https://doi.org/10.1016/j.proci.2018.06.115>)
- [19] K. P. Shrestha, L. Seidel, T. Zeuch, F. Mauss, Kinetic Modeling of NO_x Formation and Consumption during Methanol and Ethanol Oxidation, *Combust. Sci. Technol.* 191 (2019) 1627–1659. (URL: <https://doi.org/10.1080/00102202.2019.1606804>)
- [20] S. F. Ahmed, J. Santner, F. L. Dryer, B. Padak, T. I. Farouk, Computational Study of NO_x Formation at Conditions Relevant to Gas Turbine Operation, Part 2: NO_x in High Hydrogen Content Fuel Combustion at Elevated Pressure, *Energy Fuels* 30 (2016) 7691–7703. (URL: <https://doi.org/10.1021/acs.energyfuels.6b00421>)
- [21] T. Turányi, Chemical Kinetics Laboratory, ELTE, 2016. <http://garfield.chem.elte.hu/> (accessed at: 19/05/2021)
- [22] S. P. Karkach, V. I. Osheroov, Ab initio analysis of the transition states on the lowest triplet H₂O₂ potential surface, *J. Chem. Phys.* 110 (1999) 11918–11927. (URL: <https://doi.org/10.1063/1.479131>)
- [23] J. Chai, C. F. Goldsmith, Rate coefficients for fuel + NO₂: Predictive kinetics for HONO and HNO₂ formation, *Proc. Combust. Inst.* 36 (2017) 617–626. (URL: <https://doi.org/10.1016/j.proci.2016.06.133>)
- [24] S. J. Klippenstein, L. B. Harding, P. Glarborg, J. A. Miller, The role of NNH in NO formation and control, *Combust. Flame* 158 (2011) 774–789. (URL: <https://doi.org/10.1016/j.combustflame.2010.12.013>)
- [25] J. Troe, Detailed modeling of the temperature and pressure dependence of the reaction H+O₂ (+M)→HO₂ (+M), *Proc. Combust. Inst.* 28 (2000) 1463–1469. (URL: [https://doi.org/10.1016/S0082-0784\(00\)80542-1](https://doi.org/10.1016/S0082-0784(00)80542-1))
- [26] S. Javoy, R. Mevel, C. E. Paillard, A study of N₂O decomposition rate constant at high temperature: Application to the reduction of nitrous oxide by hydrogen, *Int. J. Chem. Kinet.* 41 (2009) 357–375. (URL: <https://doi.org/10.1002/kin.20401>)
- [27] C. R. Mulvihill, O. Mathieu, E. L. Petersen, The unimportance of the reaction H₂ + N₂O ⇌ H₂O + N₂: A shock-tube study using H₂O time histories and ignition delay

- times, *Combust. Flame* 196 (2018) 478–486. (URL: <https://doi.org/10.1016/j.combustflame.2018.07.003>)
- [28] M.-C. Su, S. S. Kumaran, K. P. Lim, J. V. Michael, A. F. Wagner, L. B. Harding, D.-C. Fang, Rate Constants, $1100 \leq T \leq 2000$ K, for $\text{H} + \text{NO}_2 \rightarrow \text{OH} + \text{NO}$ Using Two Shock Tube Techniques: Comparison of Theory to Experiment, *J. Phys. Chem. A* 106 (2002) 8261–8270. (URL: <https://doi.org/10.1021/jp0141023>)
- [29] F. M. Haas, F. L. Dryer, Rate coefficient determinations for $\text{H} + \text{NO}_2 \rightarrow \text{OH} + \text{NO}$ from high pressure flow reactor measurements, *J. Phys. Chem. A* 119 (2015) 7792–7801. (URL: <https://doi.org/10.1021/acs.jpca.5b01231>)
- [30] C. Olm, I. G. Zsély, R. Pálvölgyi, T. Varga, T. Nagy, H. J. Curran, T. Turányi, Comparison of the performance of several recent hydrogen combustion mechanisms, *Combust. Flame* 161 (2014) 2219–2234. (URL: <https://doi.org/10.1016/j.combustflame.2014.03.006>)
- [31] T. Turányi, A. S. Tomlin, Analysis of Kinetic Reaction Mechanisms, Ed., Springer-Verlag, Berlin, Heidelberg, 2014. (ISBN: 978-3-662-44561-7)
- [32] P. Dagaut, M. Cathonnet, J. C. Boettner, F. Gaillard, Kinetic modeling of ethylene oxidation, *Combust. Flame* 71 (1988) 295–312. (URL: [https://doi.org/10.1016/0010-2180\(88\)90065-X](https://doi.org/10.1016/0010-2180(88)90065-X))
- [33] P. Dagaut, F. Lecomte, Experiments and Kinetic Modeling Study of NO-Reburning by Gases from Biomass Pyrolysis in a JSR, *Energy Fuels* 17 (2003) 608–613. (URL: <https://doi.org/10.1021/ef020256l>)
- [34] P. Dagaut, F. Lecomte, J. Mieritz, P. Glarborg, Experimental and kinetic modeling study of the effect of NO and SO₂ on the oxidation of CO–H₂ mixtures, *Int. J. Chem. Kinet.* 35 (2003) 564–575. (URL: <https://doi.org/10.1002/kin.10154>)
- [35] F. Battin-Leclerc, J. M. Simmie, E. Blurock (Eds.), Cleaner Combustion – Developing Detailed Chemical Kinetic Models, Ed. 1, Springer-Verlag, London, UK, 2013. (ISBN: 978-1-4471-5306-1)
- [36] Y. Zhang, Z. Huang, L. Wei, J. Zhang, C. K. Law, Experimental and modeling study on ignition delays of lean mixtures of methane, hydrogen, oxygen, and argon at elevated pressures, *Combust. Flame* 159 (2012) 918–931. (URL: <https://doi.org/10.1002/kin.20218>)
- [37] P. Zhang, I. G. Zsély, V. Samu, T. Nagy, T. Turányi, Comparison of Methane Combustion Mechanisms Using Shock Tube and Rapid Compression Machine Ignition Delay Time Measurements, *Energy Fuels* 35 (2021) 12329–12351. (URL: <https://doi.org/10.1021/acs.energyfuels.0c04277>)
- [38] S. M. Burke, U. Burke, R. Mc Donagh, O. Mathieu, I. Osorio, C. Keesee, A. Morones, E. L. Petersen, W. Wang, T. A. DeVerter, M. A. Oehlschlaeger, B. Rhodes, R. K. Hanson, D. F. Davidson, B. W. Weber, C.-J. Sung, J. Santner, Y. Ju, F. M. Haas, F. L. Dryer, E. N. Volkov, E. J. K. Nilsson, A. A. Konnov, M. Alrefae, F. Khaled, A. Farooq, P. Dirrenberger, P.-A. Glaude, F. Battin-Leclerc, H. J. Curran, An experimental and modeling study of propene oxidation. Part 2: Ignition delay time and flame speed measurements, *Combust. Flame* 162 (2015) 296–314. (URL: <https://doi.org/10.1016/j.combustflame.2014.07.032>)
- [39] P. Glarborg, D. Kubel, K. Dam-Johansen, H. M. Chiang, J. W. Bozzelli, Impact of SO₂ and NO on CO oxidation under post-flame conditions, *Int. J. Chem. Kinet.* 28

- (1996) 773–790. (URL: [https://doi.org/10.1002/\(SICI\)1097-4601\(1996\)28:10<773::AID-KIN8>3.0.CO;2-K](https://doi.org/10.1002/(SICI)1097-4601(1996)28:10<773::AID-KIN8>3.0.CO;2-K))
- [40] J. Suhlmann, G. Rotzoll, Experimental characterization of the influence of CO on the high-temperature reduction of NO by NH₃, *Fuel* 72 (1993) 175–179. (URL: [https://doi.org/10.1016/0016-2361\(93\)90394-H](https://doi.org/10.1016/0016-2361(93)90394-H))
- [41] Y. Song, H. Hashemi, J. M. Christensen, C. Zou, P. Marshall, P. Glarborg, Ammonia oxidation at high pressure and intermediate temperatures, *Fuel* 181 (2016) 358–365. (URL: <https://doi.org/10.1016/j.fuel.2016.04.100>)
- [42] D. J. Seery, M. F. Zabielski, Molecular beam sampling-mass spectrometer study of H₂–O₂–NO flames, *Proc. Combust. Inst.* 18 (1981) 397–404. (URL: [https://doi.org/10.1016/S0082-0784\(81\)80044-6](https://doi.org/10.1016/S0082-0784(81)80044-6))
- [43] J. Vandooren, P. J. Van Tiggelen, J.-F. Pauwels, Experimental and modeling studies of a rich H₂/CO/N₂O/Ar flame, *Combust. Flame* 109 (1997) 647–668. (URL: [https://doi.org/10.1016/S0010-2180\(97\)00055-2](https://doi.org/10.1016/S0010-2180(97)00055-2))
- [44] O. A. Powell, P. Papas, C. B. Dreyer, Flame structure measurements of NO in premixed hydrogen–nitrous oxide flames, *Proc. Combust. Inst.* 33 (2011) 1053–1062. (URL: <https://doi.org/10.1016/j.proci.2010.06.042>)
- [45] Holthuis & Associates, Flat Flame Burners, 2013. <https://www.flatflame.com/burner-description.html> (accessed at: 2021/04/02)
- [46] A. M. Dean, D. C. Steiner, E. E. Wang, A shock tube study of the H₂/O₂/CO/Ar and H₂/N₂O/CO/Ar Systems: Measurement of the rate constant for H + N₂O = N₂ + OH, *Combust. Flame* 32 (1978) 73–83. (URL: [https://doi.org/10.1016/0010-2180\(78\)90081-0](https://doi.org/10.1016/0010-2180(78)90081-0))
- [47] M. Kopp, M. Brower, O. Mathieu, E. Petersen, F. Güthe, CO₂* chemiluminescence study at low and elevated pressures., *Appl. Phys. B* 107 (2012) 529–538. (URL: <https://doi.org/10.1007/s00340-012-5051-4>)
- [48] T. Hulgaard, K. Dam-Johansen, Homogeneous nitrous oxide formation and destruction under combustion conditions, *AIChE J.* 39 (1993) 1342–1354. (URL: <https://doi.org/10.1002/aic.690390811>)
- [49] J. Roesler, Kinetic interactions of CO, NO_x, and HCl emissions in postcombustion gases, *Combust. Flame* 100 (1995) 495–504. (URL: [https://doi.org/10.1016/0010-2180\(94\)00228-K](https://doi.org/10.1016/0010-2180(94)00228-K))
- [50] P. Glarborg, D. Kubel, P. G. Kristensen, J. Hansen, K. Dam-Johansen, Interactions of CO, NO_x and H₂O Under Post-Flame Conditions, *Combust. Sci. Technol.* 110–111 (1995) 461–485. (URL: <https://doi.org/10.1080/00102209508951936>)
- [51] M. U. Alzueta, P. Glarborg, K. Dam-Johansen, Low temperature interactions between hydrocarbons and nitric oxide: An experimental study, *Combust. Flame* 109 (1997) 25–36. (URL: [https://doi.org/10.1016/S0010-2180\(96\)00146-0](https://doi.org/10.1016/S0010-2180(96)00146-0))
- [52] P. Glarborg, P. G. Kristensen, K. Dam-Johansen, M. U. Alzueta, A. Millera, R. Bilbao, Nitric Oxide Reduction by Non-hydrocarbon Fuels. Implications for Reburning with Gasification Gases, *Energy Fuels* 14 (2000) 828–838. (URL: <https://doi.org/10.1021/ef990186r>)

- [53] H. Dindi, H.-M. Tsai, M. C. Branch, Combustion mechanism of carbon monoxide–nitrous oxide flames, *Combust. Flame* 87 (1991) 13–20. (URL: [https://doi.org/10.1016/0010-2180\(91\)90023-5](https://doi.org/10.1016/0010-2180(91)90023-5))
- [54] A. F. Sarofim, R. C. Flagan, NO_x control for stationary combustion sources, *Prog. Energy Combust. Sci.* 2 (1976) 1–25. (URL: [https://doi.org/10.1016/0360-1285\(76\)90006-X](https://doi.org/10.1016/0360-1285(76)90006-X))
- [55] A. L. Myerson, F. R. Taylor, B. G. Faunce, Ignition limits and products of the multistage flames of propane-nitrogen dioxide mixtures, *Proc. Combust. Inst.* 6 (1957) 154–163. (URL: [https://doi.org/10.1016/S0082-0784\(57\)80024-1](https://doi.org/10.1016/S0082-0784(57)80024-1))
- [56] J. O. L. Wendt, C. V. Sternling, M. A. Matovich, Reduction of sulfur trioxide and nitrogen oxides by secondary fuel injection, *Proc. Combust. Inst.* 14 (1973) 897–904. (URL: [https://doi.org/10.1016/S0082-0784\(73\)80082-7](https://doi.org/10.1016/S0082-0784(73)80082-7))
- [57] Y. B. Zeldovich, The Oxidation of Nitrogen in Combustion and Explosions, *Acta Physicochimica URSS* 11 (1946) 577–628. (URL: <https://doi.org/10.1515/9781400862979.404>)
- [58] C. P. Fenimore, Formation of nitric oxide in premixed hydrocarbon flames, *Proc. Combust. Inst.* 13 (1971) 373–380. (URL: [https://doi.org/10.1016/S0082-0784\(71\)80040-1](https://doi.org/10.1016/S0082-0784(71)80040-1))
- [59] Q. Cui, K. Morokuma, J. M. Bowman, S. J. Klippenstein, The spin-forbidden reaction $\text{CH}(^2\Pi) + \text{N}_2 \rightarrow \text{HCN} + \text{N}(^4\text{S})$ revisited. II. Nonadiabatic transition state theory and application, *J. Chem. Phys.* 110 (1999) 9469–9482. (URL: <https://doi.org/10.1063/1.478949>)
- [60] L. V. Moskaleva, M. C. Lin, The spin-conserved reaction $\text{CH} + \text{N}_2 \rightarrow \text{H} + \text{NCN}$: A major pathway to prompt NO studied by quantum/statistical theory calculations and kinetic modeling of rate constant, *Proc. Combust. Inst.* 28 (2000) 2393–2401. (URL: [https://doi.org/10.1016/S0082-0784\(00\)80652-9](https://doi.org/10.1016/S0082-0784(00)80652-9))
- [61] A. A. Konnov, Implementation of the NCN pathway of prompt-NO formation in the detailed reaction mechanism, *Combust. Flame* 156 (2009) 2093–2105. (URL: <https://doi.org/10.1016/j.combustflame.2009.03.016>)
- [62] ANSYS, Chemkin Theory Manual 17.0 (15151), *Reaction Design*, San Diego, CA, 2015. (URL: https://personal.ems.psu.edu/~radovic/ChemKin_Theory_PaSR.pdf)
- [63] R. J. Kee, F. M. Rupley, J. A. Miller, M. E. Coltrin, J. F. Grcar, E. Meeks, H. K. Moffat, A. E. Lutz, G. Dixon-Lewis, M. D. Smooke, J. Warnatz, G. H. Evans, R. S. Larson, R. E. Mitchell, L. R. Petzold, W. C. Reynolds, M. Caracotsios, W. E. Stewart, P. Glarborg, C. Wang, C. L. McLellan, O. Adigun, W. G. H. C. P. Chou, S. F. Miller, P. Ho, P. D. Young, D. J. Young, CHEMKIN Release 4.0.2: Theory Manual, *Reaction Design*, San Diego, CA, 2005.
- [64] R. J. Kee, F. M. Rupley, J. A. Miller, M. E. Coltrin, J. F. Grcar, E. Meeks, H. K. M. A. E. Lutz, G. Dixon-Lewis, M. D. Smooke, J. Warnatz, G. H. Evans, R. S. Larson, R. E. Mitchell, L. R. Petzold, W. C. Reynolds, M. Caracotsios, W. E. Stewart, P. Glarborg, C. Wang, C. L. McLellan, O. Adigun, W. G. Houf, C. P. Chou, S. F. Miller, P. Ho, P. D. Young, D. J. Young, CHEMKIN Release 4.0.2: Input Manual, *Reaction Design*, San Diego, CA, 2005.
- [65] S. Gordon, B. J. McBride, Computer program for calculation of complex chemical equilibrium compositions, rocket performance, incident and reflected shocks and

- Chapman-Jouguet detonations (NASA-SP-273), *NASA Lewis Research Center*, Cleveland, Ohio, 1971. (URL: <https://www1.grc.nasa.gov/research-and-engineering/ceaweb/publications/>)
- [66] S. Gordon, B. J. McBride, Computer program for calculation of complex chemical equilibrium compositions and applications. Part 1: Analysis (NASA-RP-1311), *NASA Lewis Research Center*, Cleveland, Ohio, 1994. (URL: <https://ntrs.nasa.gov/citations/19950013764>)
- [67] E. Keszegi, *Chemical Thermodynamics – An Introduction*, Ed. 1, *Springer-Verlag*, Berlin, Heidelberg, 2012. (ISBN: 978-3-642-19863-2)
- [68] F. A. Lindemann, S. Arrhenius, I. Langmuir, N. R. Dhar, J. Perrin, W. C. Mcc. Lewis, Discussion on “the radiation theory of chemical action”, *Trans. Faraday Soc.* 17 (1922) 598–606. (URL: <https://doi.org/10.1039/TF9221700598>)
- [69] J. Troe, Theory of Thermal Unimolecular Reactions in the Fall-off Range. I. Strong Collision Rate Constants, *Ber. Bunsenges. Phys. Chem.* 87 (1983) 161–169. (URL: <https://doi.org/10.1002/bbpc.19830870217>)
- [70] R. G. Gilbert, K. Luther, J. Troe, Theory of Thermal Unimolecular Reactions in the Fall-off Range. II. Weak Collision Rate Constants, *Ber. Bunsenges. Phys. Chem.* 87 (1983) 169–177. (URL: <https://doi.org/10.1002/bbpc.19830870218>)
- [71] P. H. Stewart, C. W. Larson, D. M. Golden, Pressure and temperature dependence of reactions proceeding via a bound complex. 2. Application to $2\text{CH}_3 \rightarrow \text{C}_2\text{H}_5 + \text{H}$, *Combust. Flame* 75 (1989) 25–31. (URL: [https://doi.org/10.1016/0010-2180\(89\)90084-9](https://doi.org/10.1016/0010-2180(89)90084-9))
- [72] J. Zádor, C. A. Taatjes, R. X. Fernandes, Kinetics of elementary reactions in low-temperature autoignition chemistry, *Prog. Energy Combust. Sci.* 37 (2011) 371–421. (URL: <https://doi.org/10.1016/j.pecs.2010.06.006>)
- [73] T. J. Rivlin, *Chebyshev Polynomials: From Approximation Theory to Algebra and Number Theory*, Ed. 2, *Wiley-Interscience*, New York, USA, 1990. (ISBN: 9780471628965)
- [74] P. K. Venkatesh, A. Y. Chang, A. M. Dean, M. H. Cohen, R. W. Carr, Parameterization of pressure- and temperature-dependent kinetics in multiple well reactions, *AIChE J.* 43 (1997) 1331–1340. (URL: <https://doi.org/10.1002/aic.690430522>)
- [75] P. Glarborg, J. A. Miller, B. Ruscic, S. J. Klippenstein, Modeling nitrogen chemistry in combustion, *Prog. Energy Combust. Sci.* 67 (2018) 31–68. (URL: <https://doi.org/10.1016/j.pecs.2018.01.002>)
- [76] C. Olm, I. G. Zsély, T. Varga, H. J. Curran, T. Turányi, Comparison of the performance of several recent syngas combustion mechanisms, *Combust. Flame* 162 (2015) 1793–1812. (URL: <https://doi.org/10.1016/j.combustflame.2014.12.001>)
- [77] Y. Zhang, O. Mathieu, E. L. Petersen, G. Bourque, H. J. Curran, Assessing the predictions of a NO_x kinetic mechanism on recent hydrogen and syngas experimental data, *Combust. Flame* 182 (2017) 122–141. (URL: <https://doi.org/10.1016/j.combustflame.2017.03.019>)
- [78] G. P. Smith, D. M. Golden, M. Frenklach, N. W. Moriarty, B. Eiteneer, M. Goldenberg, C. T. Bowman, R. K. Hanson, S. Song, W. C. G. Jr., V. V. Lissianski, Z.

- Qin, Current and Future Releases of GRI-Mech, <http://combustion.berkeley.edu/gri-mech/releases.html> (accessed at: 2021/04/04.)
- [79] Mechanical and Aerospace Engineering (Combustion Research), University of California at San Diego, Chemical-Kinetic Mechanisms for Combustion Applications, San Diego Mechanism web page, 2012. <http://web.eng.ucsd.edu/mae/groups/combustion/mechanism.html> (accessed at: 2021/04/04.)
- [80] Z. Tian, Y. Li, L. Zhang, P. Glarborg, F. Qi, An experimental and kinetic modeling study of premixed $\text{NH}_3/\text{CH}_4/\text{O}_2/\text{Ar}$ flames at low pressure, *Combust. Flame* 156 (2009) 1413–1426. (URL: <https://doi.org/10.1016/j.combustflame.2009.03.005>)
- [81] The CRECK Modeling Group (Politecnico di Milano), Previous kinetic mechanisms: Version 1412, December 2014, 2014. <http://creckmodeling.chem.polimi.it/> (accessed at: 2021/04/13)
- [82] A. Frassoldati, T. Faravelli, E. Ranzi, The ignition, combustion and flame structure of carbon monoxide/hydrogen mixtures. Note 1: Detailed kinetic modeling of syngas combustion also in presence of nitrogen compounds, *Int. J. Hydrog. Energy* 32 (2007) 3471–3485. (URL: <https://doi.org/10.1016/j.ijhydene.2007.01.011>)
- [83] N. Lamoureux, H. E. Merhubi, L. Pillier, S. De Persis, P. Desgroux, Modeling of NO formation in low pressure premixed flames, *Combust. Flame* 163 (2016) 557–575. (URL: <https://doi.org/10.1016/j.combustflame.2015.11.007>)
- [84] E. C. Okafor, Y. Naito, S. Colson, A. Ichikawa, T. Kudo, A. Hayakawa, H. Kobayashi, Experimental and numerical study of the laminar burning velocity of CH_4 – NH_3 –air premixed flames, *Combust. Flame* 187 (2018) 185–198. (URL: <https://doi.org/10.1016/j.combustflame.2017.09.002>)
- [85] The CRECK Modeling Group (Politecnico di Milano), Detailed kinetic mechanisms: C_1 – C_3 + NO_x mechanism (Version 2003, March 2020), 2020. <http://creckmodeling.chem.polimi.it/> (accessed at: 2021/04/13)
- [86] X. Han, Z. Wang, Y. He, Y. Zhu, K. Cen, Experimental and kinetic modeling study of laminar burning velocities of NH_3 /syngas/air premixed flames, *Combust. Flame* 213 (2020) 1–13. (URL: <https://doi.org/10.1016/j.combustflame.2019.11.032>)
- [87] Q.-D. Wang, Y. Sun, H. J. Curran, Comparative Chemical Kinetic Analysis and Skeletal Mechanism Generation for Syngas Combustion with NO_x Chemistry, *Energy Fuels* 34 (2020) 949–964. (URL: <https://doi.org/10.1021/acs.energyfuels.9b03440>)
- [88] M. L. Lavadera, A. A. Konnov, Laminar burning velocities of methane + formic acid + air flames: Experimental and modeling study, *Combust. Flame* 225 (2021) 65–73. (URL: <https://doi.org/10.1016/j.combustflame.2020.10.050>)
- [89] M. Frenklach, PrlMe (for Process Informatics Model), <http://primekinetics.org:8080/#/> (accessed at: 20/05/2021)
- [90] ELKH-ELTE Complex Chemical Systems Research Group, ReSpecTh information system, 2014. <https://respecTh.hu/> (accessed at: 19/05/2021)
- [91] ELKH-ELTE Research Group on Complex Chemical Systems, 2013. <http://kkrk.chem.elte.hu/kkrk/> (accessed at: 20/05/2021)
- [92] Laboratory of Molecular Structure and Dynamics, 2012. <http://kkrk.chem.elte.hu/lmsd/> (accessed at: 20/05/2021)

- [93] T. Varga, C. Olm, M. Papp, Á. Busai, I. G. Zsély, ReSpecTh Kinetics Data Format Specification v2.3, Eötvös Loránd University, Institute of Chemistry, Chemical Kinetics Laboratory, 2020.
http://respecth.chem.elte.hu/respecth/reac/ReSpecTh_Kinetics_Data_Format_Specification_v2.3.pdf
- [94] M. Papp, T. Varga, Á. Busai, I. G. Zsély, T. Nagy, T. Turányi, Computer programs for the analysis, optimization and reduction of reaction mechanisms – Optima++, <http://respecth.chem.elte.hu/respecth/reac/compProgs.php> (accessed at: 25/05/2021)
- [95] R. J. Kee, F. M. Rupley, J. A. Miller, Chemkin-II: A Fortran chemical kinetics package for the analysis of gas-phase chemical kinetics (SAND-89-8009), *Sandia National Lab. (SNL-CA), Livermore, CA (US)*, United States, 1989. (URL: <https://doi.org/10.2172/5681118>)
- [96] Institut für Technische Verbrennung, RWTH Aachen University, FlameMaster: A C++ Computer Program for 0D Combustion and 1D Laminar Flame Calculations, 2018. <https://www.itv.rwth-aachen.de/en/downloads/flamemaster/> (accessed at: 24/05/2021)
- [97] The CRECK Modeling Group (Politecnico di Milano), OpenSMOKE++: a general framework developed for numerical simulations of reacting systems with detailed kinetic mechanisms, including thousands of chemical species and reactions, 2021. <https://www.opensmokepp.polimi.it/> (accessed at: 26/05/2021)
- [98] A. Cuoci, A. Frassoldati, T. Faravelli, E. Ranzi, OpenSMOKE++: An object-oriented framework for the numerical modeling of reactive systems with detailed kinetic mechanisms, *Comput. Phys. Commun.* 192 (2015) 237–264. (URL: <https://doi.org/10.1016/j.cpc.2015.02.014>)
- [99] A. Cuoci, A. Frassoldati, T. Faravelli, E. Ranzi, Numerical Modeling of Laminar Flames with Detailed Kinetics Based on the Operator-Splitting Method, *Energy Fuels* 27 (2013) 7730–7753. (URL: <https://doi.org/10.1021/ef4016334>)
- [100] A. Stagni, A. Cuoci, A. Frassoldati, T. Faravelli, E. Ranzi, Lumping and Reduction of Detailed Kinetic Schemes: an Effective Coupling, *Ind. Eng. Chem. Res.* 53 (2014) 9004–9016. (URL: <https://doi.org/10.1021/ie403272f>)
- [101] I. N. Kosarev, S. M. Starikovskaia, A. Y. Starikovskii, The kinetics of autoignition of rich $\text{N}_2\text{O}-\text{H}_2-\text{O}_2-\text{Ar}$ mixtures at high temperatures, *Combust. Flame* 151 (2007) 61–73. (URL: <https://doi.org/10.1016/j.combustflame.2007.06.009>)
- [102] B. Ruscic, Active Thermochemical Tables: Sequential Bond Dissociation Enthalpies of Methane, Ethane, and Methanol and the Related Thermochemistry, *J. Phys. Chem. A* 119 (2015) 7810–7837. (URL: <https://doi.org/10.1021/acs.jpca.5b01346>)
- [103] B. Ruscic, R. E. Pinzon, G. v. Laszewski, D. Kodeboyina, A. Burcat, D. Leahy, D. Montoy, A. F. Wagner, Active Thermochemical Tables: thermochemistry for the 21st century, *J. Phys. Conf. Ser.* 16 (2005) 561–570. (URL: <https://doi.org/10.1088/1742-6596/16/1/078>)
- [104] B. Ruscic, R. E. Pinzon, M. L. Morton, G. Von Laszewski, S. J. Bittner, S. G. Nijssure, K. A. Amin, M. Minkoff, A. F. Wagner, Introduction to Active Thermochemical Tables: Several “Key” Enthalpies of Formation Revisited, *J. Phys. Chem. A* 108 (2004) 9979–9997. (URL: <https://doi.org/10.1021/jp047912y>)

- [105] Argonne National Laboratory, Active Thermochemical Tables (ATcT), 2021. <https://atct.anl.gov/> (accessed at: 2021/11/13)
- [106] M. Kovács, M. Papp, I. G. Zsély, T. Turányi, Determination of rate parameters of key N/H/O elementary reactions based on H₂/O₂/NO_x combustion experiments, *Fuel* 264 (2020) 116720. (URL: <https://doi.org/10.1016/j.fuel.2019.116720>)
- [107] A. G. Szanthoffer, I. G. Zsély, T. Turányi, Comparison of detailed NO_x reaction mechanisms on syngas combustion systems, *Proceedings of the European Combustion Meeting*, Paper S3_AII_11, Lisbon, Portugal, 2019, 14–17 April. (URL: http://garfield.chem.elte.hu/Turanyi/pdf/147_Szanthoffer_ECM2019_Paper_S3_AII_11.pdf)
- [108] L. Kawka, G. Juhász, M. Papp, T. Nagy, I. G. Zsély, T. Turányi, Comparison of detailed reaction mechanisms for homogeneous ammonia combustion, *Z. Phys. Chem.* 234 (2020) 1329–1357. (URL: <https://doi.org/10.1515/zpch-2020-1649>)
- [109] V. Samu, T. Varga, K. Brezinsky, T. Turányi, Investigation of ethane pyrolysis and oxidation at high pressures using global optimization based on shock tube data, *Proc. Combust. Inst.* 36 (2017) 691–698. (URL: <https://doi.org/10.1016/j.proci.2016.05.039>)
- [110] T. Varga, T. Nagy, C. Olm, I. G. Zsély, R. Pálvölgyi, É. Valkó, G. Vincze, M. Cserhádi, H. J. Curran, T. Turányi, Optimization of a hydrogen combustion mechanism using both direct and indirect measurements, *Proc. Combust. Inst.* 35 (2015) 589–596. (URL: <https://doi.org/10.1016/j.proci.2014.06.071>)
- [111] T. Varga, I. G. Zsély, T. Turányi, T. Bentz, M. Olzmann, Kinetic Analysis of Ethyl Iodide Pyrolysis Based on Shock Tube Measurements, *Int. J. Chem. Kinet.* 46 (2014) 295–304. (URL: <https://doi.org/10.1002/kin.20829>)
- [112] T. Nagy, Minimal Spline Fit Introducing Root-Mean-Square Fitting of Data Series with Akima Splines, Version: January 5 (2020), 2020, <http://respecth.chem.elte.hu/respecth/reac/compProgs.php>
- [113] T. Nagy, T. Turányi, Minimal Spline Fit: a model-free method for determining statistical noise of experimental data series, *Proceedings of the European Combustion Meeting*, Paper 337, Naples, Italy, 2021, 14–15 April. (URL: http://garfield.chem.elte.hu/Turanyi/pdf/153_Nagy_ECM21-336.pdf)
- [114] H. Akima, A New Method of Interpolation and Smooth Curve Fitting Based on Local Procedures, *J. ACM* 17 (1970) 589–602. (URL: <https://doi.org/10.1145/321607.321609>)
- [115] H. Akaike, A new look at the statistical model identification, *IEEE Trans. Automat. Contr.* 19 (1974) 716–723. (URL: <http://doi.org/10.1109/TAC.1974.1100705>)
- [116] E. J. Bedrick, C.-L. Tsai, Model Selection for Multivariate Regression in Small Samples, *Biometrics* 50 (1994) 226–231. (URL: <https://doi.org/10.2307/2533213>)
- [117] C. M. Hurvich, C.-L. Tsai, Regression and time series model selection in small samples, *Biometrika* 76 (1989) 297–307. (URL: <https://doi.org/10.1093/biomet/76.2.297>)
- [118] J. E. Cavanaugh, Unifying the derivations for the Akaike and corrected Akaike information criteria, *Stat. Probab. Lett.* 33 (1997) 201–208. (URL: [https://doi.org/10.1016/S0167-7152\(96\)00128-9](https://doi.org/10.1016/S0167-7152(96)00128-9))

- [119] O. Mathieu, M. M. Kopp, E. L. Petersen, Shock-tube study of the ignition of multi-component syngas mixtures with and without ammonia impurities, *Proc. Combust. Inst.* 34 (2013) 3211–3218. (URL: <https://doi.org/10.1016/j.proci.2012.05.008>)
- [120] O. Mathieu, A. Levacque, E. L. Petersen, Effects of N₂O addition on the ignition of H₂–O₂ mixtures: Experimental and detailed kinetic modeling study, *Int. J. Hydrog. Energy* 37 (2012) 15393–15405. (URL: <https://doi.org/10.1016/j.ijhydene.2012.07.071>)
- [121] O. Mathieu, E. L. Petersen, Experimental and modeling study on the high-temperature oxidation of Ammonia and related NO_x chemistry, *Combust. Flame* 162 (2015) 554–570. (URL: <https://doi.org/10.1016/j.combustflame.2014.08.022>)
- [122] J. A. Miller, M. C. Branch, W. J. Mclean, D. W. Chandler, M. D. Smooke, R. J. Kee, The conversion of HCN to NO and N₂ in H₂–O₂–HCN–Ar flames at low pressure, *Proc. Combust. Inst.* 20 (1985) 673–684. (URL: [https://doi.org/10.1016/S0082-0784\(85\)80557-9](https://doi.org/10.1016/S0082-0784(85)80557-9))
- [123] M. Kovács, M. Papp, I. G. Zsély, T. Turányi, Main sources of uncertainty in recent methanol/NO_x combustion models, *Int. J. Chem. Kinet.* 53 (2021) 884–900. (URL: <https://doi.org/10.1002/kin.21490>)
- [124] T. Turányi, L. Zalotai, S. Dóbe, T. Bérces, Effect of the uncertainty of kinetic and thermodynamic data on methane flame simulation results, *Phys. Chem. Chem. Phys.* 4 (2002) 2568–2578. (URL: <https://doi.org/10.1039/b109154a>)
- [125] J. Zádor, I. G. Zsély, T. Turányi, M. Ratto, S. Tarantola, A. Saltelli, Local and Global Uncertainty Analyses of a Methane Flame Model, *J. Phys. Chem. A* 109 (2005) 9795–9807. (URL: <https://doi.org/10.1021/jp053270i>)
- [126] R. Langer, J. Lotz, L. Cai, F. Vom Lehn, K. Leppkes, U. Naumann, H. Pitsch, Adjoint sensitivity analysis of kinetic, thermochemical, and transport data of nitrogen and ammonia chemistry, *Proc. Combust. Inst.* 38 (2021) 777–785. (URL: <https://doi.org/10.1016/j.proci.2020.07.020>)
- [127] S. D. Cohen, A. C. Hindmarsh, P. F. Dubois, CVODE, A Stiff/Nonstiff ODE Solver in C, *Computers in Physics* 10 (1996) 138–143. (URL: <https://doi.org/10.1063/1.4822377>)
- [128] E. J. K. Nilsson, A. A. Konnov, Role of HOCO Chemistry in Syngas Combustion, *Energy Fuels* 30 (2016) 2443–2457. (URL: <https://doi.org/10.1021/acs.energyfuels.5b02778>)
- [129] F. Battin-Leclerc, A. A. Konnov, J. L. Jaffrezo, M. Legrand, To Better Understand the Formation of Short-Chain Acids in Combustion Systems, *Combust. Sci. Technol.* 180 (2007) 343–370. (URL: <https://doi.org/10.1080/00102200701740782>)
- [130] A. Farooq, D. F. Davidson, R. K. Hanson, C. K. Westbrook, A comparative study of the chemical kinetics of methyl and ethyl propanoate, *Fuel* 134 (2014) 26–38. (URL: <https://doi.org/10.1016/j.fuel.2014.05.035>)
- [131] J. E. Johnsson, P. Glarborg, K. Dam-Johansen, Thermal dissociation of nitrous oxide at medium temperatures, *Proc. Combust. Inst.* 24 (1992) 917–923. (URL: [https://doi.org/10.1016/S0082-0784\(06\)80109-8](https://doi.org/10.1016/S0082-0784(06)80109-8))
- [132] D. L. Baulch, C. T. Bowman, C. J. Cobos, R. A. Cox, T. Just, J. A. Kerr, M. J. Pilling, D. Stocker, J. Troe, W. Tsang, R. W. Walker, J. Warnatz, Evaluated Kinetic Data for

- Combustion Modeling: Supplement II, *J. Phys. Chem. Ref. Data* 34 (2005) 757–1397. (URL: <https://doi.org/10.1063/1.1748524>)
- [133] A. P. Zuev, A. Y. Starikovskii, Reactions involving nitrogen oxides at high temperature: The unimolecular decay of N_2O , *Khim. Fiz.* 10 (1991) 52–63.
- [134] W. Tsang, J. T. Herron, Chemical Kinetic Data Base for Propellant Combustion I. Reactions Involving NO, NO_2 , HNO, HNO_2 , HCN and N_2O , *J. Phys. Chem. Ref. Data* 20 (1991) 609–663. (URL: <https://doi.org/10.1063/1.555890>)
- [135] P. S. Riley, B. Cosic, A. Fontijn, The $\text{H}+\text{NO}$ recombination reaction over a wide temperature range, *Int. J. Chem. Kinet.* 35 (2003) 374–380. (URL: <https://doi.org/10.1002/kin.10137>)
- [136] P. Glarborg, M. Østberg, M. U. Alzueta, K. Dam-Johansen, J. A. Miller, The recombination of hydrogen atoms with nitric oxide at high temperatures, *Proc. Combust. Inst.* 27 (1998) 219–226. (URL: [https://doi.org/10.1016/S0082-0784\(98\)80408-6](https://doi.org/10.1016/S0082-0784(98)80408-6))
- [137] X. Chen, M. E. Fuller, C. Franklin Goldsmith, Decomposition kinetics for HONO and HNO_2 , *React. Chem. Eng.* 4 (2019) 323–333. (URL: <https://doi.org/10.1039/c8re00201k>)
- [138] D. Fulle, H. F. Hamann, H. Hippler, J. Troe, Temperature and pressure dependence of the addition reactions of HO to NO and to NO_2 . IV. Saturated laser-induced fluorescence measurements up to 1400 bar, *J. Chem. Phys.* 108 (1998) 5391–5397. (URL: <https://doi.org/10.1063/1.475971>)